# BOEING

*SEATTLE, WASHINGTON*

Kq 3 614 3

# FEASIBILITY STUDY OF COMPUTER PREDICTION OF BROADBAND NEAR-FIELD ELECTROMAGNETIC INTERFERENCE IN A SPACE VEHICLE-FINAL REPORT

D2-90642-1

CONTRACT NUMBER NAS 8-5608

DECEMBER 31, 1964

PREPARED BY

T. K. Foley

A. Rudzitis

APPROVED BY

J. E. Maynard

V. B. Westburg

I. J. Stampalia

This report was prepared by The Boeing Company for the George C. Marshall Space Flight Center of the NASA. The work was administered under the technical direction of the Quality and Reliability Assurance Laboratory of the George Marshall Space Flight Center with James Toler acting as Project Manager.

## ABSTRACT

The objective of the research program is to investigate the
feasibility of computer prediction of broadband near-field
electromagnetic interference in a space vehicle. The
results of such a prediction program would provide useful
information on interference problems to equipment
designers and also allow selection of critical monitor
points for use during launch vehicle checkout.

The prime emphasis of the investigation has been a funda-
mental approach to the problem of analytic prediction of
radiation coupling (Section 3.0) between equipment boxes
in an enclosed vehicle structure. In addition to the radia-
tion coupling investigation, a secondary emphasis has been
given to application of a cable-to-cable computer interfer-
ence prediction program to the Saturn Instrument Unit
(Section 4.0).

## KEY WORDS

Electromagnetic Interference
Radio Interference
Computer Prediction
Cable Coupling
Radiation, Near Field
Interference Prediction

# TABLE OF CONTENTS

# 1.0 SUMMARY

*23645*

This document is the final report on an investigation into the feasibility of computer prediction of broadband near-field electromagnetic interference in a space vehicle. The prime emphasis of the investigation has been a fundamental approach to the problem of analytic prediction of radiation coupling (Section 3.0) between equipment boxes in an enclosed vehicle structure. In addition to the radiation coupling investigation, a secondary emphasis has been given to application of a cable-to-cable computer interference prediction program to the Saturn Instrument Unit (Section 4.0).

The analytic approach in the radiation coupling study has examined in detail the following possible methods of predicting the amount of coupled interference:

1) Cavity Field Expressions,
2) Lumped Circuit Models,
3) Near-Field Expressions.

In the cavity method, the vehicle structure is considered as a metallic enclosure (cavity). All equipment boxes, which are potential interference radiators (emitters), are considered as combinations of electric and magnetic dipoles. The strength and orientation of these dipoles is a function of the surface current flow on the equipment boxes.

Shielded room techniques show the most promise for the actual determination of these dipole characteristics. Other techniques using field probes on the surface of the emitter box are not satisfactory unless the disturbance of the fields caused by the presence of the probe could be evaluated.

The equipment box, whose equivalent dipole characteristics are desired, is placed in the shielded room and measurements are made of the fields at selected places on the walls. Theoretical calculations are made of

the field distributions in a cavity with the same shielded room boundary conditions. The type, strength and orientation of the equivalent dipoles for the emitter box are determined from an evaluation of the field measurements and theoretical calculations. In the future, it is entirely possible that the interference specification used by the designer will specify limits on the equivalent dipole moments equipment boxes may have.

Generalized expressions for the fields excited by these short electric and magnetic dipoles have been derived by starting with Maxwell's equations and the boundary conditions for loss-free cavities. These expressions, useful at all frequencies, allow determination of the field strengths at any point in the enclosure as a function of the emitter location, strength and orientation. With the fields known everywhere, the currents induced on a box susceptible to interference (receptor) can be found. Various analytical methods may be used to include the effects of lossy walls, openings and perturbing bodies on the resonant frequencies, and on the field configuration within the cavity. Thus, the basic feasibility of interference prediction using electromagnetic theory of cavity resonators has been established.

The applicability of the cavity expressions for prediction of coupled interference between very closely-spaced boxes (less than one box dimension apart) has not been fully substantiated. Therefore, the lumped circuit models were developed to allow prediction in this region.

The lumped circuit approach replaces the equipment box walls with the equivalent surface impedances. The coupling of emitter surface currents to a nearby receptor box is represented by inter-box capacitance, mutual inductance or conductance through interconnecting cabling. The results of predictions using the developed analytic models has been correlated with laboratory measurements, and it was found that the only significant coupling mechanisms were through inductance. The lumped-circuit models are useful when the box dimensions and spacing are much less than a wavelength.

The free-space, near-field expressions for a small loop were used to predict the radiated fields in a closed structure. The analytic predictions compared favorably with experimental data from an equivalent model set up in a screen room. However, the near-field expressions are restricted to frequencies below the structure resonant frequencies and to regions where the box separation is at least one box dimension. Therefore, near-field models will, at best, give rough approximations to the interference fields.

The second part of the study was the development of a computer program for prediction of cable-to-cable coupling of interference in the Saturn Instrument Unit. The program developed represents a modification and extension of past research efforts at Boeing on computer techniques for the predication of cable-to-cable interference coupling. The computer program is written in FORTRAN IV language and can be used on any system having a FORTRAN IV compiler such as IBM 7094, SRU 1107.

A representative set of 52 circuits in the Instrument Unit were selected for study in the computer program. Each circuit was assigned to one of six basic circuit types and given an appropriate emission and susceptibility spectra. The computer program constructed attenuation spectrums between all emitter-receptor circuit combinations. The attenuation spectrum was based on the amount of mutual circuit length and separation, the amount of inter-circuit capacity and inductance, and the shielding and twisting effectiveness of the wires.

The emission spectra of each circuit, modified by the correct attenuation spectra of the cable network, was compared to the susceptibility spectra of every other circuit for possible interference. The 52 Instrument Unit circuits examined represented over 2500 cases of possible interference. The results indicated 196 potential cases where the coupled interference might exceed a threshold 6 db below the susceptibility level of the receptor circuit. The lack of sufficient

details on Instrument Unit circuits and the resultant assumptions made on circuit characteristics definitely was a contributing factor in many of these cases.

The significant point is that the number of cases requiring more study was reduced below 8% of the original number.

## 2.0 INTRODUCTION

The problem of prediction of Electromagnetic Interference (EMI) in a complete integrated launch system is extremely complex. The agency charged with performing a successful system integration is faced with a myriad of equipment boxes, components and cabling supplied from numerous different equipment manufacturers. The only assurances on EMI the manufacturer can truthfully give the system integrator is that a particular box or component when operated by itself in a specific controlled test environment will satisfy certain prescribed specification limits on emission and susceptibility. Since the operational system environment is quite different than the test environment, the box can be expected to have a significantly different emission and susceptibility spectrum when integrated into the vehicle system.

Up to this time, there has been no practical method developed that would be useful to the system integrator in the predesign phase to determine the overall EMI environment of a large complex vehicle system. Thus, it is necessary to conduct an expensive EMI test program with all the electrical system placed in a vehicle mockup. This test is conducted after design completion and the EMI problems uncovered necessitate, in many cases, a costly retrofit program, and results in a series of launch date slippages. Thus, a predesign EMI prediction program would offer the system integrator a two-fold advantage. First, it would allow discovery of system EMI deficiencies in time for correction during the design phase. Secondly, the prediction program would pinpoint the critical interference areas for more efficient use of test time during the EMI system test.

The overall goal of the current research contract has been to determine the feasibility of prediction of broadband near-field electromagnetic interference in the predesign phase of system development. A very fundamental analysis of the various coupling paths between black boxes of an assembled vehicle system has been carried out.

The result of this approach is a prediction method applicable to all levels of system complexity (i.e., black box to black box, subsystem to stage, stage to vehicle complex, and vehicle to ground-support equipment complex).

The investigation has divided the various coupling mechanisms into two distinct parts. The first part is radiation coupling to which prime emphasis has been given in this report. The radiation coupling study represents an extension of state-of-the-art analytic techniques to vehicle interference coupling problems for which no satisfactory solutions presently exist.

The second part is a cable-to-cable coupling study which has resulted in a computer-prediction program for the Saturn Instrument Unit. This computer program represents an improved extension of past Boeing research on cable-to-cable interference prediction.

# 3.0 PREDICTION OF BROADBAND NEAR-FIELD RADIATION COUPLING

Broadband near-field radiation coupling is a term used in this report to cover a large category of coupling mechanisms. These mechanisms include box-to-box, box-to-cable, box-to-stage, stage-to-vehicle, and vehicle-to-ground complex. The prime emphasis during this investigation has been devoted to examining the feasibility of predicting box-to-box coupling and the logical extension of these prediction techniques to larger systems.

## 3.1 METHODS OF BOX LEAKAGE

Box-to-box coupling can occur from a variety of sources such as leakage through walls, seams, small apertures, cable entrances, etc. Each of these leakage sources give rise to one common effect (i.e., external surface current flow on the emitter box). It is the coupling of these emitter box external-surface currents through re-radiation or conduction to the receptor box that is the prime source of radiation coupling between boxes.

The direct radiation coupling of internal emitter-box energy to a receptor box via large apertures, such as ventilation holes, has not been considered. The reason is that the development and use of low-power dissipation solid-state circuits for space applications has resulted in forced-air cooling being replaced by cold-plate cooling. Thus, equipment boxes used in space vehicles are not expected to have large apertures.

## 3.2 CAVITY CONCEPTS APPLIED TO RADIATION COUPLING

In this report, the interference problem is investigated as applied to equipment operated in a typical closed-vehicle system. The vehicle shell forms an enclosure or cavity which contains metallic boxes

enclosing a variety of instrument and telemetry circuits. The metallic boxes are mounted on the vehicle shell and interconnected by cables. The causes of the mutual interference between the various circuits are the transmission of the electromagnetic energy directly through the metallic walls of the boxes, the leakage of the energy through apertures and seams in the walls, and the coupling of the energy through various coupling mechanisms between the interconnecting cables.

The fundamental approach to the problem of radiation coupling, which does not involve conduction currents, is to treat the interfering device as a radiating antenna which sets up electromagnetic field inside the cavity formed by the vehicle shell. The susceptibility environment of the receptor boxes is then determined by the magnitude and direction of the electromagnetic field surrounding them, and by the voltages induced in the interconnecting cables by the field. If the characteristics of the radiating source are known, the field within the excited cavity can be determined by employing the electromagnetic theory of the cavity resonators.

In this section, various aspects of the interference problem are described as applied to closed cavities. First, the radiation characteristics of the interfering equipment are considered. Second, the theory of the resonant cavities is discussed starting from the Maxwell's equations for loss-free cavities. Various analytical methods are indicated to include the effects of lossy walls, openings and perturbing bodies on the field configuration within the cavity. In conclusion, the electromagnetic leakage into receptor circuits is considered.

### 3.2.1    Equivalent Dipoles of Interference Radiators

The interfering device, which represents a radiating source in the cavity, is characterized by the currents existing on it. The strength and distribution of these currents determine the electromagnetic field everywhere in the cavity. One of the tasks of the interference prediction is the evaluation of the radiating source.

A direct calculation of the radiation characteristics of an equipment from the voltages and currents in the electronic circuits enclosed in the box is clearly impossible. Since experimental methods are required, this implies that either the interfering equipment is available for measurements or that specifications describing the radiation characteristics of the equipment are available for interference prediction. In the following discussion, it is assumed that a complete assembly of a prototype equipment box is available so that it can be activated in a laboratory under the same power and signal levels which will exist when it is operated in the assembled vehicle system.

The distribution and strength of the radiating currents may be measured directly by probe method, from which the field can be calculated at any point. This method, perhaps difficult, could yield any desired information with proper calculations. Another method is to measure the interference field under pre-specified conditions and locations. Both methods imply careful and laborious measurements under difficult conditions, since the probes and other measuring equipment will distort the measured quantity considerably.

If distances greater than the source dimensions are considered, the problem of determining the strength of the source is simplified. Provided that the interfering equipment is much smaller than the wavelength corresponding to the frequency of measurement, the important features of the source can be determined by employing the principle of superposition. The field from any radiating system may be represented by superposition of multipole sources which consist of electric and magnetic dipoles and higher-order multipoles. The relative contributions of the various multipoles to the total field around the source depend on the distance from the source. At distances greater than source dimensions, the electric and magnetic dipole terms are most important; the contributions from higher-order poles are negligible. This simplifies the problem considerably, since the strengths of the equivalent dipoles can be measured more readily. The method of measurement is to place the interfering equipment in a rectangular

shielded room or cavity, and to measure the field strength at selected places. The purpose of the shielded room is to provide a noise-free space, free from other interfering sources, and to provide a known boundary for the radiator. The known boundary condition enables exact theoretical calculations of the field inside the cavity in terms of the dipole strength, type, and orientation. These characteristics of the radiating device are then determined from field measurements taken at selected places on the walls of the shielded room. Once the equivalent dipoles of the interfering device are found, the specifications of an interference-producing device can be established in terms of the equivalent dipoles.

Considerable theoretical and experimental work regarding the determination of the equivalent dipoles of interfering equipment by shielded-room techniques has been done by the Rensselaer Polytechnic Institute. References (3) and (4) describe this work: the shielded rooms, the placing of the interfering device in the room, the design and calibration of the field-sensing devices and their locations in the shielded room. The analysis is based on the static fields of the dipoles, and is applicable to cases for which a volume distribution of electric and magnetic dipoles may be represented by an equivalent lumped electric dipole and an equivalent lumped magnetic dipole. The exact conditions regarding the size of the room and the size of the interfering device for the lumped dipole concept to be applicable are as follows:

1) The radiator should be much smaller than the wavelength of the interfering frequency;

2) The distance of observation should be smaller than a wavelength to be in the static field of the radiator;

3) The distance of the point at which the field is measured to the source should be large compared to the dimensions of the source.

The condition (1) is necessary if a piece of equipment under test is to be represented by lumped equivalent dipoles. This is possible only if the surface currents of the radiator have no phase difference along the

paths. If the greatest linear dimension, d, of the source satisfies the condition $d < \lambda/2\pi$, where $\lambda$ is the wavelength under consideration, satisfactory engineering results are obtained. The condition (2) ensures that the measurements are made in the static fields of the dipole since, for distances larger than $\lambda/2\pi$ from a source, the radiation field becomes important. The condition (3), which defines the relative sizes of the screened room and the interfering equipment, follows directly from the condition (2). If the measured field is the static field of radiator, and if the dimensions of the radiator are less than one-third of the shielded room dimensions, then the field excited by the radiator is similar to a small dipole having the same dipole moment. The shape of the screened room is chosen as a cubical room because its symmetry simplifies calculations. Under the assumptions of static fields, the computation of the field in the cavity is simplified since the principle of images is applicable.

The interfering equipment should be placed in the screen room at a location and under conditions which resemble its actual conditions in the final assembled system as closely as possible. The radiators, in general, could be classified into two types regarding their location in the assembled system: grounded radiators and isolated radiators. Equipment which is coupled to the vehicle shell directly by means of connecting cables, ground straps or indirectly by close proximity to shell are classified as grounded radiators. Any equipment which is generally used with no cable connections and is not coupled to ground or any object can be considered to be an isolated radiator. The majority of the interfering equipment fall within the class of the grounded radiators, since most equipment is expected to be located near or on the vehicle shell.

To measure the equivalent dipoles of grounded radiators, the interfering equipment is placed on the floor of the screened room (the floor representing the ground plane which is the vehicle shell). The equivalent dipoles of such equipment then contain only three components: a vertical - electric, and two horizontal-magnetic. The other two

electric and one magnetic components do not produce appreciable
fields as they are nearly cancelled by their images in the ground plane.
If the equipment is placed symmetrically at the center of the floor in
the room, then three sensing elements are required to determine the
strength of the three dipole components. This is shown in Figure 3.1
where two loop probes and one rod probe is all that is required to
determine the three dipole components. The electric rod probe placed
directly above the radiator is sensitive to the electric dipole. Hence,
the induced voltage in the electric probe is proportional to the electric
moment of the radiator. The two loops, placed to obtain maximum
sensitivity, however, are sensitive to both electric and magnetic
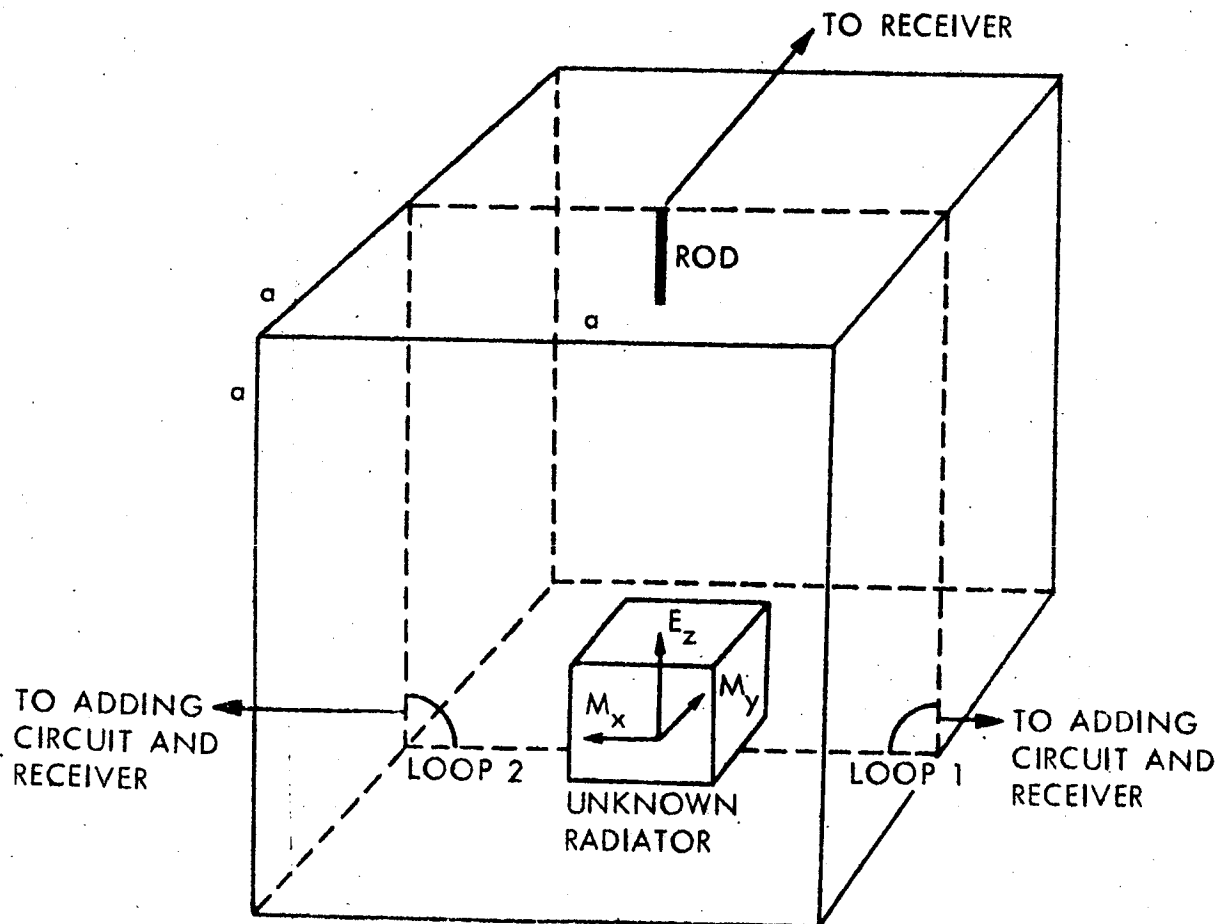dipoles.



FIGURE 3.1    SHIELDED ROOM & LOCATING OF
             SENSING DEVICES FOR GROUNDED
             RADIATOR MEASUREMENTS

The voltage induced by the electric dipole, $E_z$, in one loop is $180^{\circ}$ out of phase in the second loop; the voltage induced by the magnetic dipole, $M_y$, is in phase in both loops. Thus, subtraction of the voltage of loop 1 from that of loop 2 will give a voltage proportional to the electric dipole moment, and the addition of the two voltages will yield a value proportional to magnetic dipole moment, $M_y$. To measure the moment of the magnetic dipole $M_x$, the radiating equipment is rotated $90^{\circ}$ and the above procedure repeated. These measurements of the dipoles $E_z$, $M_x$, $M_y$ yield the values of their moments but not their relative phase differences. However, if the resulting magnitudes of the field components are added directly, the maximum possible interference field is obtained.

To measure the equivalent dipoles of large radiators, the effect of the spacial current distribution on the magnitudes of the equivalent dipoles must be determined. A method which removes the restriction of the relative sizes of the screened room and the radiator is described in the reference (3). Following this method, it is possible to evaluate approximately the magnetic dipole components of long radiators, but a correction factor is necessary for the measured electric dipole. The correction factor depends on the relative sizes of the room and of the radiator: this means that a separate calibration is required for each particular size and type of the radiator.

The most general method to determine the equivalent dipoles by the screened-room technique for all sizes of radiators and all frequency ranges is to employ the full-series expressions for the field in an excited cavity given by equations (1) and (2) in this section. As shown in reference (4) for low-frequency ranges, the field at the edges of a cubical cavity depends on the dipole strength and the spacial current distribution of the radiator. This still implies a calibration factor for each size and type of radiator. However, if an accuracy of about $\pm$ 3 db is acceptable, no calibration is required and the equivalent dipoles may be determined by using only a limited number of probes at fixed locations on the cavity walls. To obtain greater accuracy, other methods should be investigated.

Two possible solutions to the above problem may be anticipated. First, instead of probing the field at a few selected points, the field could be measured along the walls continually. This implies sliding probes and slots in the walls, but the techniques are well known from waveguide measurements. Second, the effect of resonance may be used. As shown in equation (8) in this section, the field strength at resonance can be calibrated readily at any point in the cavity if the quality factor, Q, of the cavity is known. As the field is given by comparatively simple expressions, it may be possible to deduce the characteristics of the radiator by few measurements at selected positions. Of course, this means that a room of adjustable size is required.

Finally, it can be said that, although some amount of work still remains to be done, the shielded-room technique appears to be the most promising method to determine the equivalent dipoles of the radiator. Once this is done, the noise field of the interfering device can be calculated for any condition.

At distances less than the dimensions of the radiator, higher-order multipoles contribute most to the field. There are no methods available on how to determine the multipoles of a radiator, but the problem may be approached by some other techniques as outlined in Sections 3.3 and 3.4.

3.2.2     Excitation of Ideal Cavities

After the radiation characteristics of an interfering device have been determined, the next step is to find the magnitudes and the directions of the electric and magnetic fields excited by the radiator within the cavity. The simplest case to consider is an ideal loss-free cavity formed by perfectly-conducting walls. This type of cavity supports an infinite number of source-free oscillations. To each oscillation, there corresponds a resonant frequency $f_i = \omega_i/2\pi$ and a definite field configuration $\overrightarrow{E}_i$, $\overrightarrow{H}_i$. The resonant frequency and the field distribution of each oscillation or mode is determined by the geometrical shape and size of the cavity.

A source in the cavity at a frequency off resonance will excite all the resonant modes so that the total field will be a superposition of all the resonant modes with proper amplitude factors. Since a loss-free cavity is assumed, the source supplies energy to the cavity over one part of the cycle, and the cavity acts as a reactive load on the exciting source. If the cavity is excited exactly at one of its resonant frequencies, the oscillations will build up to a very large value.

A mathematical derivation of the excited field in a cavity is given in Appendix A. The results are presented here in equations (1) and (2):

$$\overline{E} = \sum_i \frac{j\overline{E}_i}{\omega^2 - \omega_i^2} \iiint \left[ \omega \overline{J} \cdot \overline{E}_i^* + \omega_i \overline{M} \cdot \overline{H}_j^* \right] dV \tag{1}$$

$$\overline{H} = \sum_i \frac{j\overline{H}_i}{\omega^2 - \omega_i^2} \iiint \left[ \omega_i \overline{J} \cdot \overline{E}_i^* + \omega \overline{M} \cdot \overline{H}_i^* \right] dV \tag{2}$$

where $\overline{E}$ and $\overline{H}$ are the total electric and magnetic field vectors excited by the source, $\overline{E}_i$ and $\overline{H}_i$ are electric and magnetic fields of the i's resonant mode, $\overline{J}$ and $\overline{M}$ are the electric and magnetic currents of the source operating at frequency $f = \omega/2\pi$. The integration is performed over the volume, V, of the cavity.

The mode vectors, $\overline{E}_i$ and $\overline{H}_i$, are functions of the three space coordinates, and have a characteristic distribution in each direction. Therefore, the summation over the index i in the above equations actually consists of three summations:

$$\sum_i = \sum_\ell \sum_m \sum_n$$

where $\ell$, m, and n are positive integers 0, 1, 2, ... in the general case. For cavities which are formed from cylindrical waveguides, the characteristic modes are usually expressed as transverse

magnetic (TM) and transverse electric (TE) modes with respect to the longitudinal direction. Simple dipole sources oriented in the longitudinal direction require only TM or TE modes, but in general case, both TM and TE characteristic modes are necessary to expand an arbitrary field in a cavity:

$$\bar{E}_i = \bar{E}_i^{TM} + \bar{E}_i^{TE}$$

$$\bar{H}_i = \bar{H}_i^{TM} + \bar{H}_i^{TE}$$

If there are several sources in the cavity, the total field is then a superposition of the fields of equations (1), (2) from each source. The resonant frequencies, $\omega_i$, are functions of the geometry and size of the cavity. The frequencies can be calculated exactly for cavities which form coordinate surfaces u = constant, v = constant, w = constant of a coordinate system u, v, w for which the wave equation is separable. Finite conductivity of the cavity walls or the losses in the dielectric medium render the resonant frequencies complex so that the frequency has an imaginary part. This describes an exponential time decay of the energy in a lossy cavity due to the flow of energy into the walls or due to the losses in the dielectric medium. The complex resonant frequencies can be calculated approximately by perturbational and variational methods, as discussed in paragraph 3.2.3.

The equations (1), (2), have been derived assuming ideal cavities and general electric and magnetic current sources. The main difficulty in evaluating the forced fields is the integral over the volume of the cavity. Even if the analytical expressions of current distributions $\bar{J}$, $\bar{M}$ are known, it may not be possible to evaluate the volume integrals in a closed form so that numerical methods are necessary.

The forced fields due to simple electric and magnetic dipole sources in rectangular and circular cylindrical cavities are derived in Appendix A.

### 3.2.3 Approximate Solutions of Cavity Perturbation Problems

The theory derived in Section 3.2.1 is applicable to ideal cavities with perfect boundaries enclosing homogeneous isotropic loss-free dielectric medium with dielectric constant $\varepsilon$ and magnetic permeability $\mu$. In the interference problem, the vehicle shell forms lossy metallic walls. Also enclosed within the cavity are various instrument and telemetry chassis, cables and possibly other equipment. These factors represent a wide variety of irregularities which influence the resonant frequencies and the field in a cavity. Exact calculations of the effects of irregularities on the resonant frequencies and the characteristic modes are seldom possible with present mathematical techniques, but approximate values can be obtained by applying perturbational and variational methods. These methods employ the fact that the electromagnetic problems can be expressed in a form of integral equations instead of differential equations. Integration is a summation process, and it is not necessary that each element of the summation be correct. It is more important that the elements contributing most to the summation be correct, than that the elements of minor contribution be correct. Even for the problems which can be solved exactly, it may be more convenient to employ approximate methods; for the evaluation of the exact solution may be much too complicated.

The derivation of the approximate methods can be found in standard texts (references 1 and 2). Some of the problems and the approximate solutions, as encountered in the interference prediction, are outlined here.

The perturbational methods are applicable when a cavity differs but little from a cavity whose characteristic modes and resonant frequencies are known. The characteristic modes and the resonant frequencies will differ but little from those of the known cavity. The change in resonant frequency and the quality factor, Q, of a cavity due to lossy walls can be calculated by perturbational method. The theory

of the skin effect for metallic boundaries permits one to obtain a first approximation for the change in resonant frequency from equation (A.16), Appendix A,

$$\omega - \omega_0 = \frac{-j \oiint Z_s \vec{H} \cdot \vec{H}_0 \, dS}{\iiint (\epsilon \vec{E} \cdot \vec{E}_0 - \mu \vec{H} \cdot \vec{H}_0) \, dV} \qquad (3)$$

where $E$, $H$, $\omega$ represent the field and resonant frequency of the cavity with lossy walls, having a surface impedance $Z_s$; and $\vec{E}_0$, $\vec{H}_0$, $\omega_0$ represent the corresponding quantities of the original cavity with perfectly-conducting walls. The surface and volume integrals are taken over the cavity. Equation (3) is an exact expression for the change in resonant frequency due to the lossy walls of the cavity. Since the surface impedance of metallic boundaries is a very small quantity at most frequencies, it can be deduced that the tangential electric field at the walls is still very small, and that the field distribution within the lossy cavity is nearly identical to the field distribution within the corresponding loss-free cavity. As a result of this, the unknown field $\vec{E}$, $\vec{H}$ in equation (3) may be approximated by the known field $\vec{E}_0$, $\vec{H}_0$. When this is done, the change in resonant frequency is given by

$$\omega - \omega_0 = \frac{j \oiint Z_s |H_0|^2 \, dS}{\iiint (\epsilon |E_0|^2 + \mu |H_0|^2) \, dV} \qquad (4)$$

As mentioned before, the resonant frequency becomes complex when the losses in a cavity are considered:

$$\omega = \omega_r + j\omega_j \qquad (5)$$

where,

$$\omega_r - \omega_0 \approx -\frac{\oiint X_s |H_0|^2 \, dS}{2\iiint \mu |H_0|^2 \, dV} \; ,$$

$$\omega_j \approx \frac{\oiint R_s |H_0|^2 \, dS}{2\iiint \mu |H_0|^2 \, dV}$$

and $\quad Z_s = R_s + j X_s$ .

The quality factor, Q, for a cavity is defined by

$$Q = \frac{\omega \times \text{energy stored in the cavity}}{\text{energy lost per cycle to the walls}}$$

and can be shown to be (for a perturbed cavity)

$$Q \approx \frac{\omega_0 \iiint \mu |H_0|^2 dV}{\oiint R_s |H_0|^2 \, dS} \tag{6}$$

The complex resonant frequency then can be written as

$$\omega = \omega_r \left( 1 + \frac{j}{2Q} \right) \tag{7}$$

19

The forced fields in equations (1), and (2) are now functions of complex resonant frequencies

$$\omega_{\ell mn} = (\omega_r)_{\ell mn} + j(\omega_j)_{\ell mn}$$

$$(\omega_j)_{\ell mn} = \frac{1}{2Q_{\ell mn}}$$

For a loss-free cavity, the field becomes indeterminate with $\omega = \omega_{\ell mn}$, $\omega$ and $\omega_{\ell mn}$ being real. Physically, a loss-free cavity is an unrealizable limiting case: so that, in all practical cases, resonance cannot be achieved with real frequencies. The forced field near a complex resonant frequency can be calculated from equation (A.17), Appendix A,

$$\vec{E}(\omega \rightarrow \omega_i) = \frac{j\vec{E}_i}{2(\omega - \omega_i)} \iiint \left[ \vec{J} \cdot \vec{E}_i^* + \vec{M} \cdot \vec{H}_i^* \right] dV \tag{8}$$

with a similar expression for the magnetic field $\vec{H}(\omega \rightarrow \omega_i)$.

In the case of a degeneracy, when one unperturbed resonant frequency corresponds to several characteristic modes, such as $TM_{\ell mn}$ and $TE_{\ell mn}$ modes in a rectangular cavity, a number of complex resonant frequencies of the perturbed cavity may be near each other. In these cases, the forced field is obtained from (A.18), Appendix A,

$$\vec{E}(\omega) \quad \sum_{r=1}^{k} \frac{j\vec{E}_{ir}}{2(\omega - \omega_{ir})} \iiint \left[ \vec{J} \cdot \vec{E}_{ir}^* + \vec{M} \cdot \vec{H}_{ir}^* \right] dV \tag{9}$$

$$\omega \rightarrow \omega_{ir}, \quad r = 1, 2, \ldots k$$

The equipment boxes within the cavity influence not only the resonant frequencies but also change the field. As a starting point, the effect of a small conducting body in an ideal cavity is investigated. By a reasoning similar to the one used to derive equation (3), the change in the resonant frequency due to a conducting perturbation is given by

$$\omega - \omega_0 = \frac{j \oiint_{\Delta S} \vec{H} \times \vec{E}_0^* \cdot \vec{dS}}{\iiint_{V'} (\epsilon \, \vec{E} \cdot \vec{E}_0^* + \mu \, \vec{H} \cdot \vec{H}_0^*) \, dV} \tag{10}$$

where the integrations are performed throughout the volume, $V'$, of the deformed cavity, and over the surface, $\Delta S$, of the deformation. Expression (10) is exact if the fields $\vec{E}$, $\vec{H}$ are used. If the volume of the perturbing body is small and if it forms a smooth inward perturbation of the cavity wall, the unknown field $\vec{E}$, $\vec{H}$ may be replaced by the unperturbed field $\vec{E}_0$, $\vec{H}_0$. As seen from equation (10), the change in resonant frequency depends on the size and on the location of the perturbation.

If the perturbing body is large, the perturbational technique becomes difficult as the approximation $\vec{E}_0$, $\vec{H}_0$ for the unknown field introduces a large error. A procedure which allows one to calculate the changes in resonant frequencies and to determine the unknown fields $\vec{E}$, $\vec{H}$ is the variational method. This method employs the principle that the eigenvalues or some other characteristic quantities of a boundary-value problem is stationary. For example, if a resonant frequency of a cavity is expressed as a variational integral of the field inside the cavity, first-order approximation of the field results in a second-order approximation of the resonant frequency. The resonant frequency is insensitive to small variations of the field about the true field. A systematic scheme for determining a finite set of approximate mode functions and characteristic values to a given boundary value problem is the Rayleigh-Ritz method which may be used when the cavity encloses

a large number of perturbing bodies. The Rayleigh-Ritz method is based on the variational integral, whose stationary values correspond to the true eigenvalues, when the true mode vectors are employed in the integrand.

The details of the perturbational and variational methods are developed in references (1), (2). Reference (5) is an exhaustive treatment of waveguides and cavities.

3.2.4    Electromagnetic Leakage into Receptor Circuits

In order for any interference to become effective, it must (in some way or other) reach the receptor circuits. Complete shielding of the receptor circuits is never possible because there always are connecting cables entering the equipment, and there may be discontinuities in the metal shielding. These factors provide coupling between the external and internal space of an equipment box.

The coupling takes the form of electromagnetic energy leakage through apertures (such as seams, long slits, connectors) and conduction interference via cables. The leakage through apertures has been extensively studied by the Rensselaer Polytechnic Institute in reference (8), and will not be considered in this report. If the field outside the enclosure is known, the leakage may be calculated from Bethe's theory of small apertures. The conduction interference via cables is considered in Section 4.0 of this report.

One coupling mechanism which has not been considered before is the magnetic induction via cables or wires entering the enclosure.

Cables or wires together with equipment enclosures and the ground plane may form a closed loop in which a voltage is induced by the external field. The current in the loop may be conducted inside the enclosure and may interfere with the electronic circuits directly or

establish a field by reradiation. A typical example is shown in Figure 3.2 where a loop is formed by two equipment boxes, cable shield, and the cavity wall.
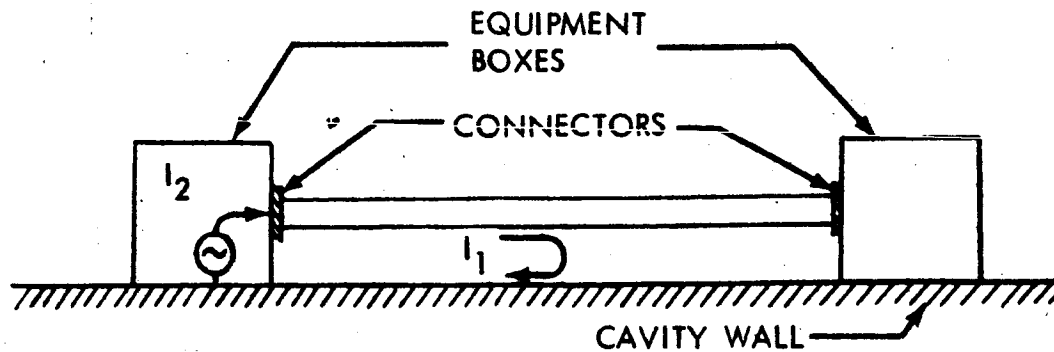


FIGURE 3.2. · LOOP FORMED BY COAXIAL
CABLE & EQUIPMENT BOXES

The voltage in the loop which produces the current, I, is calculated from

$$V = -j\omega\mu \iint \overline{H} \cdot \overline{dS}$$

where $\overline{H}$ is the magnetic field in the cavity enclosed by the loop, and $\overline{S}$ is the area enclosed by the loop. The current, $I_2$, in the inner conductor is created by the leakage of current $I_1$ through the shield. If a twisted pair instead of a coaxial cable is considered, the interference is carried by longitudinal currents in the twisted pair.

The energy leakage through walls is possible for low-impedance fields. In most instances, the strength of the external field surrounding the enclosure will not be known exactly unless numerical methods are used to solve the boundary-value problem. As a first approximation, it can be assumed that the enclosure is immersed in the undisturbed

field $\vec{H}_0$, $\vec{E}_0$. The surface current on the enclosure is then

$$\vec{J}_s = \vec{n} \times \vec{H}_0$$

where $\vec{n}$ points into the region of field. In case of apertures in the walls, the field $\vec{E}_0$, $\vec{H}_0$ is a first approximation to use for calculations of equivalent dipoles of an aperture.

## 3.3    LUMPED CIRCUIT MODELS FOR CLOSELY-SPACED BOXES

The cavity expressions of Section 3.2 have been shown to be valid for box coupling at all regions except for very closely-spaced boxes. Other methods have been investigated to develop analytic prediction models for the case of closely-spaced boxes. One of the more promising methods, involving lumped-circuit approximations, is described in this section.

Lumped circuits are usable when the dimensions of the system being considered are much less than a wavelength (about 1/16 of a wavelength or less).

At these frequencies, the radiation resistance is negligible, and the inductances are constant and equal to the low-frequency values.

In order to test the lumped-circuit model predictions, it was decided to use a set-up which was simpler than actual box-to-box coupling, but still approximating it. Instead of standard boxes, "degenerate" boxes or sheets were used as receptors and emitters, as shown in Figure 3.1.6. Here, the situation is much simpler, and it was deemed necessary to be thoroughly familiar with this situation in order to understand the more complicated box-to-box case. As a check to the degree of electromagnetic similarity between the two cases, a box as a receptor was connected to ground through a short

wire. A Stoddart current probe was used to monitor the current in the wire. The results, Paragraph 3.5.4, agreed closely to the sheets which were used as receptors throughout the rest of the experimental work.

In the lumped-circuit approach, it was assumed that the current on the emitter surface was sinusoidally varying in time, and that it was constant in direction and magnitude along the surface. The input current to the emitter is approximately twice the current on the outer surface of the emitter, since the current splits evenly and flows on both sides of the sheet.

### 3.3.1    Capacitive Coupling Between Closely-Spaced Boxes

Consider the situation illustrated in Figure 3.3. A box is radiating with the characteristics of an electrical current loop in a plane perpendicular to a ground plane. A box at a distance d from the emitter is the receptor of the electromagnetic radiation. To determine whether interference will occur or not, it is necessary to know the current induced on the receptor box surface. When the product of frequency, f, and distance, d, is much less than $\frac{1}{2\pi}$ times velocity of light, then the lumped-circuit model can be used to predict the current. The capacitive equivalent-circuit model is shown in Figure 3.4.
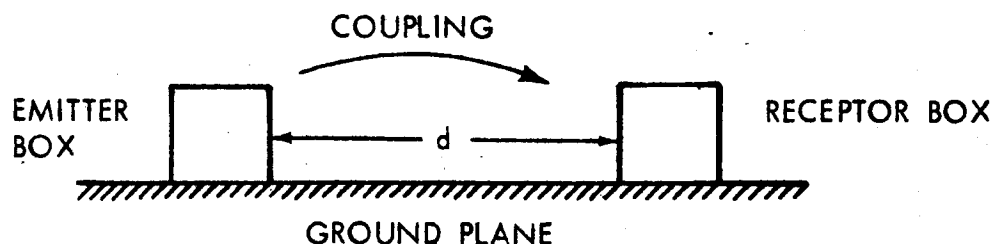
COUPLING

EMITTER BOX          d          RECEPTOR BOX
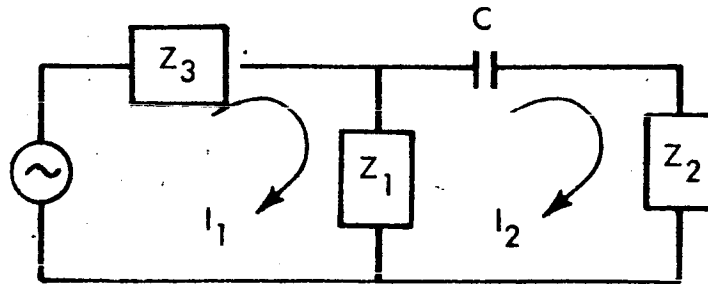
GROUND PLANE

FIGURE 3.3

FIGURE 3.4

The capacitance represents the mode of coupling between the receptor sheet (represented by $Z_2$) and the emitter sheet (represented by $Z_1$). The current $I_1$ is the current on the emitter surface, and $I_2$ is the current on the receptor surface. The voltage around the second loop of Figure 3.4 is

$$(I_2 - I_1) Z_1 + \left(Z_2 + \frac{1}{j \omega C}\right) I_2 = 0$$

by Kirchoff's voltage law. Thus, the magnitude of the surface current ratio is

$$\frac{I_1}{I_2} = \frac{Z_1 + Z_2 + \frac{1}{j \omega C}}{Z_1}$$

$Z_1$ and $Z_2$ are the impedances of the emitter and receptor sheets, respectively, and C is the capacitance between the two plates.

To obtain the worst case, the value of C was taken as that between two parallel plates. Thus,

$$C = \frac{\epsilon_0 A}{d},$$

where $\varepsilon_0$ is the dielectric constant of air, A is the area of the plates, and d is the plate separation.

The impedances of the two sheets are given by

$$Z_1 - Z_2 = (1 + j)\sqrt{\frac{\omega\mu}{2\sigma}}\ \frac{L}{W} \qquad\qquad (11)$$

where $\omega$ is the frequency in radian/sec., $\sigma$ the conductivity of the metal being used, $\mu$ the permeability, L the length of the conductor and W its width.

Typical values of $I_1/I_2$ were calculated and plotted in Figure 3.5. An electrically clean, controlled situation was set up in the laboratory to verify the results. Because of measurement problems, it was decided to simulate the actual situation in the laboratory, as shown in Figure 3.16 in Paragraph 3.5.2.1. The reason for this set-up is that no method for determining absolute values of surface current had been determined. Thus, the Stoddart No. 91550-1 current probe was used to determine the current flowing through a wire inter-connected between the plate and ground. The set-up is a first approximation to the actual one likely to occur in the Instrument Unit. Figure 3.17 (of 3.5.2.1) shows the method of measuring $I_2$. To check that the full current through $Z_2$ was being measured, the capacitance between the plate and ground was measured.

The capacitive reactance was determined to be about 100 $\Omega$ at 40 Mc and a distance of 1/4 inch away from the ground plane, while the internal impedance of the wire and plate is about $3 \times 10^{-2} \Omega$. Thus, it was shown that only negligible leakage occurred between the plate and the ground through the capacitance.
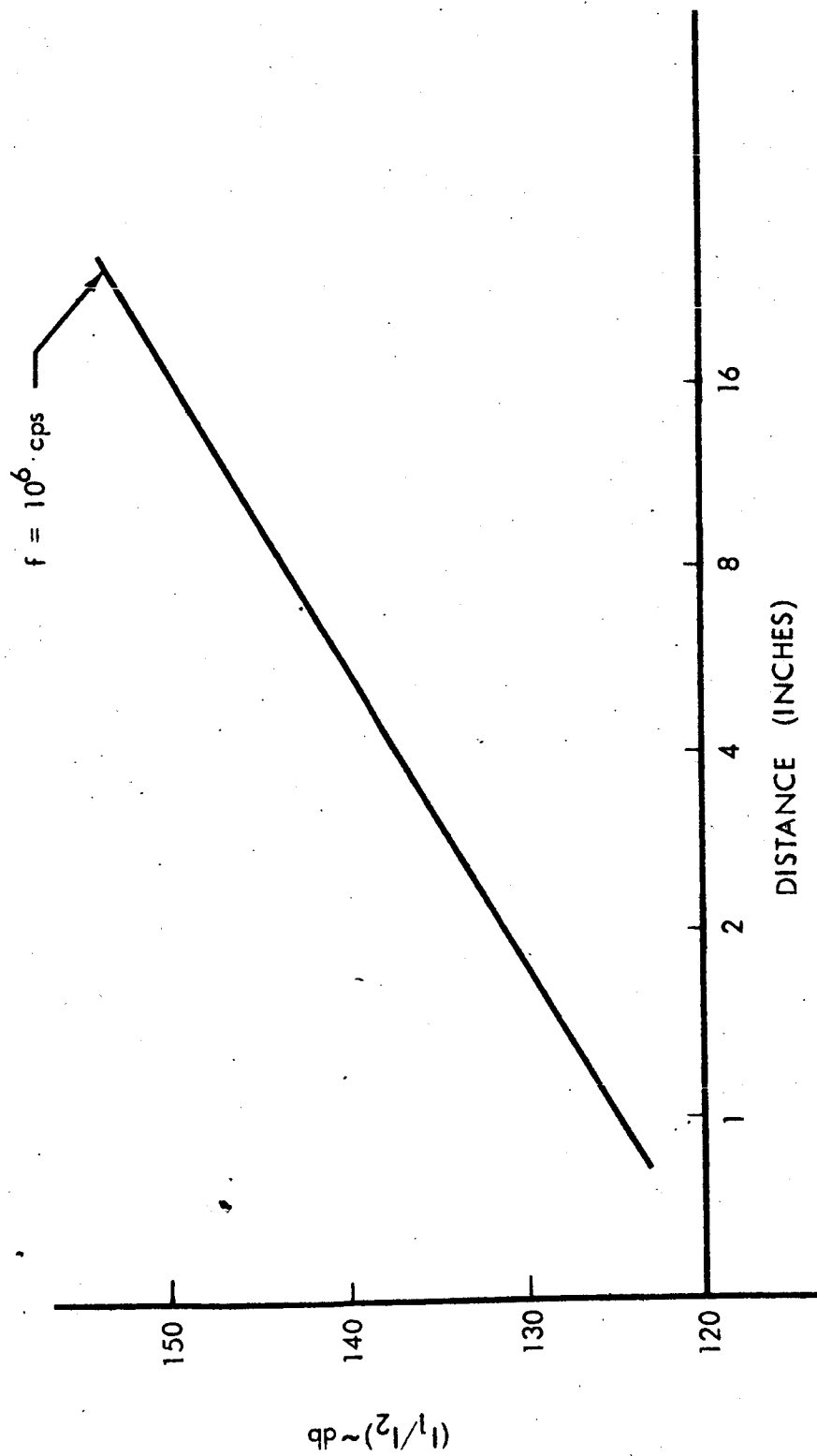
FIGURE 3.5   CAPACITIVE COUPLING BETWEEN
CLOSELY-SPACED BOXES

### 3.3.2    Coupling Between Boxes Interconnected by A Cable

The other lumped-circuit model which was studied is that of coupling between two boxes inter-connected by a cable as shown in Figure 3.6
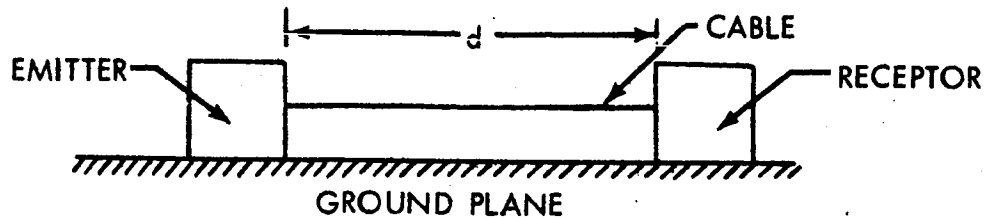


**FIGURE 3.6**

Originally, two possible mechanisms of coupling were considered. One was the conduction of a portion of the emitter-box surface current to the receptor box via the inter-connecting wire.  The second was the inductive coupling between the emitter magnetic dipole and the loop formed by the wire and ground plane.  It was determined experimentally (Paragraph 3.5.4) that resistive coupling through the cable was negligible compared to the inductive coupling.

Figure 3.7 shows the lumped equivalent-circuit model for the case of inductive coupling which holds when $2\pi \, fd \ll c$.  For this model, the surface current ratio is given by

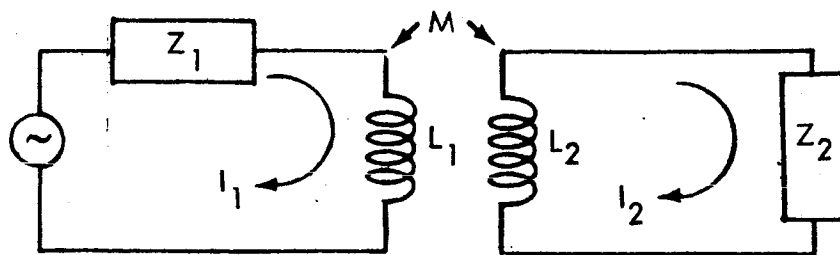$$\left| \frac{I_2}{I_1} \right| = \left| \frac{j\omega M}{Z_2 + j\omega L_2} \right|$$

FIGURE 3.7

Predictions have not been made using this model because of the com-
plexity of determining a value for M. However, two methods are
available adaptable to computer solution.

One method of determining M, the mutual inductance, is to take two
experimental readings of the ratio $I_2$ to $I_1$ at two different frequen-
cies. Then eliminating $L_2$, M can be solved for since $Z_2$ is known
from equation 11. However, since magnitudes are being taken, this
procedure is lengthy. The other method involving direct calculation
of M from its definition is lengthy also. The method essentially con-
sists of replacing portions of the current paths by straight-line
sections, and estimating the coupling from these. The mutual
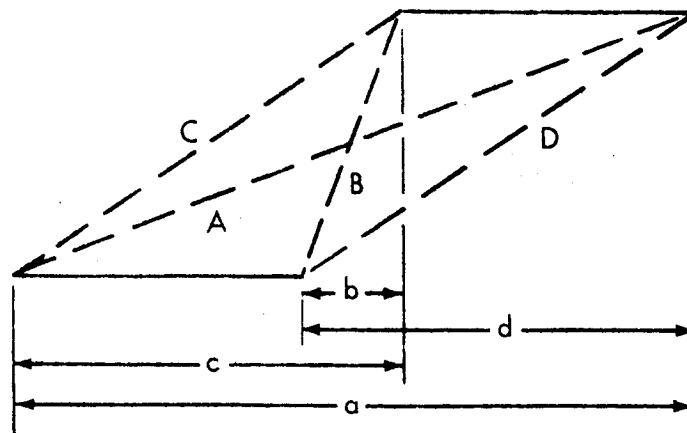inductance for one such parallel pair is given in Figure 3.8.



FIGURE 3.8

$$M = \frac{\mu}{4\pi} \ln \left\{ \frac{(A + a)^a (B + b)^b}{(C + c)^c (D + d)^d} \right\} + (C + D) - (A + B)$$

A computer subroutine could be developed for the solution of this equation, which will allow application of the prediction model to the variety of box geometries that will be encountered.

### 3.3.3 Results and Conclusions

The results for capacitive coupling as discussed in Paragraph 3.5.2.1 indicate that this type will not cause interference below 10 Mc. Typical values of surface-current ratios were calculated and checked by experiment (see Figure 3.5). The predicted values of -130 db were verified by the measurements at frequencies less than 2 Mc. At higher frequencies, there was a noticeable rise in the ratio. This was attributed to inductive coupling increase and to resonances of the shielded room, wherein the measurements were taken. The requirement that $2\pi$ f'd $< < c$ is not satisfied above frequencies of 10 Mc. Thus, this model no longer holds, and correlation with experiment was not expected. However, up to 10 Mc, the measured results were close to predicted values.

Further work needs to be done to extend the frequency range wherein coupling can be predicted.

### 3.4 PREDICTION BY NEAR-FIELD EXPRESSIONS

A preliminary investigation has been made into the feasibility of interference prediction in an enclosure using the free-space, near-field expressions for electric and magnetic dipoles. The purpose of considering this approach is to see if the resultant expressions are more readily adaptable to computer solution than the cavity expressions of Paragraph 3.2.1.

### 3.4.1   The Near Fields of An Emitter Loop in A Cavity

The analytic model selected to evaluate the applicability of the near-field expressions was an emitter loop acting as a magnetic dipole.

The complete theoretical expressions for the fields in spherical coordinates in the vicinity of such a source are given by the following equations

$$H_r = \frac{IS}{2\pi} e^{-ikr}\left(\frac{ik}{r^2} + \frac{1}{r^3}\right) \cos\theta$$

$$H_\theta = \frac{IS}{4\pi} e^{-ikr}\left(-\frac{k^2}{r} + \frac{ik}{r^2} + \frac{1}{r^3}\right) \sin\theta$$

$$E_\omega = \frac{\eta IS}{4\pi} e^{-ikr}\left(\frac{k^2}{r} - \frac{ik}{r^2}\right) \sin\theta$$

where     $k = 2\pi f \sqrt{\mu\epsilon}$

f = frequency

r = distance to the observation point

I = current

s = area enclosed by the loop

and the time dependence, $e^{j\omega t}$, is understood.  These field expressions are valid at distances r large compared to the loop radius $r_0$.

It will be recognized that these equations are identical to the field equations for an infinitesimal oscillating magnetic dipole except that the magnetic dipole moment m has been replaced by IS, the product of the loop current and loop area.

The three spacial components of the field are mutually perpendicular at any point with two being magnetic ($H_r$ and $H_\theta$) and one electric ($E_\phi$). It will be noted that there are terms in these field equations that vary as

$$\frac{1}{r^3}, \quad \frac{1}{r^2}, \quad \text{and} \quad \frac{1}{r}.$$

These describe the quasi static, the induction, and the radiation components, respectively. The quasi static term in $1/r^3$ does not involve K, and so is independent of frequency. The induction field term is proportional to frequency being an induced field, and the radiation term is proportional to the square of frequency.

In the vicinity of the emitter and with $K < 1/r$, the fields are magnetic with the $1/r^3$ term dominant. The magnetic field components are then given by

$$H_r = \frac{IS}{2\pi} \frac{\cos\theta}{r^3}$$

$$H_\theta = \frac{IS}{4\pi} \frac{\sin\theta}{r^3}$$

Calculations were made to determine the accuracy of these expressions in predicting the fields of an emitter loop in a cavity. The configuration examined is shown in Figure 3.9, where it is seen that only the $H_\theta$ component will couple to the pickup loop. Thus, calculations of $H_\theta$ were compared to the corresponding measured values as shown in Figure 3.33, Paragraph 3.5.8.

The presence of a finite ground plane is considered by bounding the problem with theoretical curves for both no ground plane and an infinite ground plane.
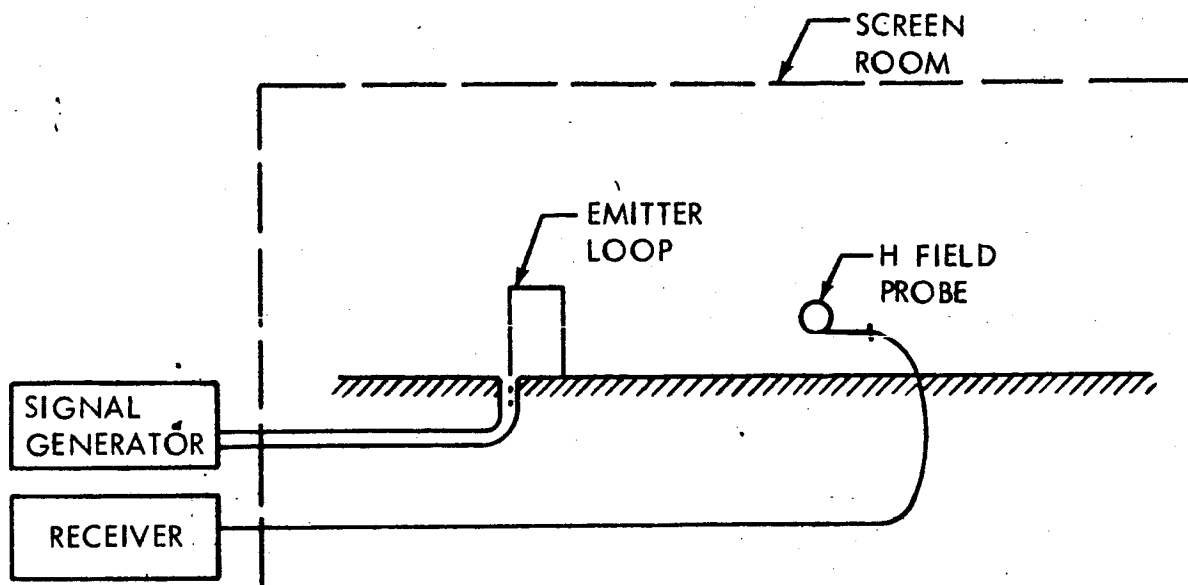
FIGURE 3.9

The results show that the prediction is good at distances greater than one emitter dimension away.

Because of the preliminary nature of the study in this area, no definite conclusions on the applicability of near-field expressions for prediction should be made. It is recognized that this approach would at best give rough approximations to the fields, and will require further evaluation in follow-on work.

## 3.5    EXPERIMENTAL INVESTIGATION

Experimental investigation of various modes of coupling between equipment boxes in a closed structure has been directed primarily toward obtaining measurements to confirm theoretical results. However, other experiments have been intended to obtain coupling data under conditions that cannot be readily analyzed theoretically. The ultimate purpose of all experimental measurements is to determine realistic input data for a digital computer interference-prediction program.

### 3.5.1    Determination of Leakage Sources per MIL-I-6181D

When considering electromagnetic coupling between two circuits, it is desirable to know the path or paths of maximum energy transfer. MIL-I-6181D has a standardized method of obtaining radiation levels. It was decided to use this method to determine the primary radiation sources of a typical "black box". This method leaves much to be desired, as far as obtaining an absolute level of radiation, but it is often satisfactory for making relative comparisons. As such, the data obtained should be evaluated as a comparison of different radiation mechanisms.

### 3.5.1.1    Test Configurations

The MIL-I-6181D test set-up is shown in Figures 3.10 and 3.11. The "black box" used in this test was a 12" x 10" x 9" brass box with a removable lid. A coaxial cable from a signal generator external to the screen room was connected to the box and terminated in a rod antenna inside the box. This excitation was designed to give maximum current flowing over the seam between the lid and the box. The radiation level was measured with the lid on loose and on tight. These measurements were made with no wires connected to the box.

A three-wire cable was connected between the box and the line-stabilization networks (LSN's) simulating a power cable. The power line was two feet in length and mounted two inches above the table top. Each of the ungrounded leads was terminated in a line-stabilization network (LSN). The third wire was grounded to the box at several different positions. It was noted that a considerable variation in radiation level occurred as a function of the grounding position.

In addition, shielded pairs and coaxial lines were connected to simulate signal leads.
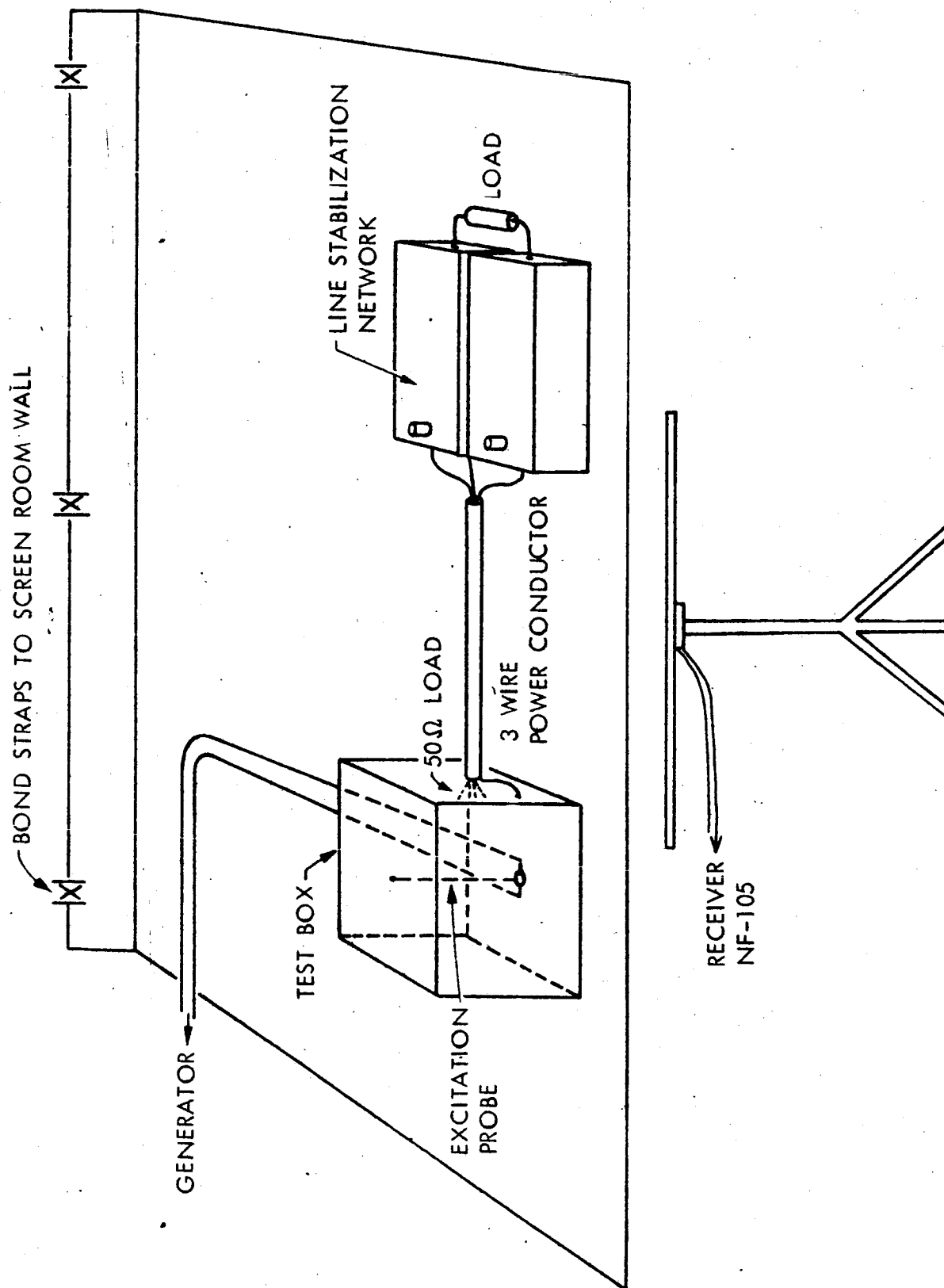
FIGURE 3.10
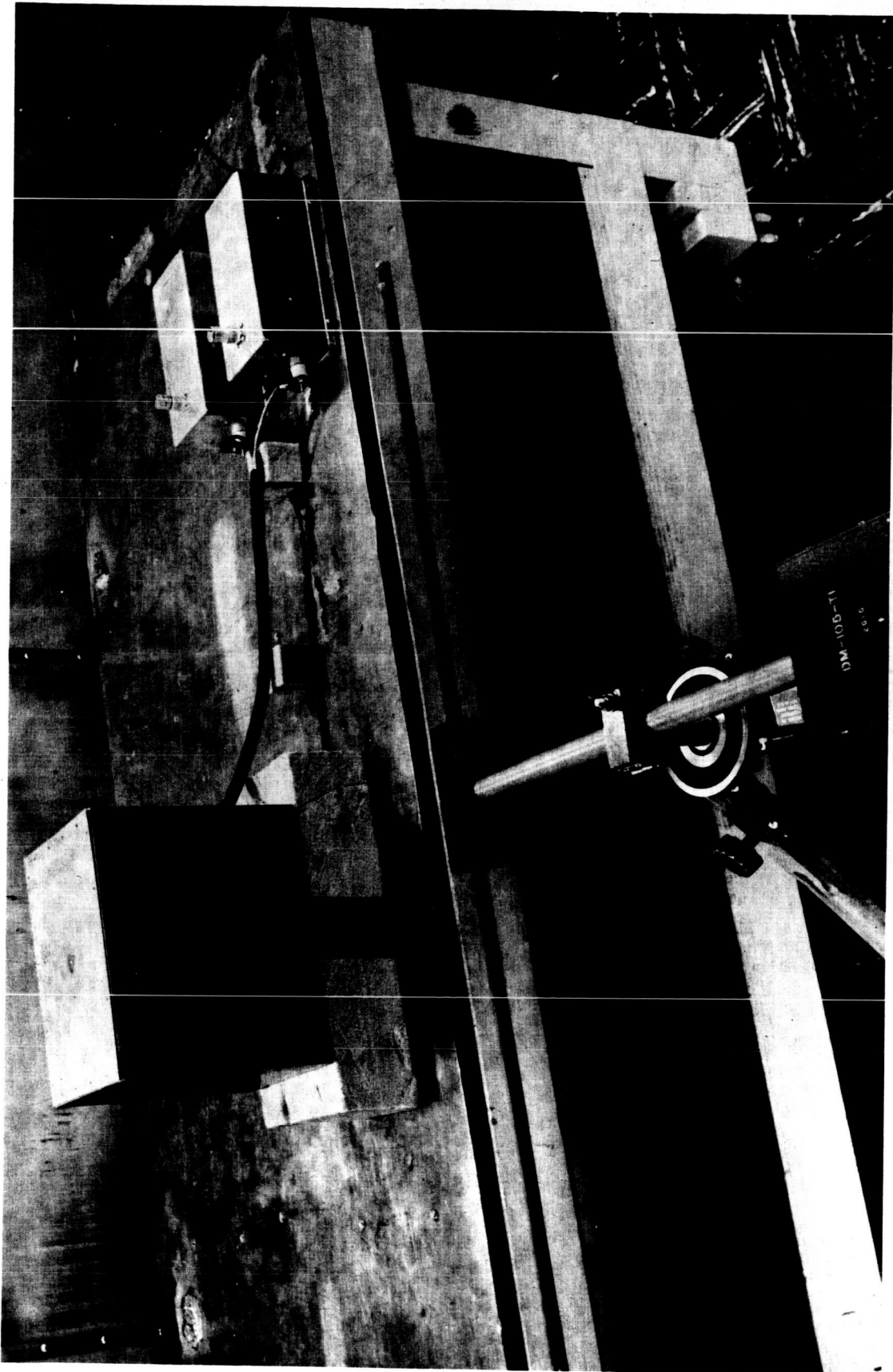TEST SET UP PER MIL-I-6181D FOR LEAKY BOX AND CABLE

FIGURE 3.11
MIL-I-6181D TEST SETUP

### 3.5.1.2    Results

A low-signal level could be detected with the lid on tight.   There was
an increased level with the screws loosened (see Figure 3.12).   How-
ever, when a three-wire power cord was added (terminated in 50 ohms
inside the box and terminated in a LSN outside), the radiated level
increased substantially (Figure 3.12).   An increase also occurred
with a shielded twisted pair terminated in a 50-ohm load in the box.
It was determined that the tightness of the lid did not affect the
measured level from the wires.   This indicates that the lower signal
levels do not measurably add to the radiation levels of higher energy
leakage sources.   It was found that when the third wire ground and
shields were grounded internal to the box, rather than outside, the
radiated level was measurably higher (see Figures 3.13, 3.14, and
3.15).

The results of this type of test indicate that the radiation level
measured under these conditions is primarily from wires connecting
to the box.

### 3.5.2    Simulation of Emitter Box as A Magnetic Dipole

A possible source of radio interference is the current flow on the out-
side surface of metallic equipment boxes.   A laboratory simulation of
an emitter box acting as a magnetic dipole was made.   The emitter
was simulated by a sheet of brass, 12 inches square and 0.032 inches
thick, with the bottom edge firmly attached to the copper-covered
table.   The sheet was fed from a signal source outside of the screen
room through a well-grounded coaxial cable.   The outer conductor of
the coax was grounded to the table at the level of the copper cover
while the inner conductor continued to the top of the brass sheet.   To
improve the uniformity of the current sheet, the center conductor was
split to attach at the three points along the upper edge of the brass
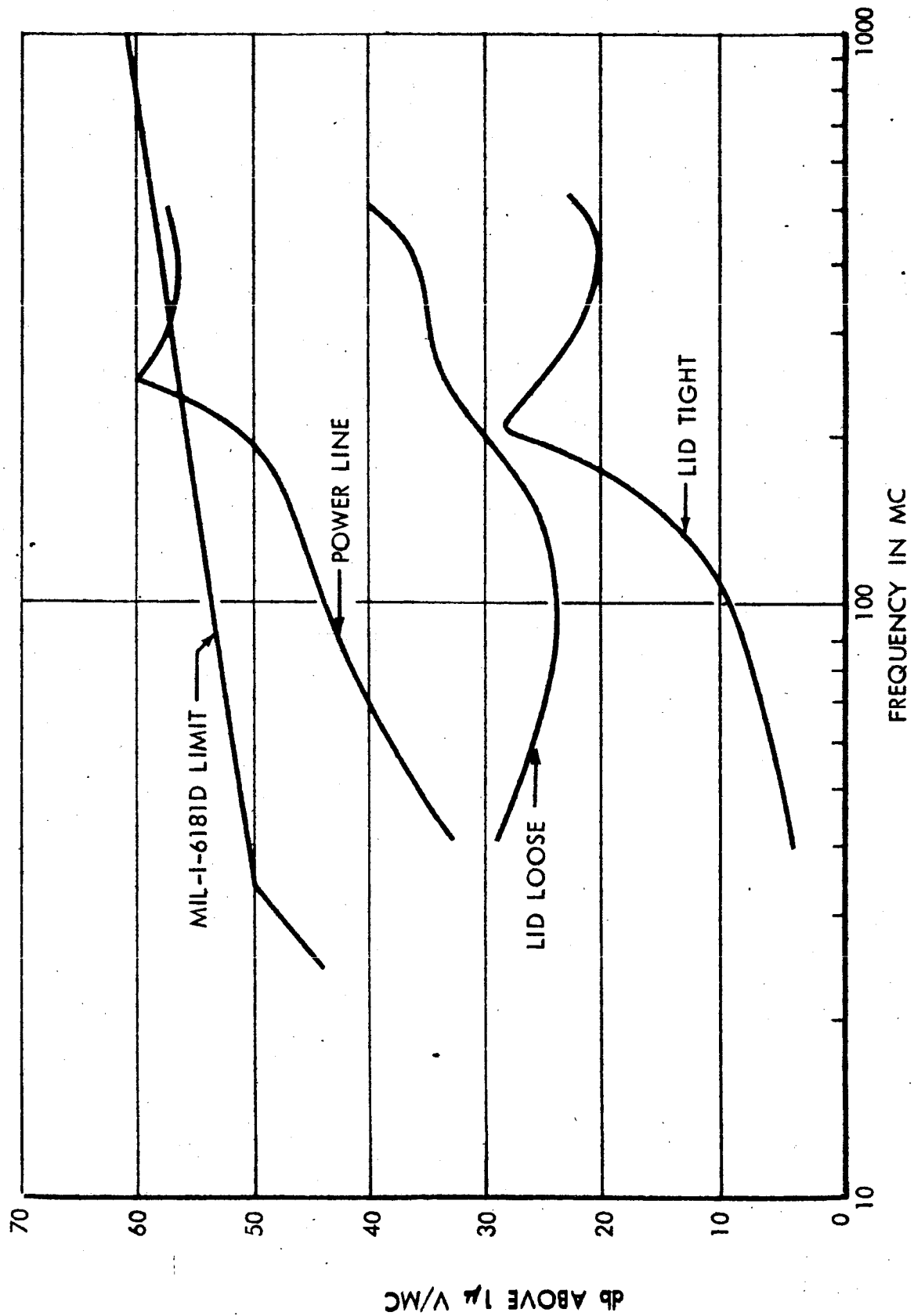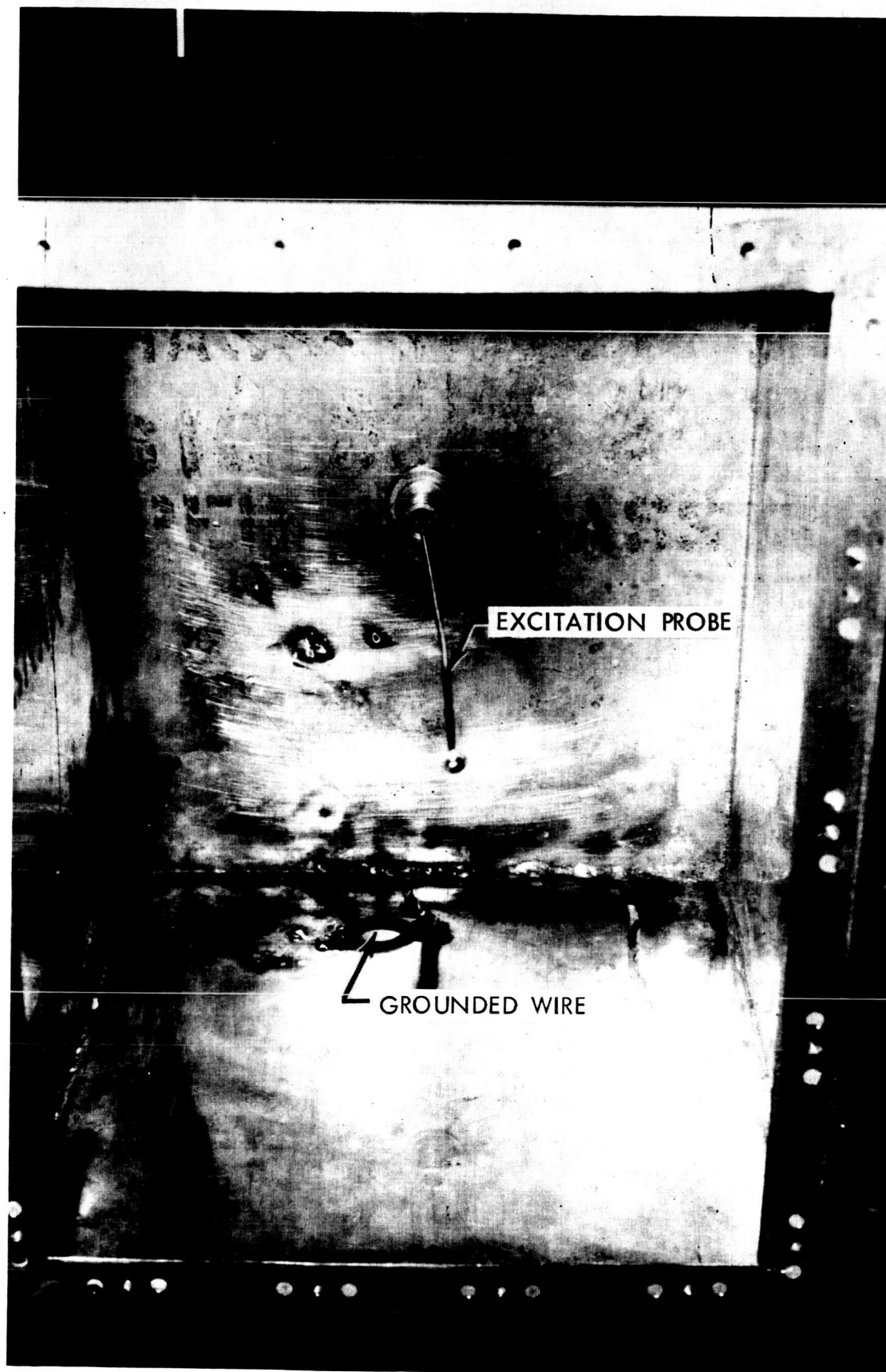sheet.   Input current was monitored by a Stoddart Model 91550-1

FIGURE 3.12

FIGURE 3.13
WIRE GROUNDED INTERNALLY

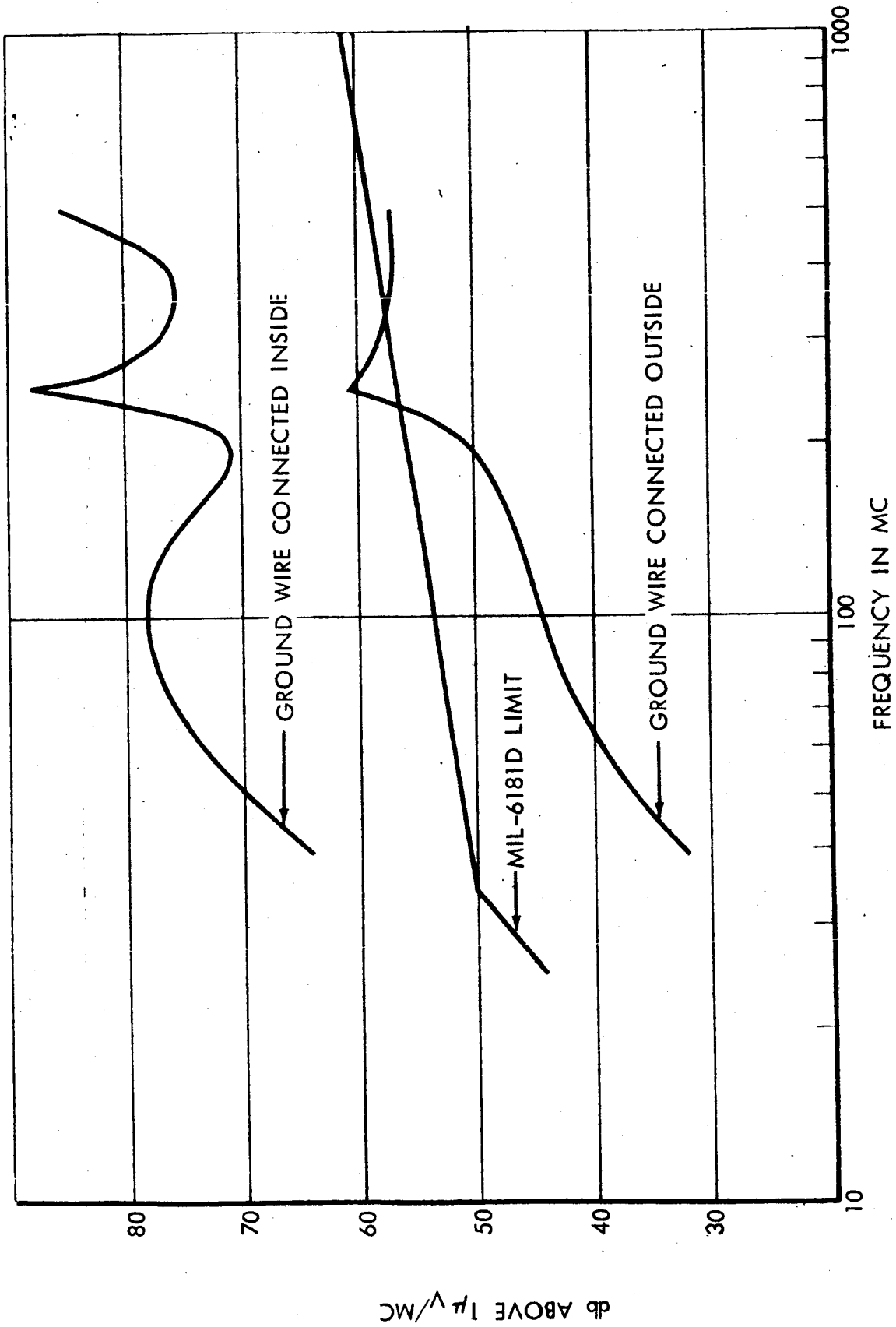FIGURE 3.14
WIRE GROUNDED EXTERNALLY

FIGURE 3.15

dB ABOVE 1μV/MC

FREQUENCY IN MC

GROUND WIRE CONNECTED INSIDE

MIL-6181D LIMIT

GROUND WIRE CONNECTED OUTSIDE

current probe surrounding the extended center conductor of the coax. With the emitter box acting as a magnetic dipole, measurements were made of the induced currents in various types of receptor configurations. Some of the more significant laboratory simulations and results are discussed below.

### 3.5.2.1 Receptor Box as Electric Dipole

The coupling between the simulated emitter box and a receptor as an electric dipole was determined as shown in Figure 3.16 and 3.17. A twelve-inch square sheet parallel to the emitter sheet was tested as a receptor.

The current from the bottom of the receptor sheet to the table top was monitored. This simulated a box with connection to the common ground plane only through the box mounting. At frequencies lower than approximately two megacycles, the coupling was less than the sensitivity of the test equipment (100 db). At higher frequencies, the readings increased as a function of frequency at a rate of approximately 15 db per octave, and were independent of the spacing between emitter and receptor; thus, these readings were actually due to stray fields created by high-frequency effects such as resonant effects and standing waves on various structural elements of the test set-up. The only positive result of the test is that the induced current in the receptor is at least 100 db below the input current to the emitter at frequencies below two megacycles. This result agrees with the lumped-circuit prediction models which are discussed in Paragraph 3.3. Figure 3.18 illustrates the test data. Although a smooth point-by-point plot of the data is meaningless because of the resonances, the general trend of the data is obvious.

BOND STRAP TO SCREEN
ROOM WALL

TO NF-105 RECEIVER

COPPER COVERED
TABLE

CURRENT PROBE
$(I_2)$

CURRENT PROBE
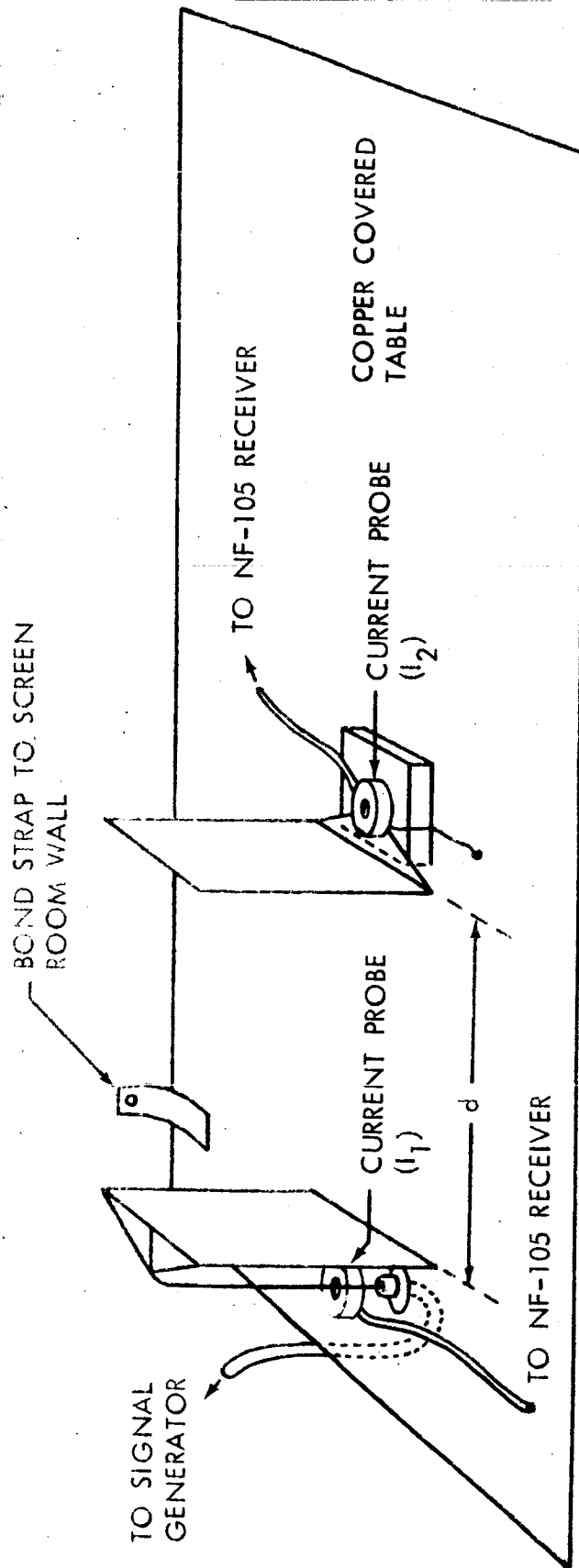$(I_1)$

d

TO NF-105 RECEIVER

TO SIGNAL
GENERATOR

FIGURE 3.16
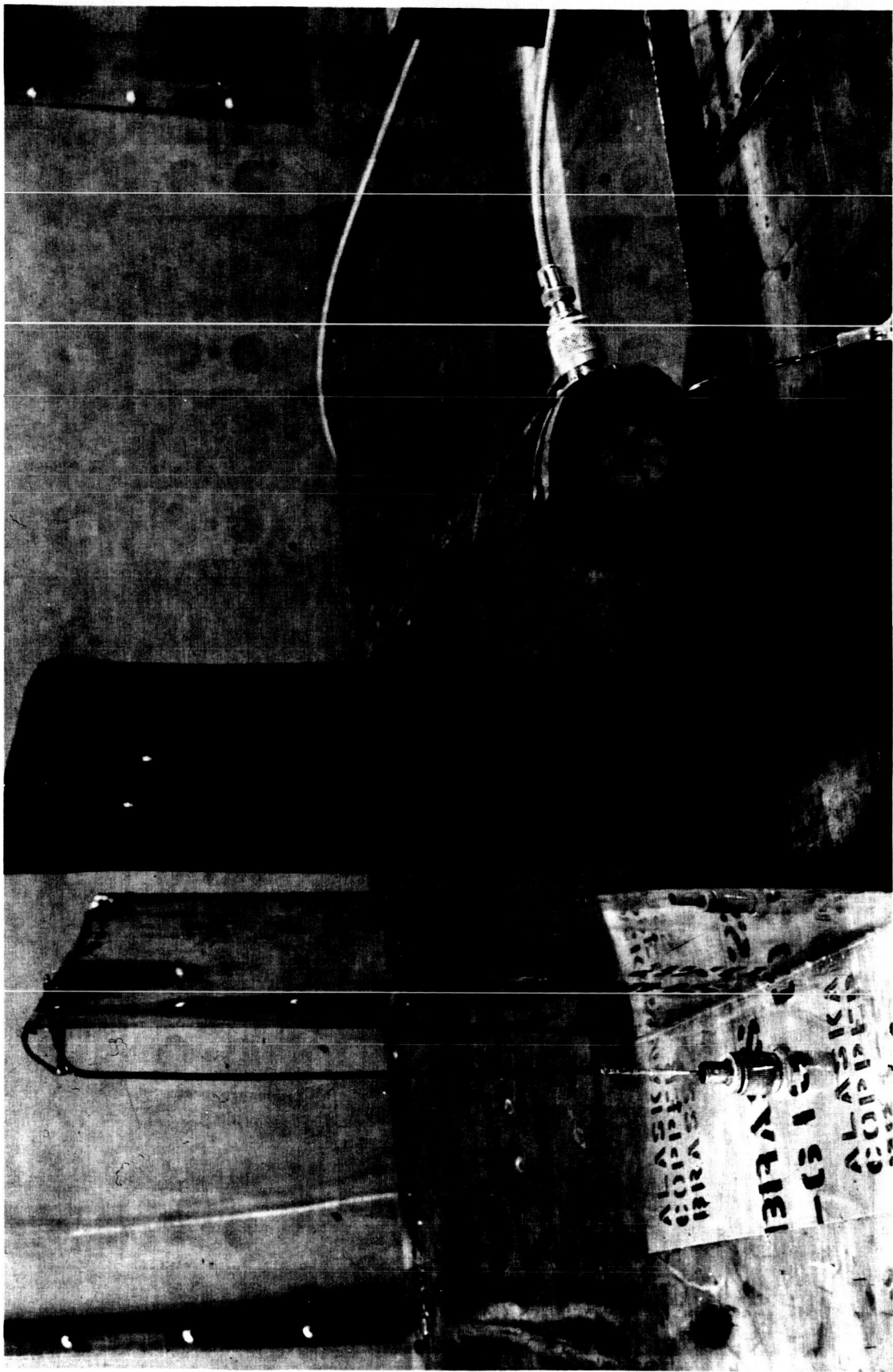TEST SET-UP SIMULATING BOX-TO-BOX COUPLING

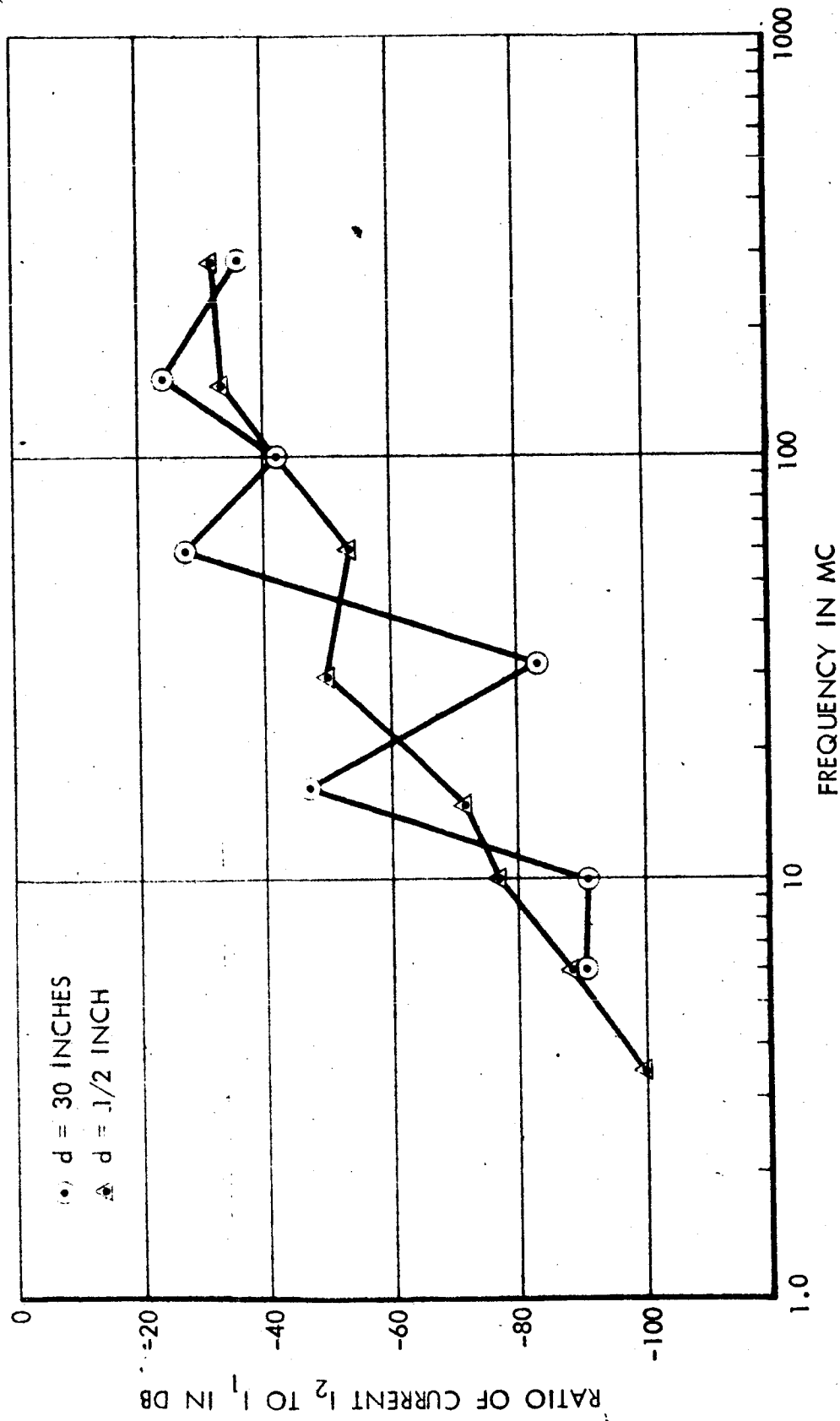FIGURE 3.17
BOX-BOX COUPLING SIMULATION

FIGURE 3.18
BOX-BOX COUPLING, RECEPTOR AS ELECTRIC DIPOLE

### 3.5.2.2   Receptor Box as A Magnetic Dipole

Tests were also conducted under conditions differing from that discussed above by having the wire that carried the induced current connected to the top of the receptor sheet instead of the bottom. This simulated a box grounded only through internal wiring. The copper sheet-to-ground plane capacity completed a receptor loop and was expected to increase magnetic coupling. A comparison of data under this condition (Figure 3.19) with Figure 3.18 shows the same general increase of coupling with frequency of 15 db per octave. However, the current level was higher, as expected, and a decrease in coupled current as a function of emitter-receptor spacing was evident.

When the bottom and top edges of the receptor sheet were both grounded (the rest of the set-up remaining as described above), the induced current varied with frequency and spacing as shown by Figure 3.20. In this case, the receptor forms a complete conductive loop, so that considerable magnetic coupling should occur. Below ten megacycles, the induced current was a slow function of frequency, increasing only about 0.75 db per octave, and a nearly linear function of spacing, about 1.25 db per inch. However, above ten megacycles, the same 15-db-per-octave increase in current with frequency and the spacing independence observed under the two conditions described above was again observed.

It is probable that the curves of Figure 3.18 and 3.19 at lower frequencies would resemble those of Figure 11, if the measuring equipment had sufficient sensitivity.

### 3.5.3   Comparison of Current Sheets to Actual Boxes

The box-to-box coupling experiments were further extended to the use of actual boxes for receptors. The purpose of the test was to show correspondence between the measurements using simulated and actual
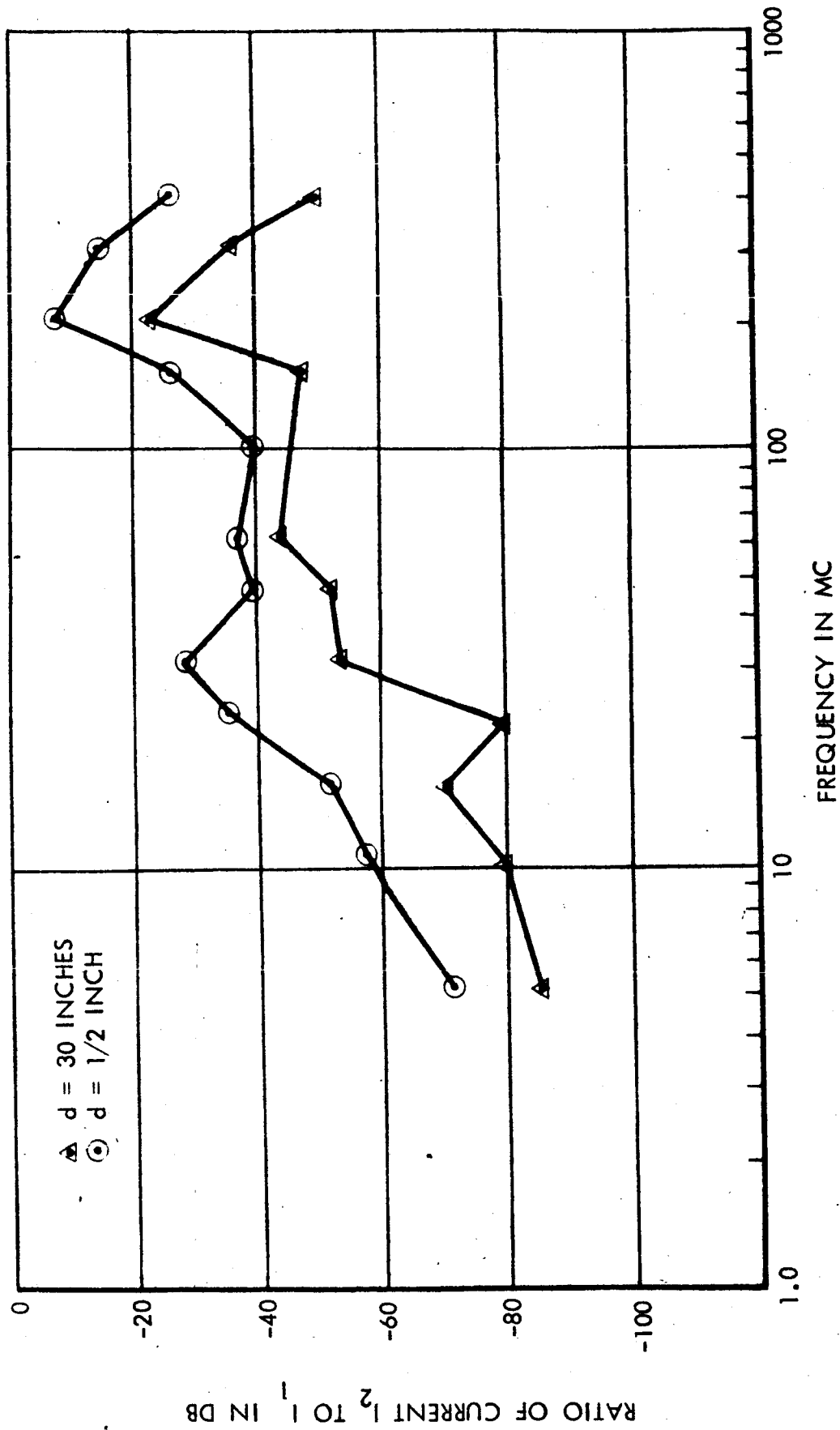
FREQUENCY IN MC

FIGURE 3.19

BOX-BOX COUPLING, RECEPTOR AS MAGNETIC DIPOLE
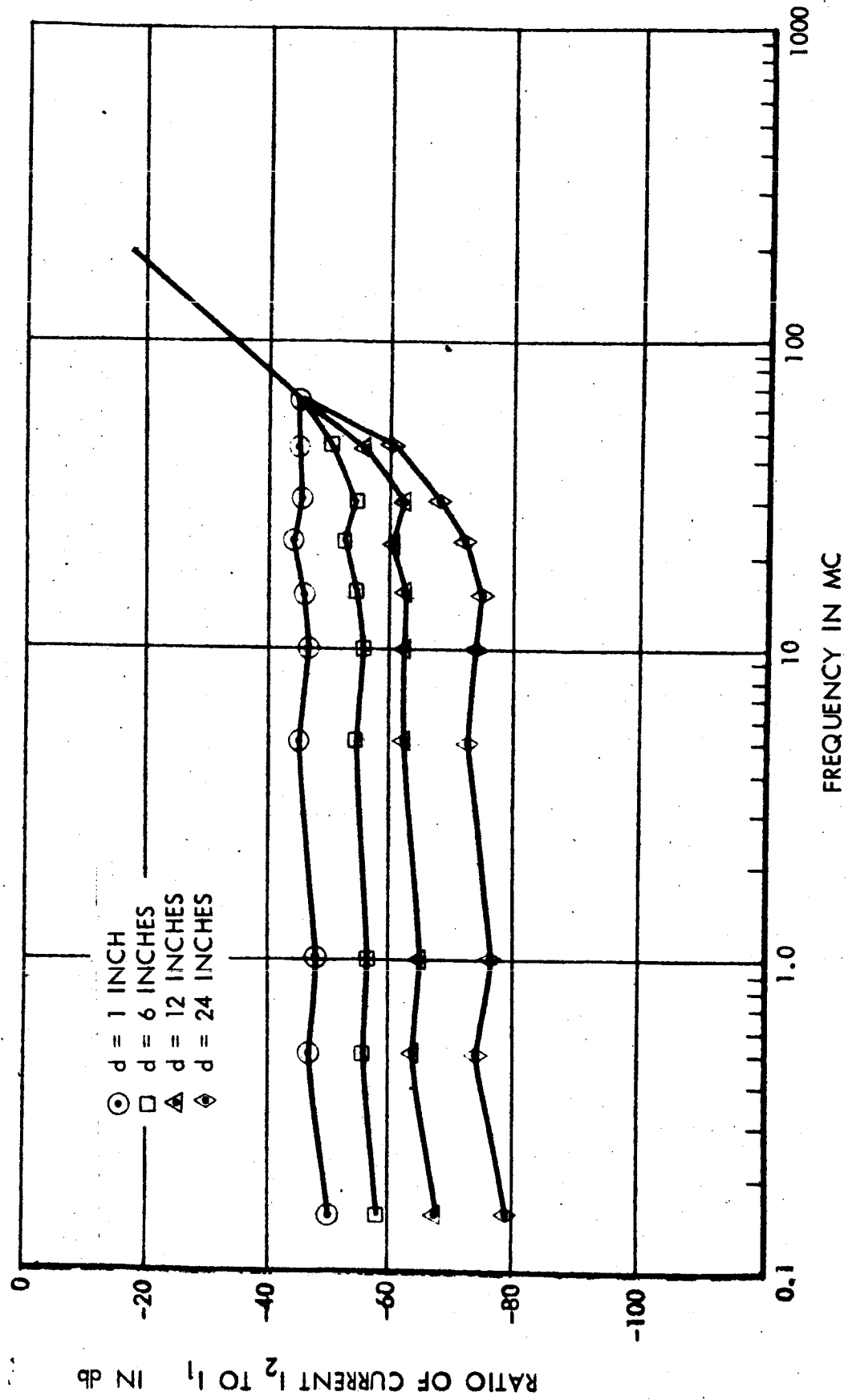
FIGURE 3.20
BOX-BOX COUPLING, RECEPTOR AS GROUNDED MAGNETIC DIPOLE

boxes. Measurements were made using boxes of the following configurations:

a)  An aluminum box with all twelve edges carefully welded with continuous bead (Figure 3.21),

b)  A brass box having the lid tightly secured by machine screws spaced two inches apart (Figure 3.22).

The induced current was measured by a current probe, placed around a wire running from a corner nearest the table top ground plane but most remote to the emitter sheet. Measured data, shown as Figure 3.23, has the same general characteristic as the data for the thin-sheet simulation (Figure 3.18). The induced current at frequencies below six megacycles was again too low to be measured.

3.5.4    Box-to-Box Coupling with Interconnecting Cable

Experimental tests were conducted to find the predominate mode of two proposed modes of box-box coupling, in the presence of an interconnecting cable. The first proposed mode was based on the conduction of emitter currents to the receptor through the interconnecting cable. The second mode postulated that the receptor currents were a result of inductive coupling of emitter magnetic field (transformer action) into the loop formed by the cable and ground plane.

To evaluate the first mode, a wire was stretched between the emitter current sheet and a similar receptor sheet mounted on the copper table cover nine feet away, as shown by Figures 3.24 and 3.25. This test set-up simulated two boxes having a direct interconnecting cable. The test results, Figure 3.26, show that the current along the wire is independent of frequency up to about 20 megacycles. The current along the wire was also independent of the distance from the emitter, below 20 megacycles.
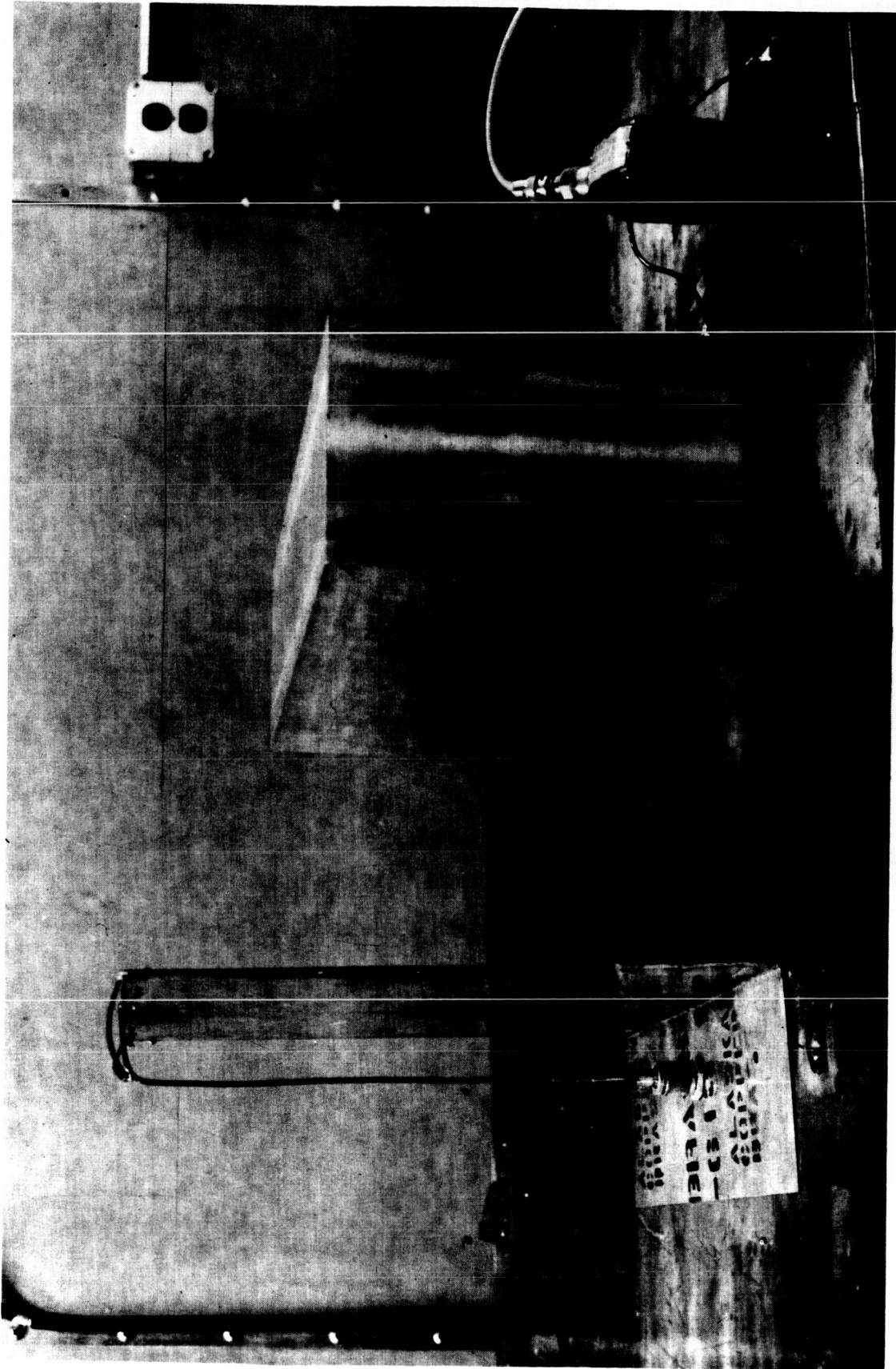
FIGURE 3.21
COUPLING SHEET TO ALUMINUM BOX
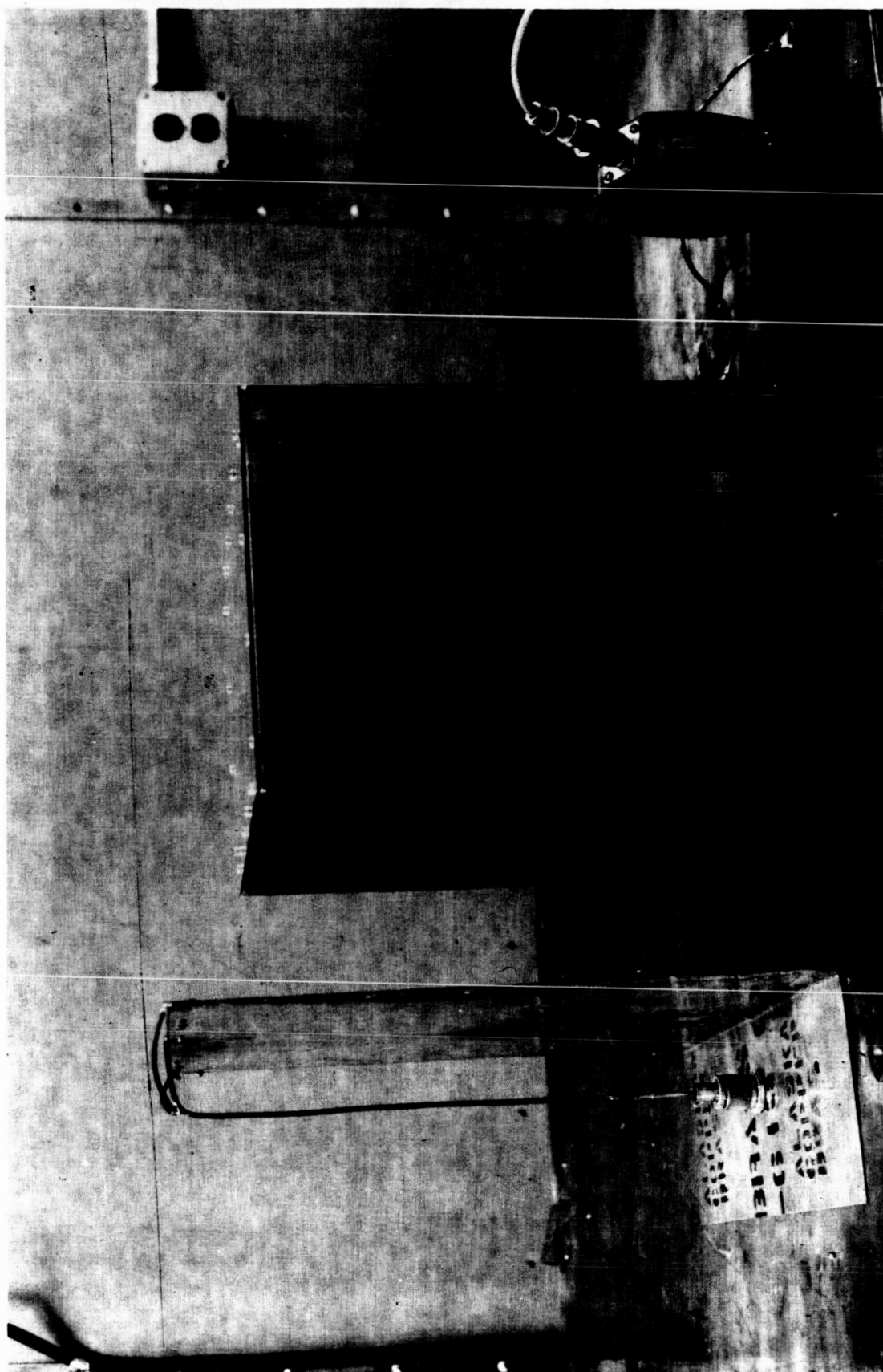
FIGURE 3.22
COUPLING SHEET TO BRASS BOX

ALUMINUM BOX
BRASS BOX

FREQUENCY IN MC
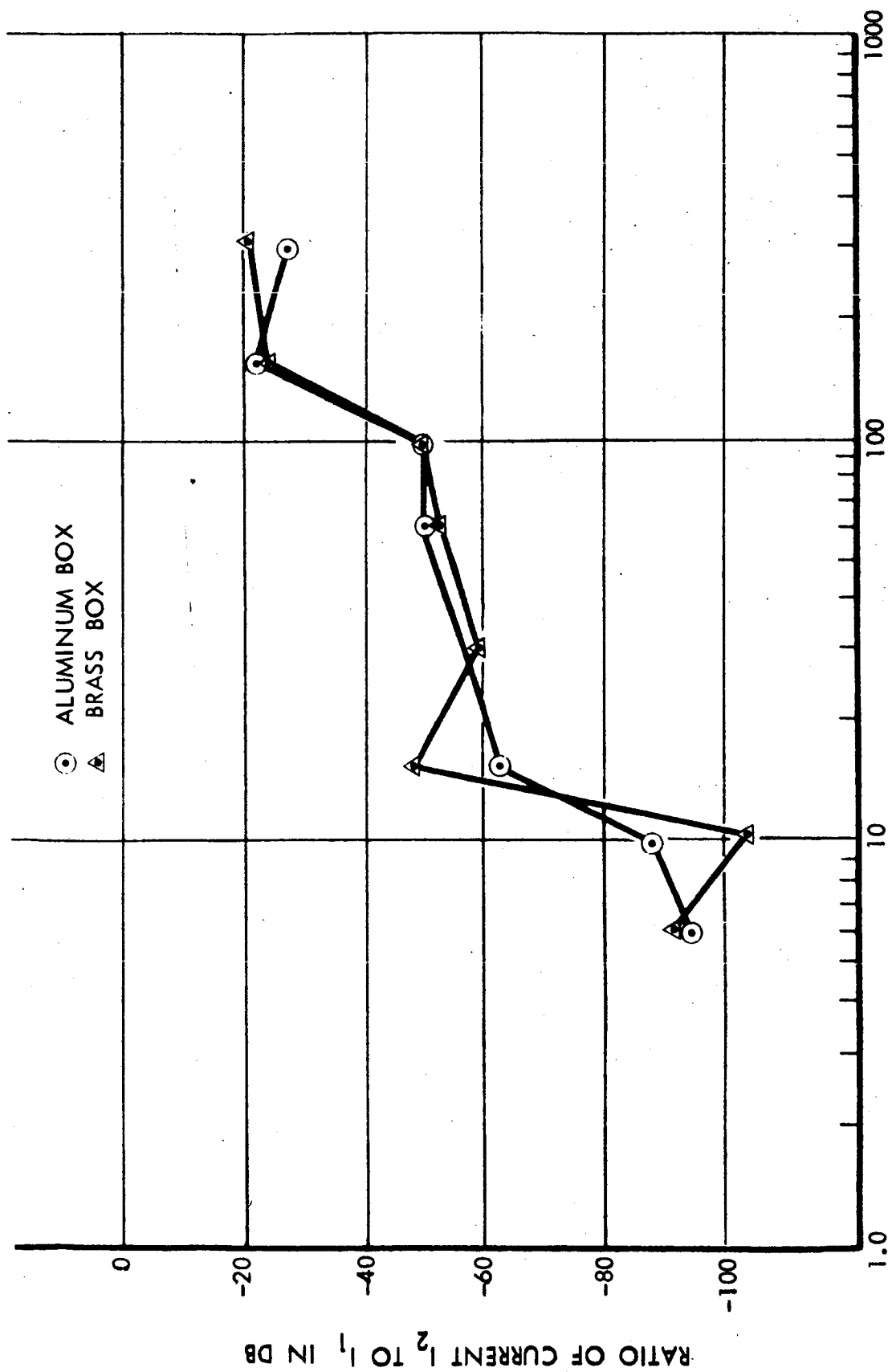
FIGURE 3.23
BOX-BOX COUPLING, ACTUAL BOXES AS RECEPTORS

RATIO OF CURRENT $I_2$ TO $I_1$ IN DB
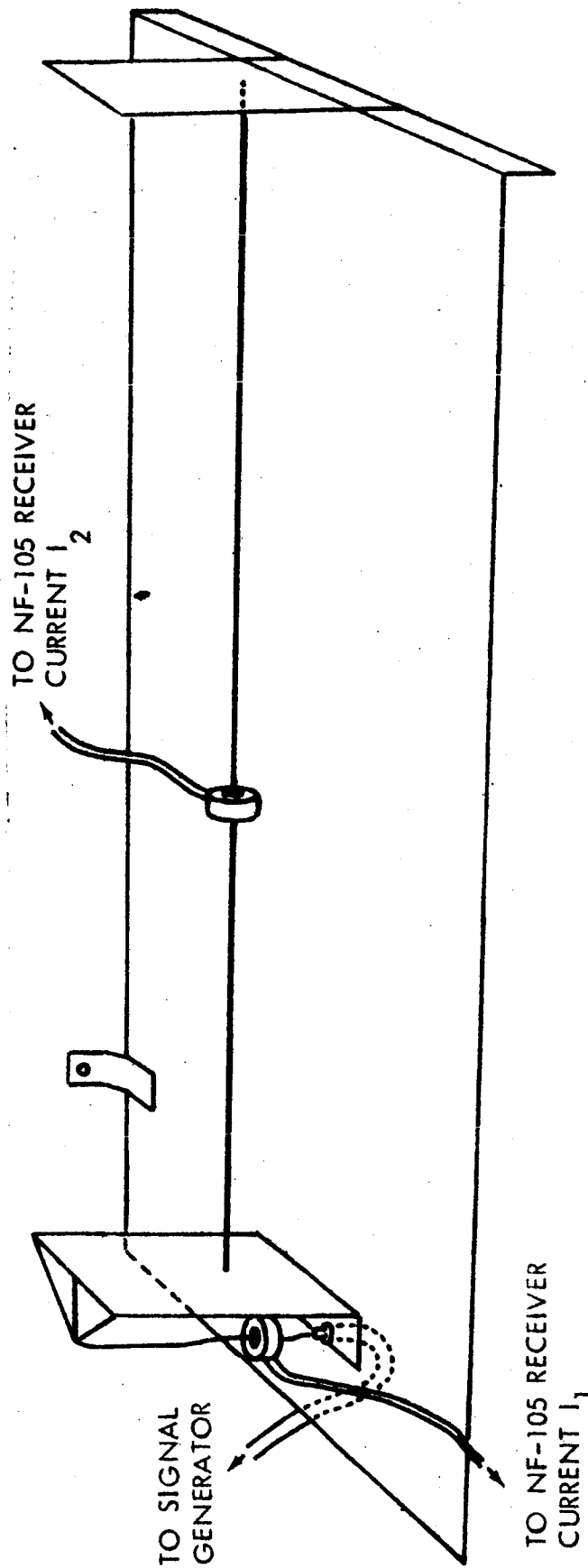
FIGURE 3.24
BOX-TO-BOX COUPLING WITH INTERCONNECTING CABLE

TO NF-105 RECEIVER
CURRENT $I_2$

TO SIGNAL
GENERATOR

TO NF-105 RECEIVER
CURRENT $I_1$

FIGURE 3.25
BOX COUPLING WITH INTERCONNECTING WIRE

FREQUENCY IN MC
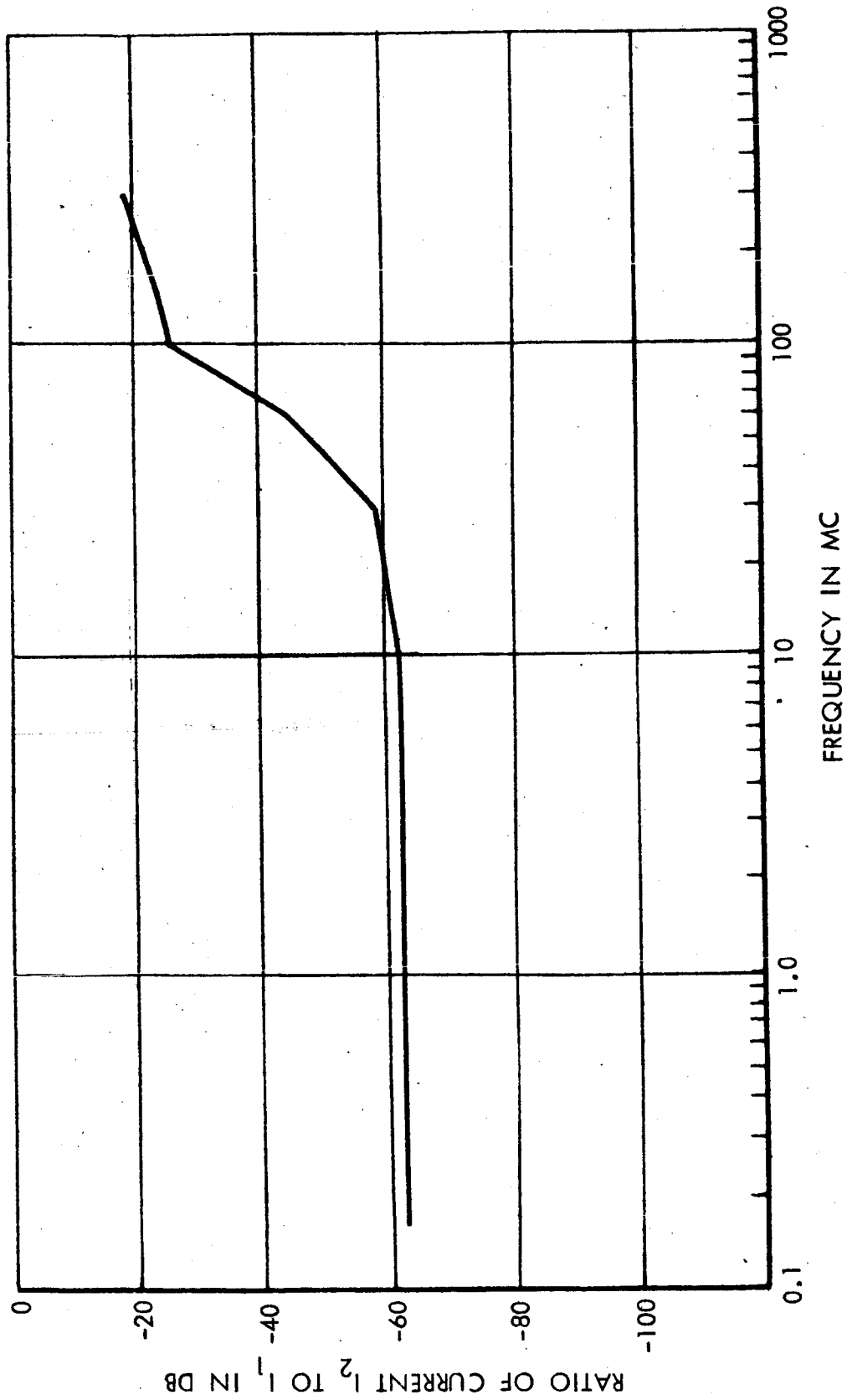
FIGURE 3.26

CURRENT INDUCED ON WIRE RUNNING BETWEEN TWO PLATES
(CONNECTED TO EMITTER PLATE)

RATIO OF CURRENT $I_2$ TO $I_1$ IN DB

FREQUENCY IN MC

FIGURE 3.27

CURRENT INDUCED ON WIRE RUNNING BETWEEN TWO PLATES
(NOT CONNECTED TO EMITTER PLATE)

RATIO OF CURRENT I₂ TO I₁ IN DB

The wire was removed from direct contact with the emitter for a test of the second mode of coupling. This time, the wire ran perpendicular to the ground plane, one-quarter inch from the emitter face for four inches; after a right-angle bend, it continued on to the receptor plate as for the first mode test.
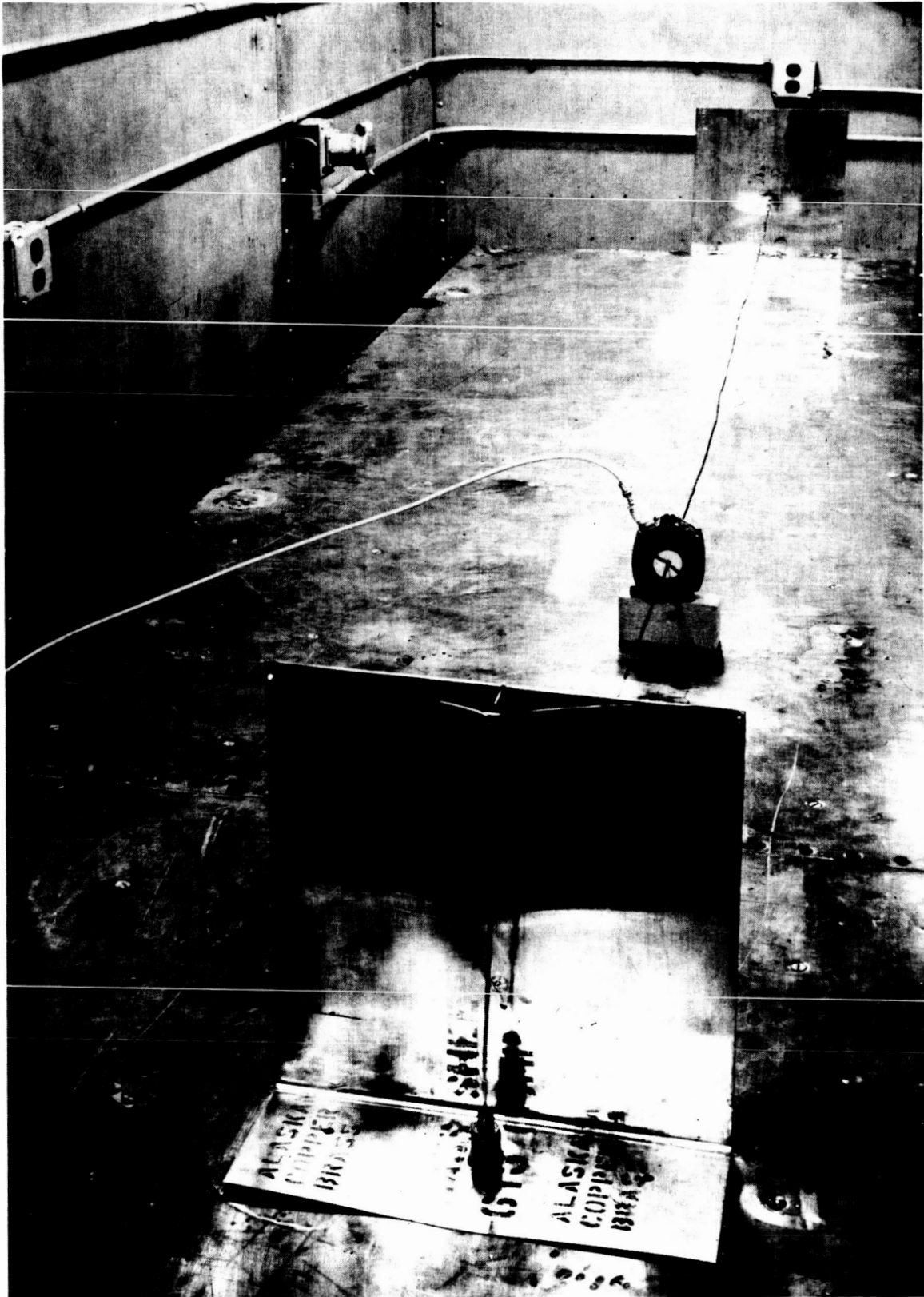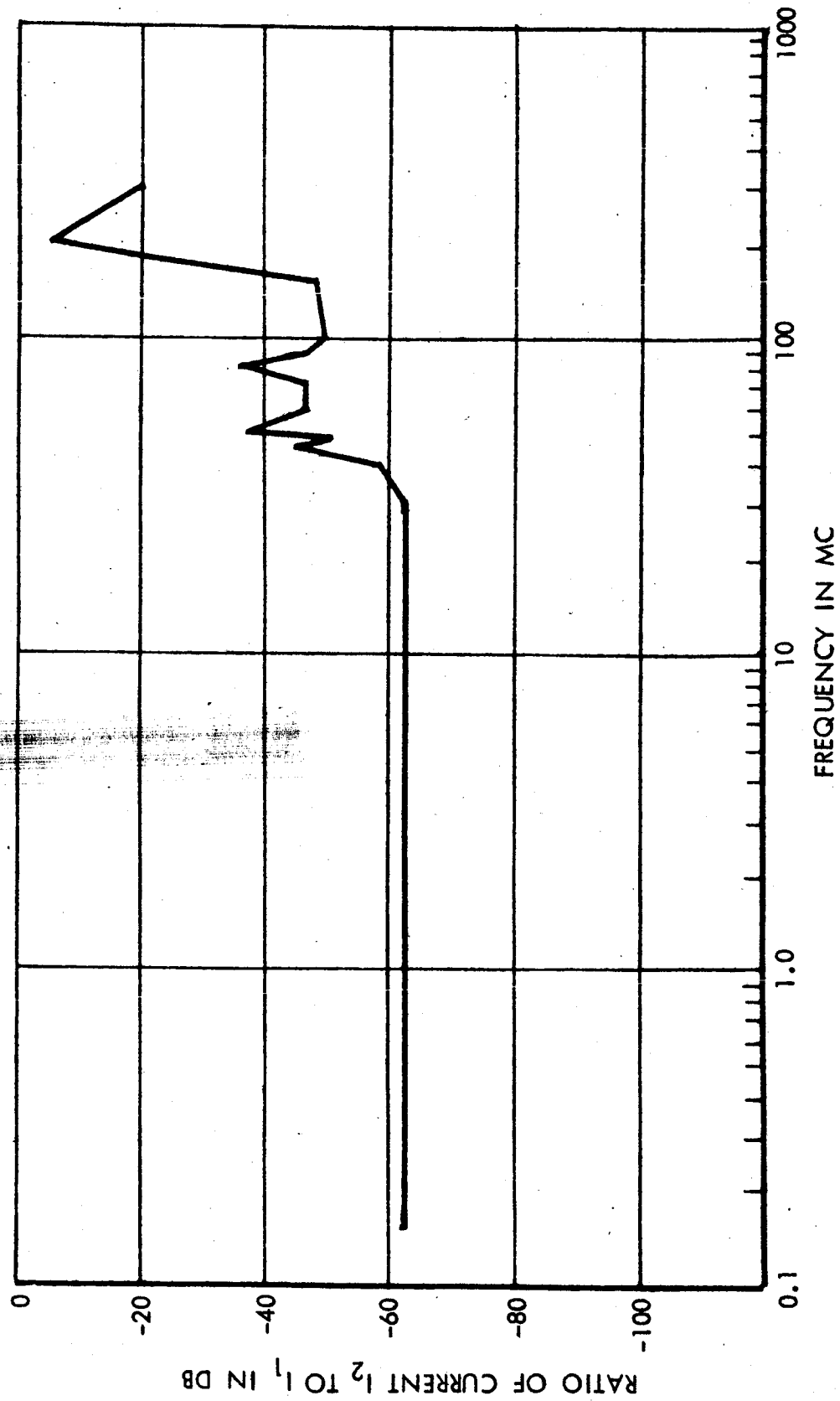
As shown on Figures 3.26 and 3.27, there is very little difference between the current along the wire when it is connected to the emitter or when it is not connected. Thus, it has been established that the magnetic coupling is predominant.

### 3.5.5    Box-to-Grounded Cable Coupling Measurements

An experiment was conducted to determine the current induced in a wire or cable shield as a function of the distance between grounding points. The test configuration and results are shown by Figure 3.28. The current measured on the horizontal wire near the emitter plate actually decreased at a slow rate as a function of wire length. The decrease was probably because the principle mode of coupling was between the current in the emitter face and the portion of the wire which was parallel to the current. Adding length to the wire loop increased the impedance of the current path without materially increasing the induced voltage.

### 3.5.6    Determination of Receptor-to-Ground Plane Capacitance

The capacity between the copper-covered table and a perpendicular conducting plate of the size used for box-to-box coupling simulation was measured as a function of height above the ground plane. The result of this measurement and a similar measurement, using a box instead of a thin plate, is shown by Figure 3.29.

RATIO OF CURRENT $I_2$ TO $I_1$ IN DB

$\ell$ IN INCHES

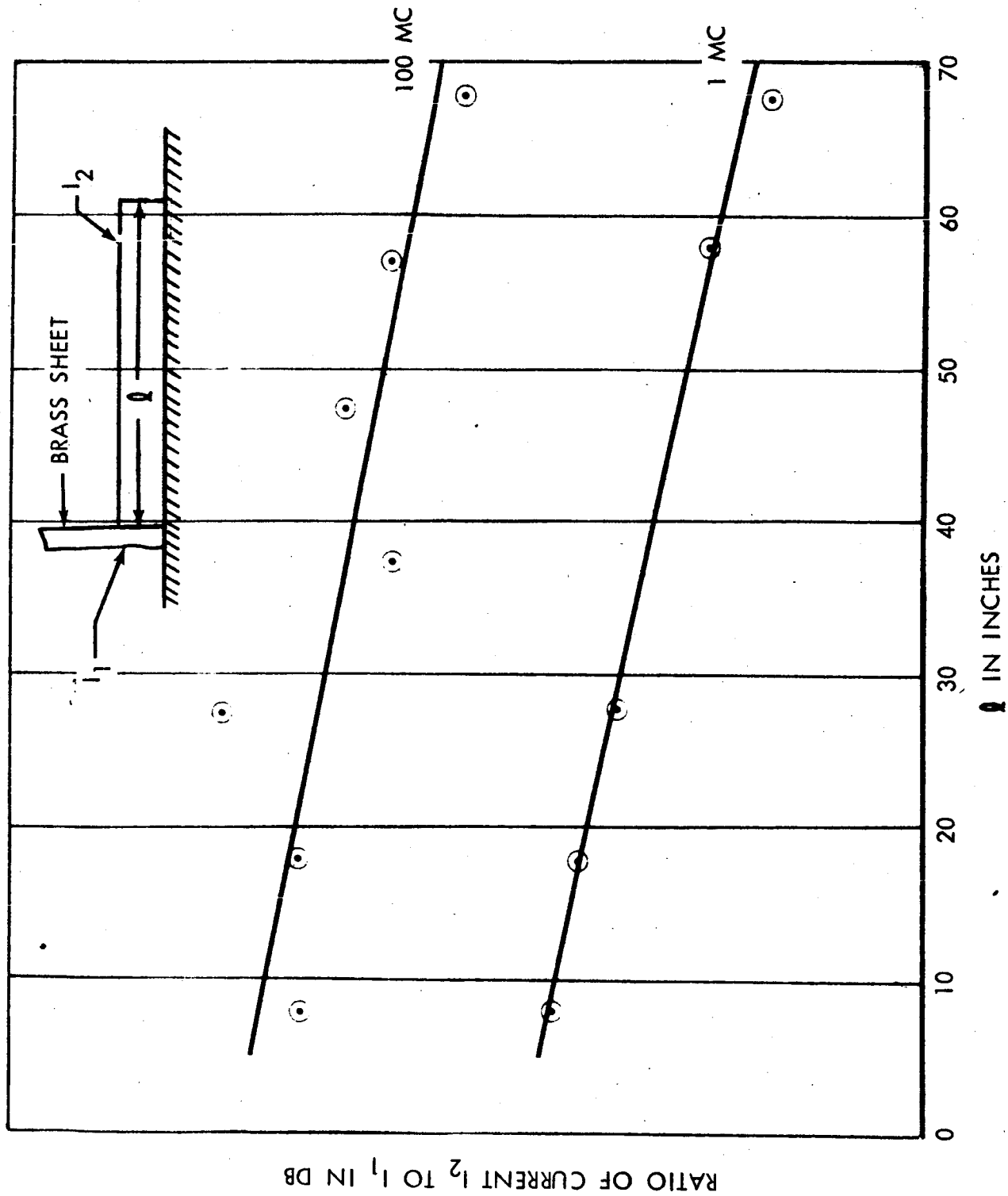FIGURE 3.28

INDUCED CURRENT AS A FUNCTION OF LENGTH TO GROUND
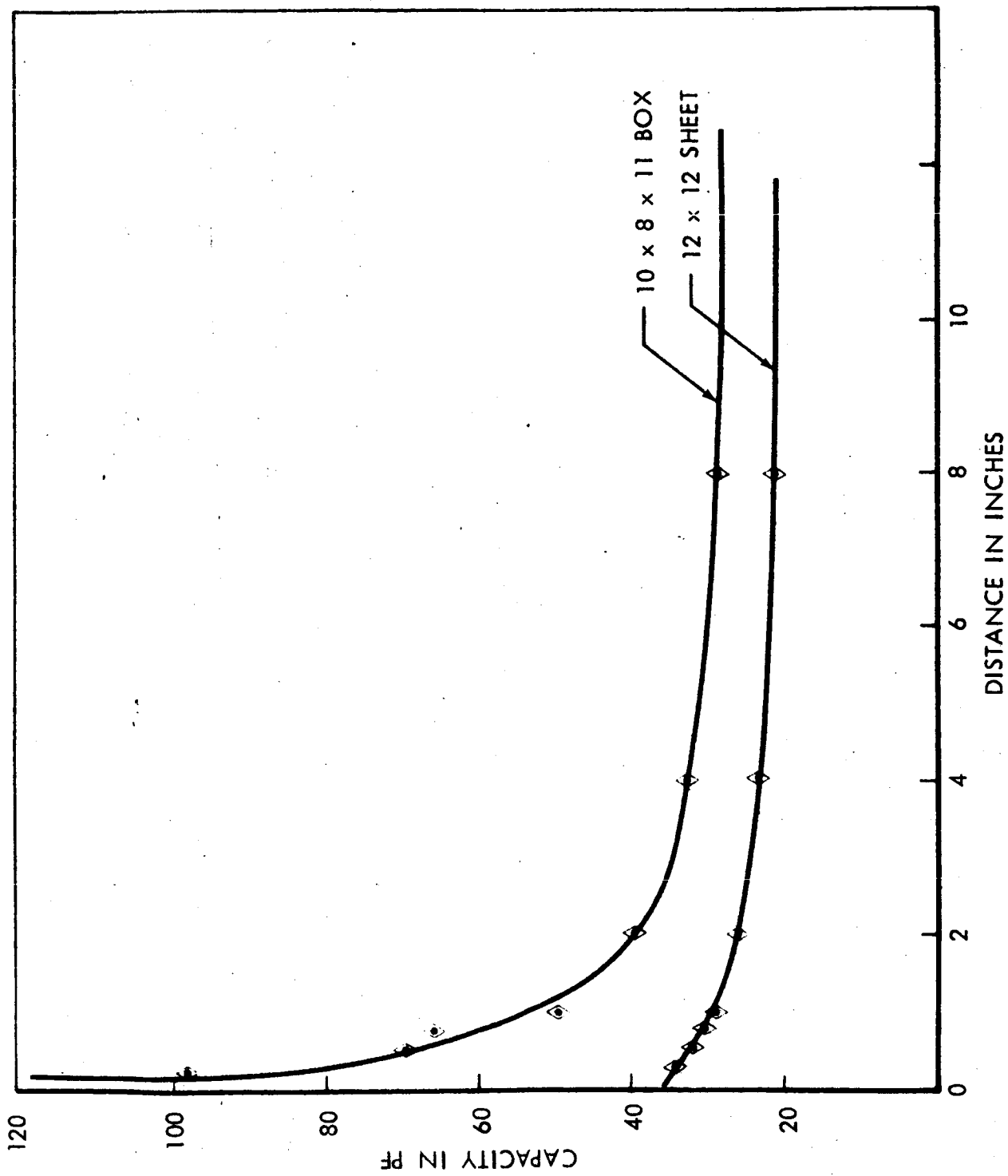
CAPACITY BETWEEN EQUIPMENT BOX & GROUND PLANE
AS A FUNCTION OF SEPARATION

FIGURE 3.29

DISTANCE IN INCHES

10 x 8 x 11 BOX

12 x 12 SHEET

CAPACITY IN PF

### 3.5.7    Magnetic Field Probe Calibration

In order to measure the magnetic field intensity produced by an emitter, it was necessary to calibrate a Boeing-built probe. The probe, sketched as a part of Figure 3.30, is an electrostatic shielded loop. The center conductor forms a loop, with its end short circuited to the outer conductor. The outer conductor is split so that electric field coupling is neutralized.

Calibration, as shown in Figure 3.31, was accomplished by measuring the voltage induced in the small probe when placed in the center of the large probe (uniform field region) as a function of the input current in the large circular loop. The magnetic field intensity in the center of the large loop was calculated from the measured current and loop diameter, and plotted as a function of probe output voltage. The results are shown by the family of calibration curves, Figure 3.30.

### 3.5.8    Magnetic Field Produced by A Rectangular Loop

The magnetic field intensity produced by a rectangular loop of wire was measured with the calibrated probe of Paragraph 3.3.7 as a function of distance from the loop (see Figure 3.32). The loop had the same configuration as the current sheet emitter of Paragraph 3.5.2, except that the thin plate was replaced with wire. Figure 3.33 shows the measured magnetic field intensity along with the theoretical field intensity, assuming an infinite ground plane and assuming no ground plane. Since the actual measured data for frequencies higher than 200 kilocycles were essentially independent of frequency, a single average curve was used to represent the field from 200 Kc to 30 Mc.

FIGURE 3.30

MAGNETIC PROBE CALIBRATION
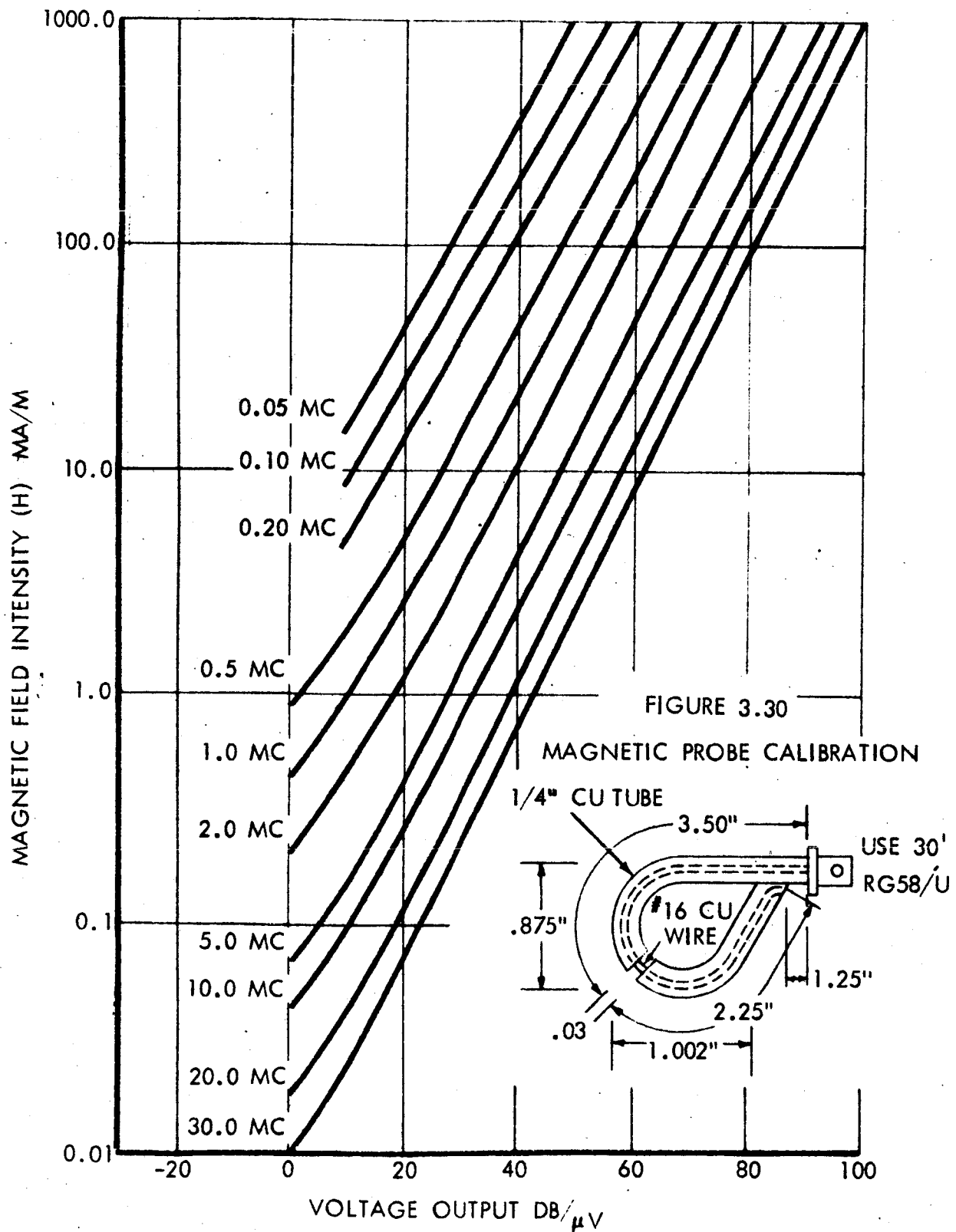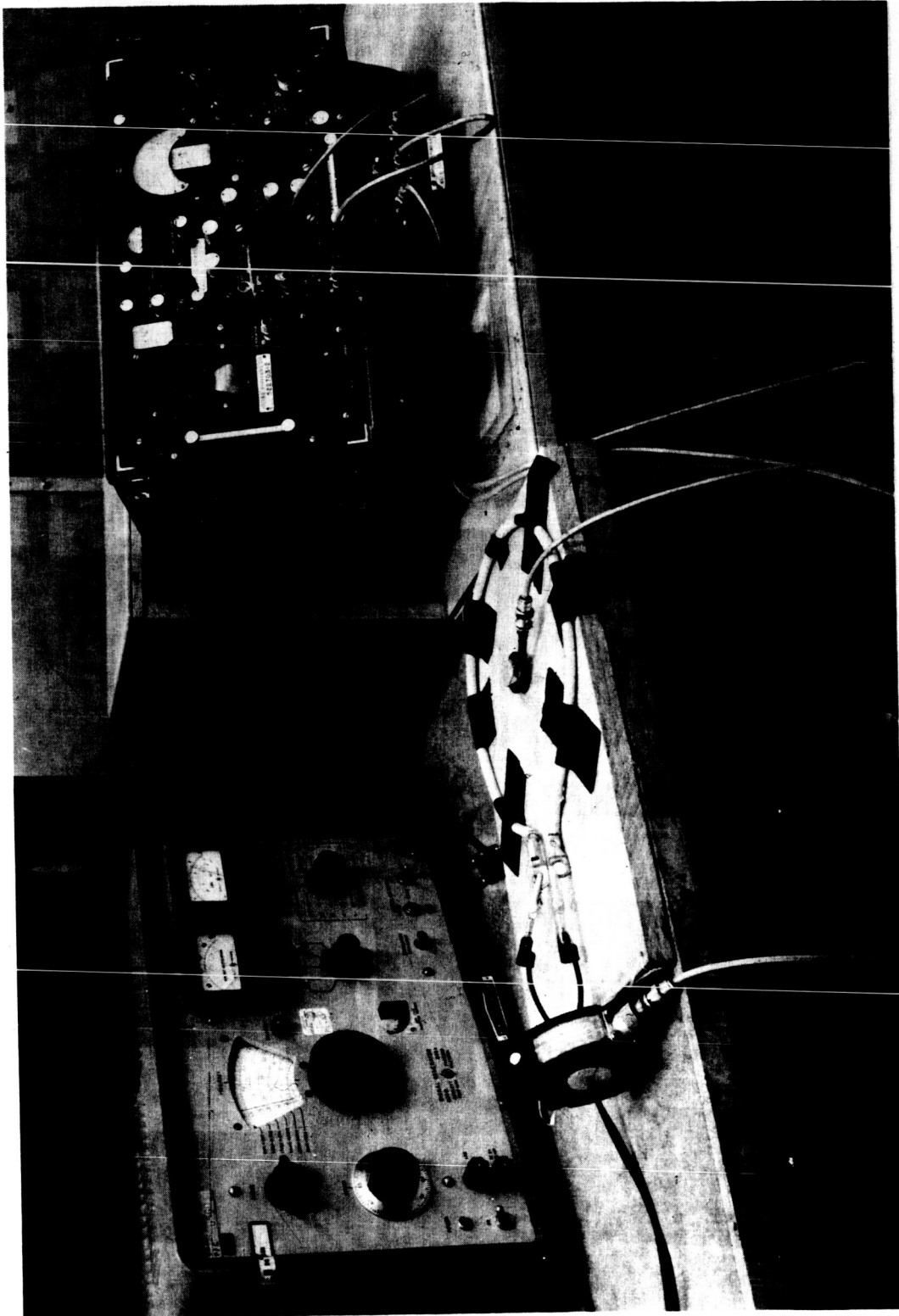
FIG. 3.31
MAGNETIC PROBE CALIBRATION
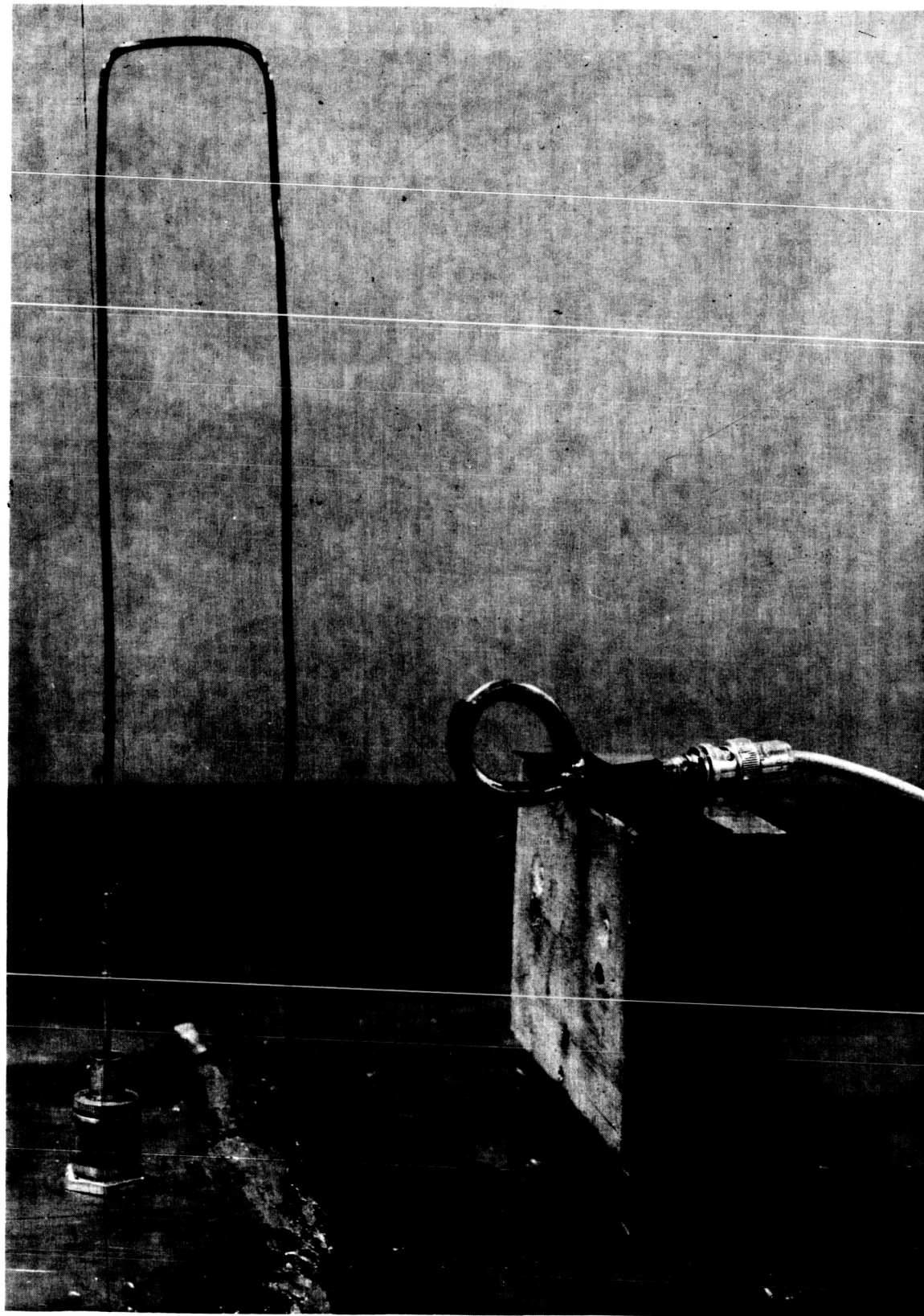
FIGURE 3.32
MAGNETIC FIELD MEASUREMENTS

MAGNETIC FIELD INTENSITY MA/METER
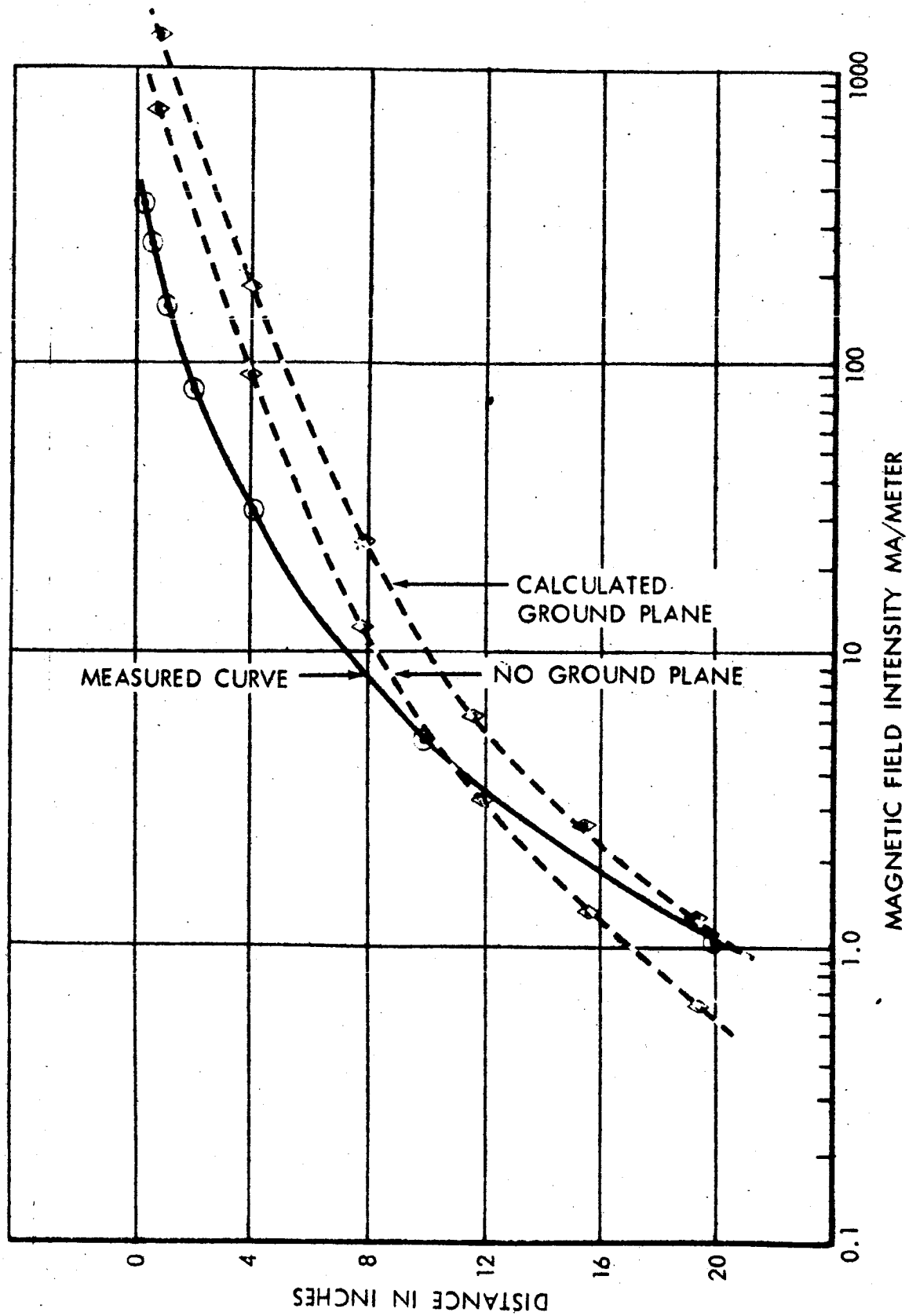
FIGURE 3.33
MAGNETIC FIELD INTENSITY PRODUCED BY CURRENT LOOP

CALCULATED
GROUND PLANE

MEASURED CURVE

NO GROUND PLANE

DISTANCE IN INCHES

# 4.0 CABLE-TO-CABLE INTERFERENCE
## PREDICTION COMPUTER PROGRAM

Prediction of cable-to-cable coupling by means of a computer program has been the subject of extensive research efforts at Boeing for many years. The knowledge gained from past research programs has been extended and modified for application to the Saturn Instrument Unit.

## 4.1 SPECTRUM CONCEPT

The basic method of approach in the computer program is shown pictorially in Figure 4.1.
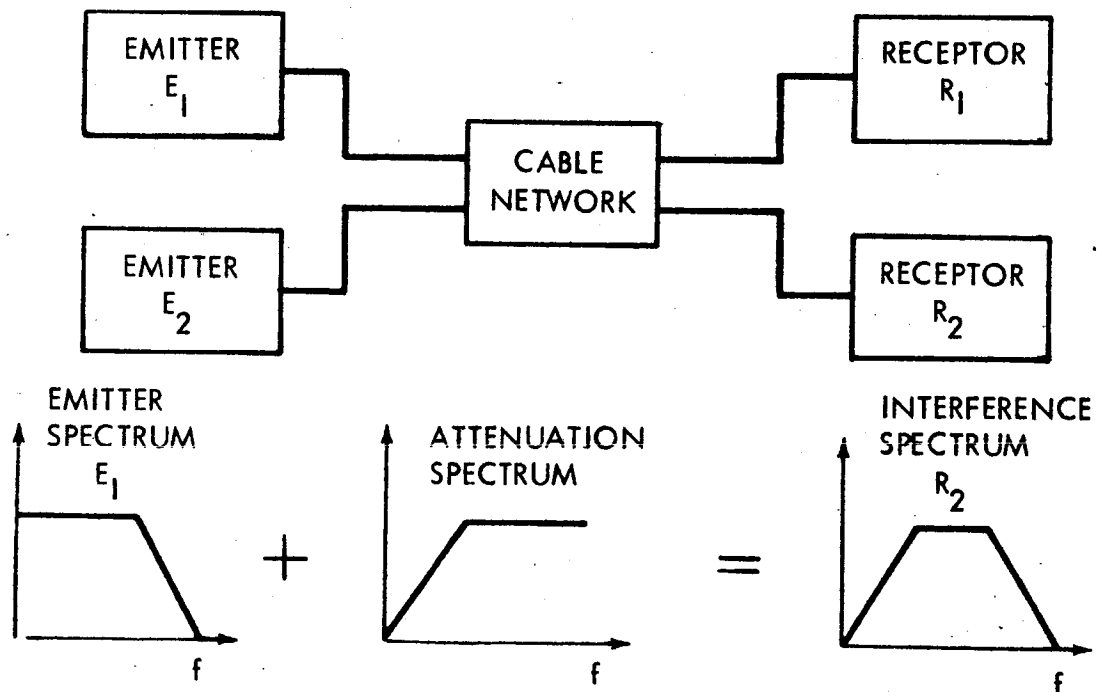


FIGURE 4.1    SPECTRUM CONCEPT

Each circuit is given an appropriate emission and susceptibility spectrum, since every circuit is capable of being both an emitter and a receptor of energy.

The emission spectrum is a composite output spectrum of the normal signal as well as the harmonic and spurious components the circuit will generate. The susceptibility spectrum indicates what input levels would cause significant interference when the circuit is considered as a receptor.

Six broad categories of basic circuit types have been selected to cover all anticipated types of circuits. These basic circuit types are:

1)  Power,
2)  Switch,
3)  Signal,
4)  Modulated,
5)  Servo,
6)  Squib.

Appendix B contains the development of the emitter and receptor susceptibility spectra corresponding to these basic circuit types.

The emission spectrum of one circuit can be coupled as interference into a second circuit by either intercable capacity or mutual inductance as shown in the equivalent circuit of Figure 4.2.

The computer program generates an effective attenuation spectrum to represent the cable-coupling network. The attenuation spectrum modifies the emission spectrum, and with additional allowances for shielding and twisting, the resultant spectrum is that present at the receptor input. A check is made to see if the level of this resultant spectrum approaches or exceeds the level of the susceptibility spectrum of the receptor. A 6-db safety factor is used in the spectrum comparison. The computer program will predict an interference condition if the computed spectrum which can be coupled to the input of a receptor is within 6 db of the receptor's susceptibility level. This safety margin
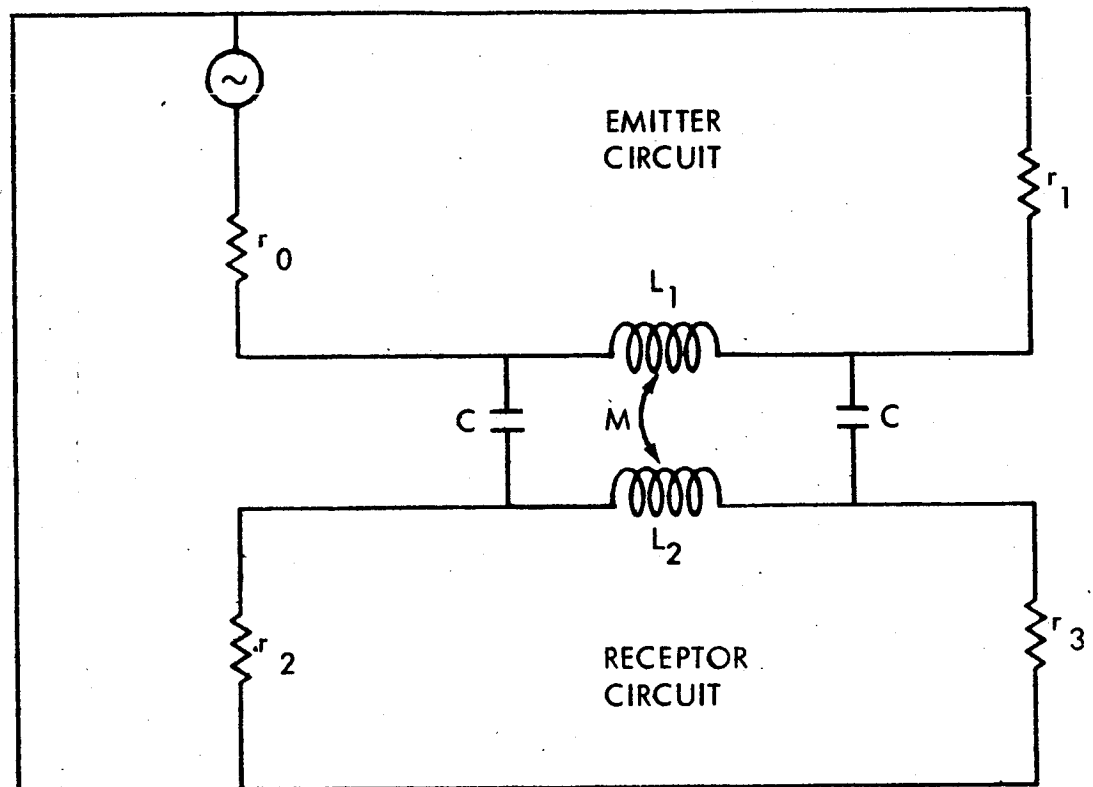
FIGURE 4.2    SYSTEM EQUIVALENT CIRCUIT

can be changed depending on judgment and the fineness required for the analysis. The 6-db value was selected primarily because it is the same margin of safety which must be proven in MIL-E-6051C system compatibility tests.

When the computer finds a potential interference condition, a printout of the parameters of the two circuits and other diagnostic information is made. The computer program continues to run until all the emitters have been checked to see if any one would interfere with any one of the receptors.

## 4.2    DERIVATIONS OF COUPLING EQUATIONS

The equivalent circuit of Figure 4.2 is used to find the amount of cable-coupled interference. This circuit has been extensively analyzed (Appendix C) to determine an optimum method of solution for use in the computer prediction program. The five methods of solution considered are:

Method   I.        Complete Loop Equations,

Method  II.        Capacitive & Magnetic Coupling calculated separately and then added together,

Method III.        Same as Method II except capacitance to ground and receptor circuit self inductance is neglected,

Method IV.         Same as Method III but impedances considered real numbers,

Method  V.         Straight-Line Approximation with no self inductance.

These five methods have been compared as to validity and analytic complexity. All five methods include both capacitive and magnetic coupling, and all give identical answers at frequencies below one megacycle. Above one megacycle, the solutions vary from the exact solution (Method I), depending upon the amount of simplification used.

It is desirable to employ the simplest approach possible consistent with the attainment of specified prediction accuracy. The results, Table I, show that the simplest approach (Method V) is by far the most practical, because it does not impair accuracy beyond tolerable limits and greatly reduces the computation time of the computer prediction program.

TABLE I.

| Method | Error at 1 Mc | Error at 10 Mc | Maximum Error | Normalized Computation Time |
|--------|---------------|----------------|---------------|-----------------------------|
| I      | 0 db          | 0 db           | 0 db          | 1.0                         |
| II     | 0 db          | 2 db           | 6 db          | 0.5                         |
| III    | 0 db          | 1.5 db         | 6 db          | 0.25                        |
| IV     | 0 db          | 3 db           | 6 db          | 0.09                        |
| V      | 0 db          | 5 db           | 6 db          | 0.009                       |

The computer has been programmed to use the coupling equations of Method V given in Appendix C. By use of these equations, a single calculation to find the corner frequency allows complete determination of the attenuation spectrum of the coupling networks.

4.3     COMPUTER DETERMINATION OF MUTUAL
        LENGTH BETWEEN CIRCUITS

The interference coupling between circuits is caused by intercable capacity and mutual inductance. Each of these quantities is a function of the mutual length existing between the two circuits. Thus, a computer prediction program must have the capability of determining

mutual length between arbitrary wire routes. A practical method to do this has been developed for the cylindrical structure represented by the Saturn Instrument Unit.

### 4.3.1    Coordinate System

A cylindrical coordinate system has been chosen wherein any point is defined by Station (S), Radius (R), and Angle (A), as shown in Figure 4.3.
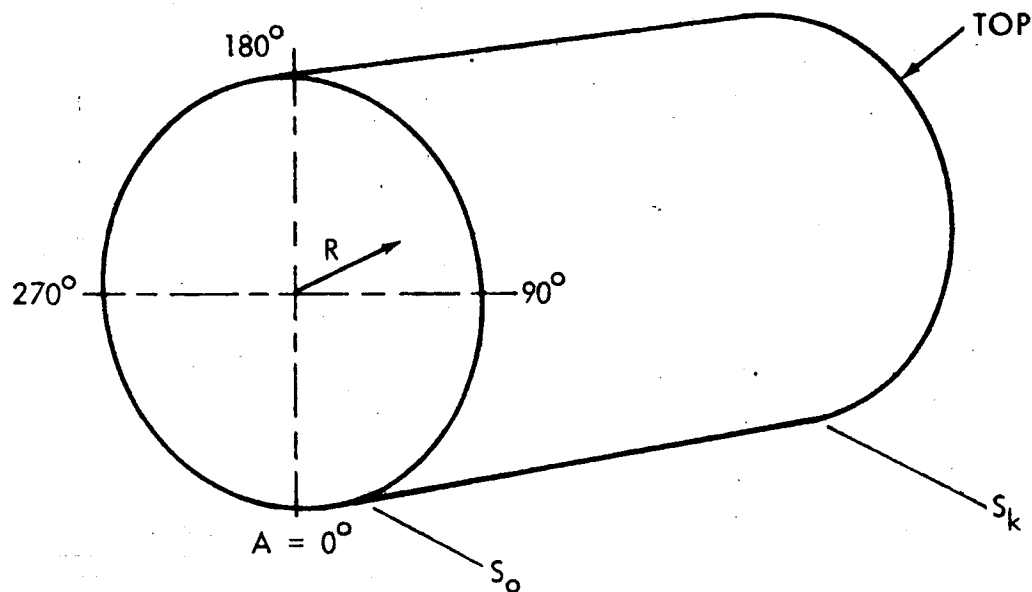


FIGURE 4.3    VEHICLE COORDINATE SYSTEM

For the specific geometry and equipment layout of the Saturn Instrument Unit, all the radius values can be considered constant. Each circuit will be given a wiring routing code in terms of the S and A parameters (e.g., $S_m A_m$, $S_m A_1$, $S_1 A_1$, ... , $S_n A_n$), where m

subscripts are the originating plug coordinates and the n subscripts
are the terminal plug coordinates.  Thus as an example, the routing
of the two circuits shown in Figure 4.4 would be encoded as Table II.

TABLE II.
WIRE ROUTE TABLE

| CIRCUIT 1 | CIRCUIT 2 |
|-----------|-----------|
| $S_2 A_1$ | $S_3 A_3$ |
| $S_2 A_2$ | $S_3 A_2$ |
| $S_1 A_2$ | $S_1 A_2$ |
| $S_1 A_4$ | $S_1 A_5$ |



FIGURE 4.4     CYLINDER ROLLOUT VIEW

## 4.3.2 Mutual Length Determination

To determine the mutual length, the wire routing table for the two circuits will be tested as follows. Circuit (1) route table is searched for two consecutive station entries that are identical such as $S_2A_1$, $S_2A_2$. Then, circuit (2) is searched for the identical consecutive station entries. When none is found, this means that there is no mutual length along that station line. The circuit (1) table is searched for the next consecutive station en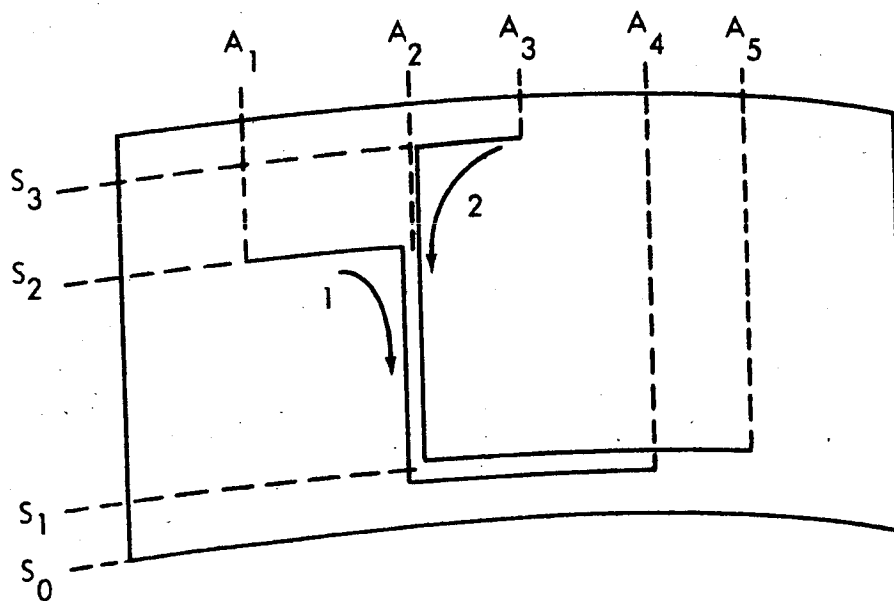try $(S_1A_2, S_1A_4)$. Searching circuit (2) shows it has the same identical consecutive station entry $(S_1A_2, S_1A_5)$. Thus, there is a potential of mutual length at Station $S_1$ between circuits (1) and (2).

The amount of mutual length is found by arranging the angle values in ascending order as shown.

| | X | Y |
|---|---|---|
| (1) | $A_2$ | $A_4$ |
| (2) | $A_2$ | $A_5$ |

The computer compares the X column entries and selects the largest. (This is the start of the mutual length.) For this case, it is $A_2$. The minimum of the Y column is selected (this is the end of the mutual length), and for this case, it is $A_4$. Finally, $Y_{min} - X_{max} = A_4 - A_2$ if found. This last answer is the mutual length if positive. Note, if it comes out negative, there is no mutual length. The latter occurs when circuit (1) stops before circuit (2) starts.

The mutual length so determined is expressed as an angle in degrees or radians and must be converted to units of length using the relation

$$\ell = RA;$$

      R is the cylinder radius
      A is the angle in radians .

The same procedure is followed in searching the circuit route tables for two identical consecutive angle entries in each circuit. This indicates a potential mutual length along an angle line. The resulting pairs are ordered again in table form,

|  | X | Y |
|---|---|---|
| (1) | $S_1$ | $S_2$ |
| (2) | $S_1$ | $S_3$ |

and testing as before, the mutual length is found to be $S_2 - S_1$ with the same check on polarity as before. The total mutual length is then

$$\ell_m = R(A_4 - A_2) + (S_2 - S_1).$$

## 4.4     GENERAL PROGRAM OPERATION

### 4.4.1     Program Flow Chart

The general operation of the computer prediction program is given in the Program Flow Chart in Figure 4.5.

The card input data to the program describes the collection of circuits to be examined for the purpose of prediction of cable-to-cable EMI. A collection of wire routes is also input on cards; the data sheet for each circuit includes a reference to one of these wire routes, thereby defining the position of the circuit within the vehicle.
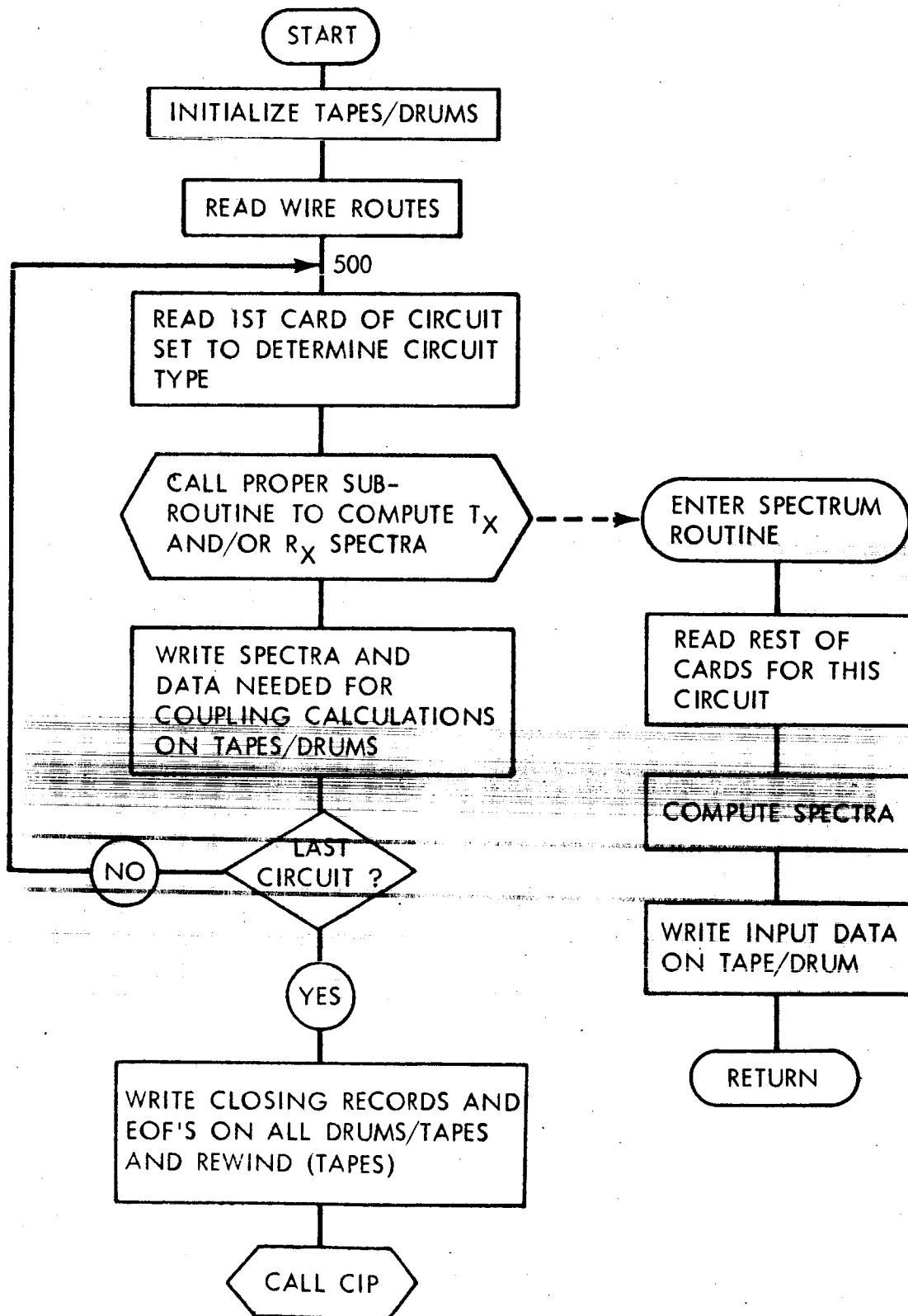
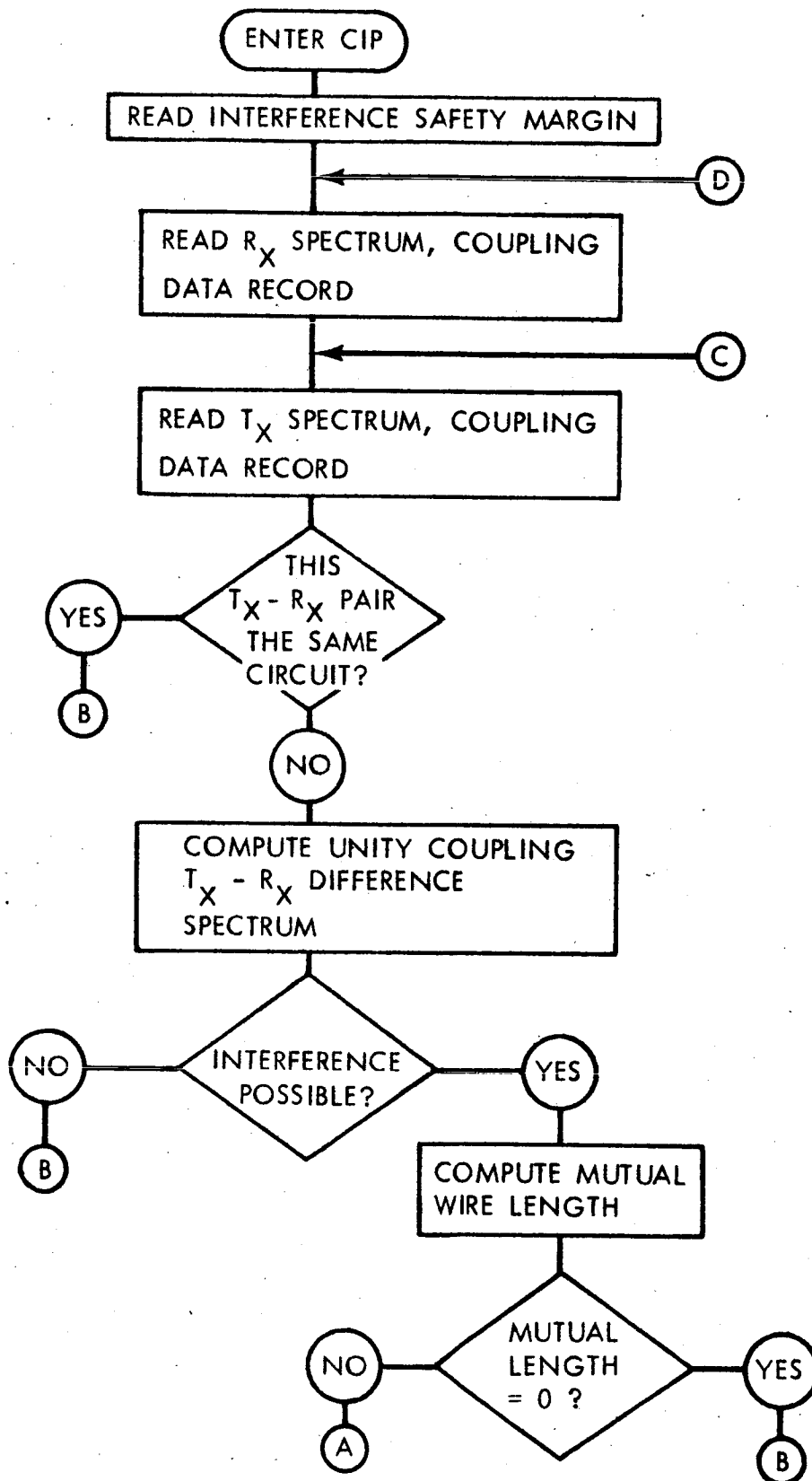FIGURE 4.5    PROGRAM FLOW CHART SHEET # 1
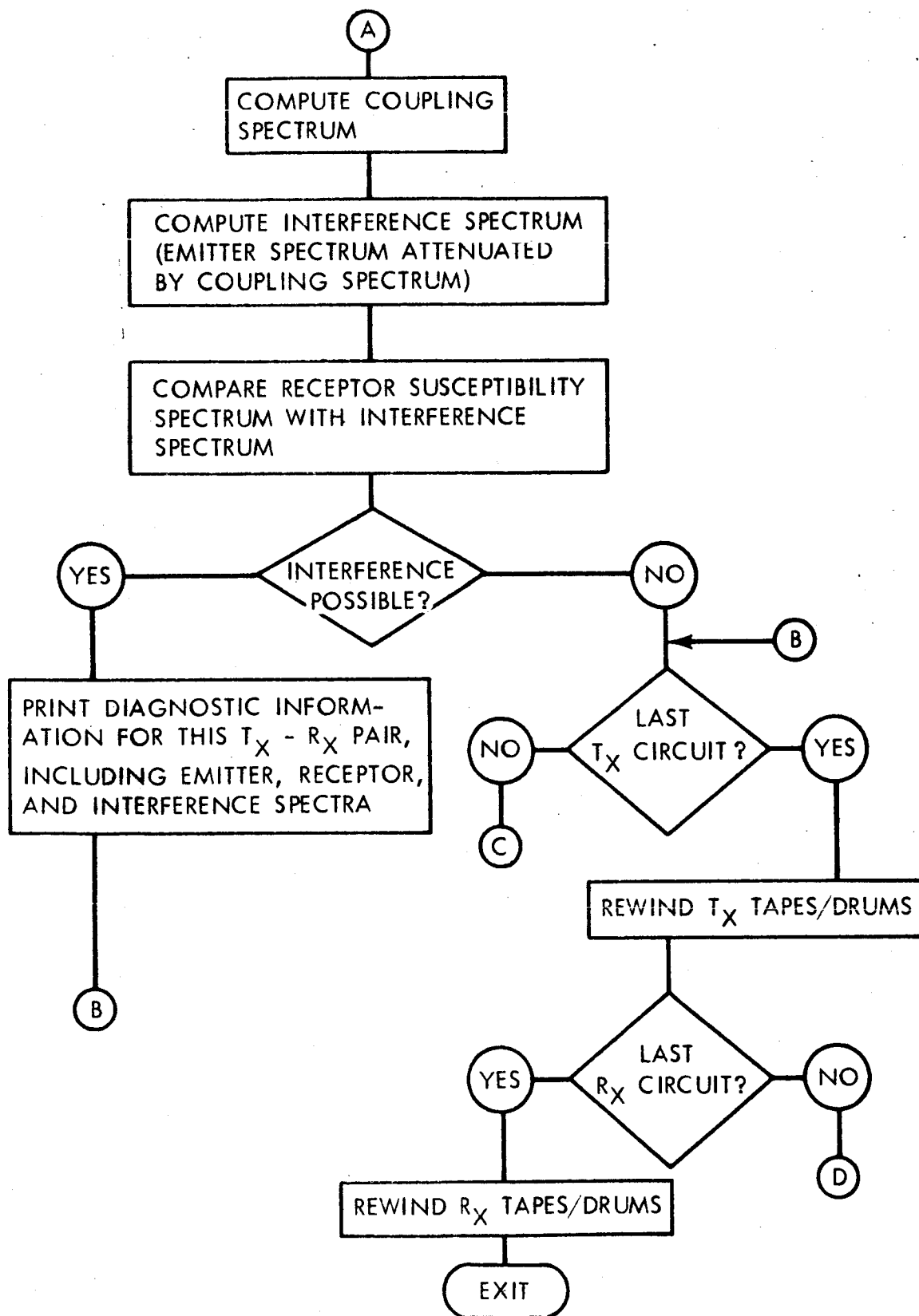
FIGURE 4.5    PROGRAM FLOW CHART SHEET # 2

FIGURE 4.5   PROGRAM FLOW CHART SHEET # 3

Each circuit represented in the input data must be one of the following six types, according to its signal characteristics: power, switch, signal, modulated signal, servo, and squib. A description of these circuit classes and the models used for the emitter and receptor susceptibility spectra for each class of circuit are described in Appendix B.

As each set of input data cards describing a single circuit is read, the emitter and receptor spectra are constructed for that circuit. When an emitter spectrum has been so constructed, that spectrum and all coupling information input for the circuit is written on magnetic tape or drum. A similar set of data is recorded on tape or drum whenever a receptor susceptibility spectrum is constructed for a circuit. After all sets of circuit-description data cards have been read and the spectra constructed, then two lists of spectra and coupling information are available. All circuits which may function as emitters have the necessary descriptive information entered in one list, while the second list is similarly made up of such information for each of the receptor circuits.

For each emitter-receptor circuit pair to be examined, the program first makes a unity coupling test (i.e., checks for the possibility of interference when all the emitter energy is coupled into the receptor circuit). If no interference can result under this condition, no further examination of this emitter-receptor pair is made. Otherwise, if interference is a possibility, the program computes a "mutual wire length" for the emitter-receptor pair, the mutual wire length being the distance the circuit leads travel together in the vehicle. No further examination need be made if the mutual length is zero; the emitter-receptor pair is not considered a potential interference pair. Otherwise, a coupling spectrum is computed on the basis of mutual wire length, mutual inductance and capacitance between the circuits, and whether the circuit leads are twisted or shielded.

The emitter spectrum is then "attenuated" by this coupling spectrum to provide an interference spectrum. If, at any frequency, an ordinate (voltage level) of this interference spectrum is within the safety margin of being greater than the ordinate of the receptor susceptibility spectrum at that same frequency, the two circuits are considered a potential interference pair. The emitter, receptor susceptibility, and interference spectra are then printed to assist in diagnosis. The entire process is continued until all possible emitter-receptor circuit pairs have been examined.

A detailed discussion of the program input preparation and major subroutines can be found in Appendix D.


4.4.2    Storage Requirements

The major requirement for data storage is for storing computed spectra data and circuit input data. (The input data for each circuit is to be retained throughout execution by the program for use in printing diagnostic information whenever any circuit is one of a pair of predicted potential interference circuits.) Each circuit may have either an emitter spectrum or a receptor susceptibility spectrum, or both. For the models currently used to define the various spectra types, an average of about 30 computer words are required for the storage of each spectrum and the associated circuit coupling data. Thus, for a vehicle system consisting of up to n circuits, up to 60 n words are needed to store this spectra and coupling data. (A more exact estimate would, of course, be $30[2n - n_e - n_r]$ words, where $n_e$ the number of circuits having no emitter spectrum, and similarly for $n_r$ and receptor susceptibility spectra.)

The present phase of the EMI program stores all spectra-coupling data and circuit input data on drum and tape.

It is estimated that a program which stored all spectra-coupling data in core rather than on tape or drum would require 10,000 - 13,000 core locations for storage of the program itself and other necessary data. In a 32 K computer*(e.g., the IBM 7094) then, some 20,000 core locations would be available for storage of spectra-coupling data; so that a vehicle system consisting of somewhat more than 300 circuits could be handled by the program. In a 64 K computer (e.g., the SRU 1107), some 50,000 core locations would be available for such use, and in this case up to 800 + circuits could be dealt with. In either case (a 32 K computer or a 64 K computer), it is assumed that all circuit input data would be stored on tape or drum, as is the case in the present program. It is also assumed the models used for spectrum computation (coupling attenuation, etc.) would require approximately the same amount of core area for the storage of the program itself as do the presently-used models.

The present phase of the cable-to-cable EMI program uses both core and auxiliary tape/drum storage.

Six system input-output units (magnetic tape or drum) are used for intermediate storage of the original circuit input data , and the computed emitter and receptor susceptibility spectra. The program currently uses three of the tape units and three of the logical drum units available on the Boeing SRU 1107 for this scratch storage.

Each record or collection of information describing a single spectrum consists of 25 - 35 computer words, so for a vehicle system consisting of n circuits, storage of up to n records of 25 - 35 words each on a single tape or drum unit is required. Three units are used for such storage. The number of words required for the storage of the circuit input data is about 25 n. Three units are used for the storage of this input data.

---

*    A "32 K Computer" is a computer having 32,000 core storage words.

Wire route information is currently placed in core storage after being read from the input cards. Only if very large numbers of wire routes are used in the future, for any one vehicle system, will it be necessary to assign an additional tape or drum unit for storage of wire route information.

Approximately 9,000 core locations are required for the storage of the program itself, as compiled on the SRU 1107. The core data storage requirement is approximately $(1000 + 5n_w + 2n_r + 2n_p)$ words, where $n_w$ is the number of wire codes available (currently $n_w = 41$), $n_r$ is the number of wire routes to be included in the data card input to the program, and $n_p$ is the total number of station-angle pairs in all the $n_r$ wire routes.

With respect to the present program then, any large scientific computer system has a more than adequate core and auxiliary storage capability (e.g., the Boeing IBM 7094 - 32 K core storage, 18 tape units on 3 channels; or the Boeing SRU 1107 - 64 K core storage, 6 tapes, 4 drums on 3 channels).

## 4.4.3    Adaptibility to Other Computers

The present program is written in the FORTRAN IV programming language; so it may be used with only minor changes on any computer system having a FORTRAN IV compiler, such as IBM 7094, SRU 1107. Such changes would include reassignment of logical input-output unit numbers or substitution of program names used for standard library subroutines.

Future phases of the program will also be written in FORTRAN IV so as to make the program as compatible as possible with various computing systems. One possible exception to this general FORTRAN IV compatibility is discussed in the section on future program optimization, Paragraph 4.8.

## 4.5    AUXILIARY PROGRAM CHARACTERISTICS

### 4.5.1    Wire Table Characteristics

The coupling of energy between wires can be calculated in accordance with formulas presented in Appendix C of this report. These formulas include the physical properties and dimensions of wires. Since any cabling system contains many sizes of wire, shielded and unshielded, a table of look-up (Table III) was made and coded so that the computer could refer to the code and store all the necessary wire parameters. This avoids the burdensome task of entering wire characteristic information on each data input sheet. This table was developed after the Saturn wiring drawing 40M30627 was reviewed to assure that the table would include all the wire types used.

For each wire code number, the table indicates whether the wire is twisted and/or shielded, the diameter of the metallic conductor, and the total diameter of the wire bundle (this takes into account a twisted pair, twisted triad, and twisted quadrad).

In addition to this table, the dielectric constant of the wire insulation is specified for the system.

The table is adaptable to any system and can be expanded for larger or smaller wires.

### 4.5.2    Data Sheets

When determining electromagnetic coupling between circuits, a number of variables affect the coupling. Likewise, a number of variables affect the degree to which circuits are susceptible to this coupled energy.

# TABLE III

## WIRE CHARACTERISTICS TABLE

| Wire Code | Size | Twisted | Shielded | d Cond. Diam. (mils) | Diam. of Wire and Insulation (mils) | d₁ Total Diam. of Bundle (mils) | Configuration |
|---|---|---|---|---|---|---|---|
| 00 | 26 | 0 | 0 | | | | |
| 01 | 24 | 0 | 0 | 26 | 43 | 43 | |
| 02 | 22 | 0 | 0 | 33 | 50 | 50 | |
| 03 | 20 | 0 | 0 | 41 | 58 | 58 | |
| 04 | 18 | 0 | 0 | 52 | 70 | 70 | |
| 05 | 16 | 0 | 0 | 60 | 80 | 80 | |
| 06 | 14 | 0 | 0 | | | | |
| 07 | 12 | 0 | 0 | | | | |
| 08 | 10 | 0 | 0 | | | | |
| 09 | 8 | 0 | 0 | 140 | 160 | 160 | |
| 10 | 26 | 1 | 0 | | | | |
| 11 | 24 | 1 | 0 | 26 | 43 | 90 | |
| 12 | 22 | 1 | 0 | 33 | 50 | 104 | |
| 13 | 20 | 1 | 0 | 41 | 58 | 120 | |
| 14 | 18 | 1 | 0 | 52 | 70 | 144 | |
| 15 | 16 | 1 | 0 | 60 | 80 | 164 | |
| 16 | 14 | 1 | 0 | | | | |
| 17 | 12 | 1 | 0 | | | | |
| 18 | 10 | 1 | 0 | | | | |
| 19 | 8 | 1 | 0 | | | | |
| 20 | 26 | 1 | 0 | | | | |
| 21 | 24 | 1 | 0 | 26 | 43 | 99 | |
| 22 | 22 | 1 | 0 | 33 | 50 | 114 | |
| 23 | 20 | 1 | 0 | 41 | 58 | 131 | |
| 24 | 18 | 1 | 0 | 52 | 70 | 157 | |
| 25 | 16 | 1 | 0 | 60 | 80 | 178 | |
| 26 | 14 | 1 | 0 | | | | |
| 27 | 12 | 1 | 0 | | | | |
| 28 | 10 | 1 | 0 | | | | |
| 29 | 8 | 1 | 0 | | | | |
| 30 | 26 | 1 | 0 | | | | |
| 31 | 24 | 1 | 0 | 26 | 43 | 110 | |
| 32 | 22 | 1 | 0 | 33 | 50 | 127 | |
| 33 | 20 | 1 | 0 | 41 | 58 | 146 | |
| 34 | 18 | 1 | 0 | 52 | 70 | 176 | |
| 35 | 16 | 1 | 0 | 60 | 80 | 204 | |
| 36 | 14 | 1 | 0 | | | | |
| 37 | 12 | 1 | 0 | | | | |
| 38 | 10 | 1 | 0 | | | | |
| 39 | 8 | 1 | 0 | | | | |

## TABLE III (cont.)

### WIRE CHARACTERISTICS TABLE

| Wire Code | Size | Twisted | Shielded | d Cond. Diam. (mils) | Diam. of Wire and Insulation (mils) | d₁ Total Diam. of Bundle (mils) | Configuration |
|---|---|---|---|---|---|---|---|
| 40 | 26 | 0 | 1 | | | | |
| 41 | 24 | 0 | 1 | 26 | 43 | 87 | |
| 42 | 22 | 0 | 1 | 33 | 50 | 94 | |
| 43 | 20 | 0 | 1 | 41 | 58 | 102 | ⊙ |
| 44 | 18 | 0 | 1 | 52 | 70 | 114 | |
| 45 | 16 | 0 | 1 | 60 | 80 | 120 | |
| 46 | 14 | 0 | 1 | | | | |
| 47 | 12 | 0 | 1 | | | | |
| 48 | 10 | 0 | 1 | | | | |
| 49 | 8 | 0 | 1 | | | | |
| 50 | 26 | 1 | 1 | | | | |
| 51 | 24 | 1 | 1 | 26 | 43 | 130 | |
| 52 | 22 | 1 | 1 | 33 | 50 | 144 | |
| 53 | 20 | 1 | 1 | 41 | 58 | 166 | ⊙⊙ |
| 54 | 18 | 1 | 1 | 52 | 70 | 184 | |
| 55 | 16 | 1 | 1 | 60 | 80 | 204 | |
| 56 | 14 | 1 | 1 | | | | |
| 57 | 12 | 1 | 1 | | | | |
| 58 | 10 | 1 | 1 | | | | |
| 59 | 8 | 1 | 1 | | | | |
| 60 | 26 | 1 | 1 | | | | |
| 61 | 24 | 1 | 1 | 26 | 43 | 139 | |
| 62 | 22 | 1 | 1 | 33 | 50 | 154 | |
| 63 | 20 | 1 | 1 | 41 | 58 | 171 | ⊙⊙⊙ |
| 64 | 18 | 1 | 1 | 52 | 70 | 197 | |
| 65 | 16 | 1 | 1 | 60 | 80 | 218 | |
| 66 | 14 | 1 | 1 | | | | |
| 67 | 12 | 1 | 1 | | | | |
| 68 | 10 | 1 | 1 | | | | |
| 69 | 8 | 1 | 1 | | | | |
| 70 | 26 | 1 | 1 | | | | |
| 71 | 24 | 1 | 1 | 26 | 43 | 150 | |
| 72 | 22 | 1 | 1 | 33 | 50 | 167 | |
| 73 | 20 | 1 | 1 | 41 | 58 | 186 | ⊙⊙⊙⊙ |
| 74 | 18 | 1 | 1 | 52 | 70 | 216 | |
| 75 | 16 | 1 | 1 | 60 | 80 | 244 | |
| 76 | 14 | 1 | 1 | | | | |
| 77 | 12 | 1 | 1 | | | | |
| 78 | 10 | 1 | 1 | | | | |
| 79 | 8 | 1 | 1 | | | | |

When using a computer for prediction of coupling and susceptibility, the variables need to be programmed into the computer. To accomplish this, data sheets have been prepared for the six basic circuit types discussed in Paragraph 4.1. A sample of each data sheet is given in Figures 4.6 through 4.11. One of the prime considerations in developing the data sheets was to minimize the time required of the user to fill out the sheets.

Information is required to define the specific circuit and wire in a cable. The route that the wire follows is defined by a route plan number. This has the advantage of not requiring this information to be included on each data sheet. Likewise, only a wire code number needs to be entered on that data sheet. This again saves the time required to enter wire size, diameter, shielding, etc.

The circuit characteristics required to define the coupling, generated spectrum, and the susceptibility levels have been kept to a minimum. Further details and refinements could be used that might give levels slightly closer to the true values. However, worst-case situations have been assumed in making approximations. These approximations are extremely useful, since even the minimum information is difficult to obtain. The more detailed circuit parameters often are not known until late in a program. The net results are a considerable savings in time, and the ability to approximate many parameters based on previous programs.

4.5.3    Shielding Effectiveness

On the basis of laboratory measurements made under controlled conditions, several significant changes and simplifications have been made in the shielding effectiveness curves used in the computer prediction program for the Saturn Instrument Unit.

**FIGURE 4.6 1.- KEYPUNCH DATA FOR POWER CIRCUITS**

ORID

CIRCUIT

1 2

VOLTAGE AMPLITUDE VOLTS

1 6

CONNECTOR CONTACT CONNECTOR CONTACT CONNECTOR CONTACT CIRCUIT ID ROUTE PLAN WIRE CODE

8 12 14 18 20 21 24

LOAD IMPEDANCE OHMS

9 16

POWER SUPPLY (AC, DC)

17

FREQUENCY TOLERANCE CPS

7 10

LOAD POWER FACTOR

11

MEASURED NO. OF SPECTRUM DATA AVAILABLE

NO. OF GENERATED SPECTRUM POINTS

NO. OF SUSCEPTIBILITY SPECTRUM POINTS

14 15 16 18

AC SUPPLY

FREQUENCY CPS

1 6

MAXIMUM ALLOWABLE RIPPLE VOLTAGE

1 7

RIPPLE FREQUENCY

8

DC SUPPLY

MEASURED SPECTRUM DATA AVAILABLE
1 YES
2 NO

14 15

NO. OF GENERATED SPECTRUM POINTS

16 18

*DATA TYPE

M - MEASURED
D - DOCUMENTED
E - ESTIMATED

MEASURED BROADBAND GENERATED SPECTRUM

AMPLITUDE FREQUENCY

AMPLITUDE FREQUENCY

FREQUENCY

MEASURED BROADBAND SUSCEPTIBILITY SPECTRUM

AMPLITUDE FREQUENCY

AMPLITUDE FREQUENCY

FREQUENCY

FIGURE 4.7
2 – KEYPUNCH DATA FOR SERVO UNITS

FIGURE 4.8

3 – KEYPUNCH DATA FOR SIGNAL CIRCUITS

FIGURE 4.9
4-KEYPUNCH DATA FOR SWITCH CIRCUITS

WIRE CODE — 24

CIRCUIT ROUTE PLAN — 21

CIRCUIT ID — 5 — 20

CONTACT — 18

CONNECTOR CONTACT — 14

CONNECTOR — 12

CONNECTOR — 8

CIRCUIT — 2

ORID — 1

SQUIB INPUT IMPEDANCE — OHMS * — 32 — 25

IMPEDANCE OF BRIDGE WIRE — OHMS — 16

MAXIMUM NO-FIRE VOLTAGE (1) — VOLTS * — 15 — 9

MAXIMUM NO-FIRE CURRENT (1) — AMPS * — 8 — 1

* DATA TYPE
D – DOCUMENTED
M – MEASURED
E – ESTIMATED

(1) DATA FIELD NOT USED

FIGURE 4.10
5–KEYPUNCH DATA FOR SQUIB CIRCUITS

**SIGNAL CODING**

CIRCUIT

CONNECTOR CONTACT CONNECTOR CONTACT CIRCUIT ID ROUTE PLAN WIRE CODE

**SIGNAL CODING**

RX INPUT IMPEDANCE OHMS

RX BANDPASS FROM CPS TO CPS

TX SOURCE IMPEDANCE OHMS

**FOR AM OR FM ONLY**

FUNDAMENTAL OPERATING FREQUENCY CPS

MAXIMUM AMPLITUDE OF FUNDAMENTAL VOLTS

MAXIMUM DEVIATION FOR FM CPS

PERCENT MODULATION (AM)

BANDWIDTH OF MODULATING SIGNAL FROM TO

**FOR PCM ONLY**

MINIMUM PULSE WIDTH µ SEC

RISE TIME OF MINIMUM PULSE µ SEC

FALL TIME OF MINIMUM PULSE µ SEC

VOLTAGE AMPLITUDE VOLTS

MAXIMUM PULSE WIDTH µ SEC

RISE TIME OF MAXIMUM PULSE µ SEC

FALL TIME OF MAXIMUM PULSE µ SEC

(1) SIGNAL CODING
2 - PCM
3 - FM
4 - AM

DATA TYPE
D - DOCUMENTED
M - MEASURED
E - ESTIMATED

FIGURE 4.11
6 - KEY PUNCH DATA FOR PCM, FM, AND AM CIRCUITS

For the testing, wires were mounted inside a 69" diameter aluminum cylinder, 29' long. The wires were separated 15 inches from the cylinder wall by wooden supports. Shielding effectiveness against interference coupling can meaningfully be measured only when the electrical length of each wire under test is short compared to the wavelength of the signal it carries. Laboratory results indicate the line length should be less than 1/16 wavelength.

Initially, coupling between unshielded wires was measured for several circuit configurations. Magnetic (low impedance) fields for these measurements were produced by terminating the transmitting wire in a short circuit. Electric (capacitive or high impedance) fields were obtained by terminating the transmitting wire in an open circuit. The receiving wire was terminated in 50 ohms at the far end, and in the receiver 50-ohm impedance at the near end.

Based on laboratory measurements made under controlled conditions, several significant changes and simplifications have been made in the shielding effectiveness curves used in previous computer-prediction programs.

Figure 4.12 shows the shielding effectiveness against capacitive coupling. It should be noted that a shield is more effective when it is on the receiving wire. This is because the capacitance between the wire and shield lowers the effective impedance of the receiving circuit, making it less susceptible to capacitive coupling.

Figure 4.13 shows the shielding effectiveness against inductive coupling. Here again, the shield is more effective on the receiving wire. This is because, for the same applied voltage on the transmission wire, the current is increased when the wire is shielded. The larger current will induce a larger voltage in the receiving wire and reduce the apparent shielding effectiveness.
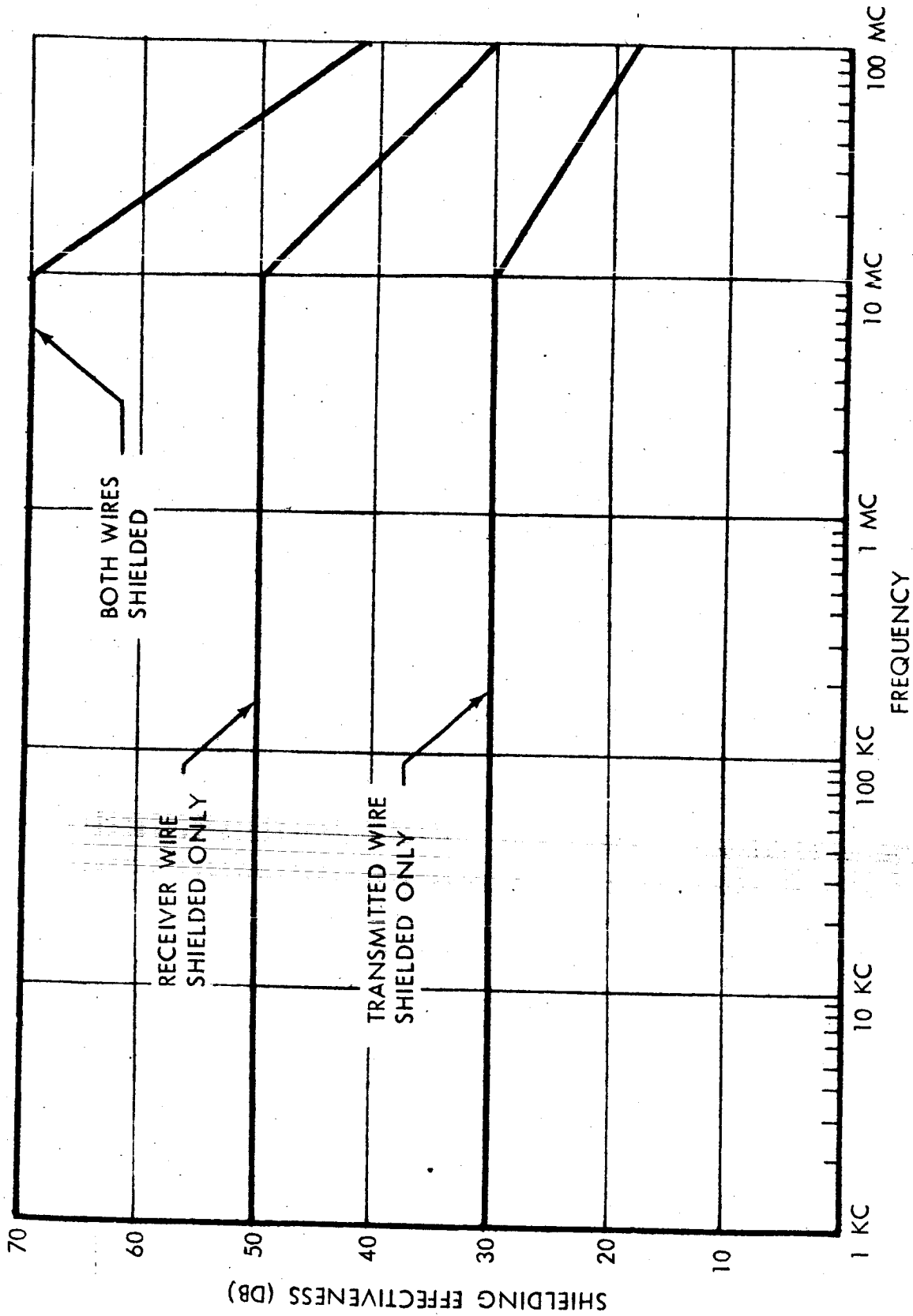
FIGURE 4.12
NEW SHIELDING EFFECTIVENESS ON CAPACITIVE COUPLING

FREQUENCY
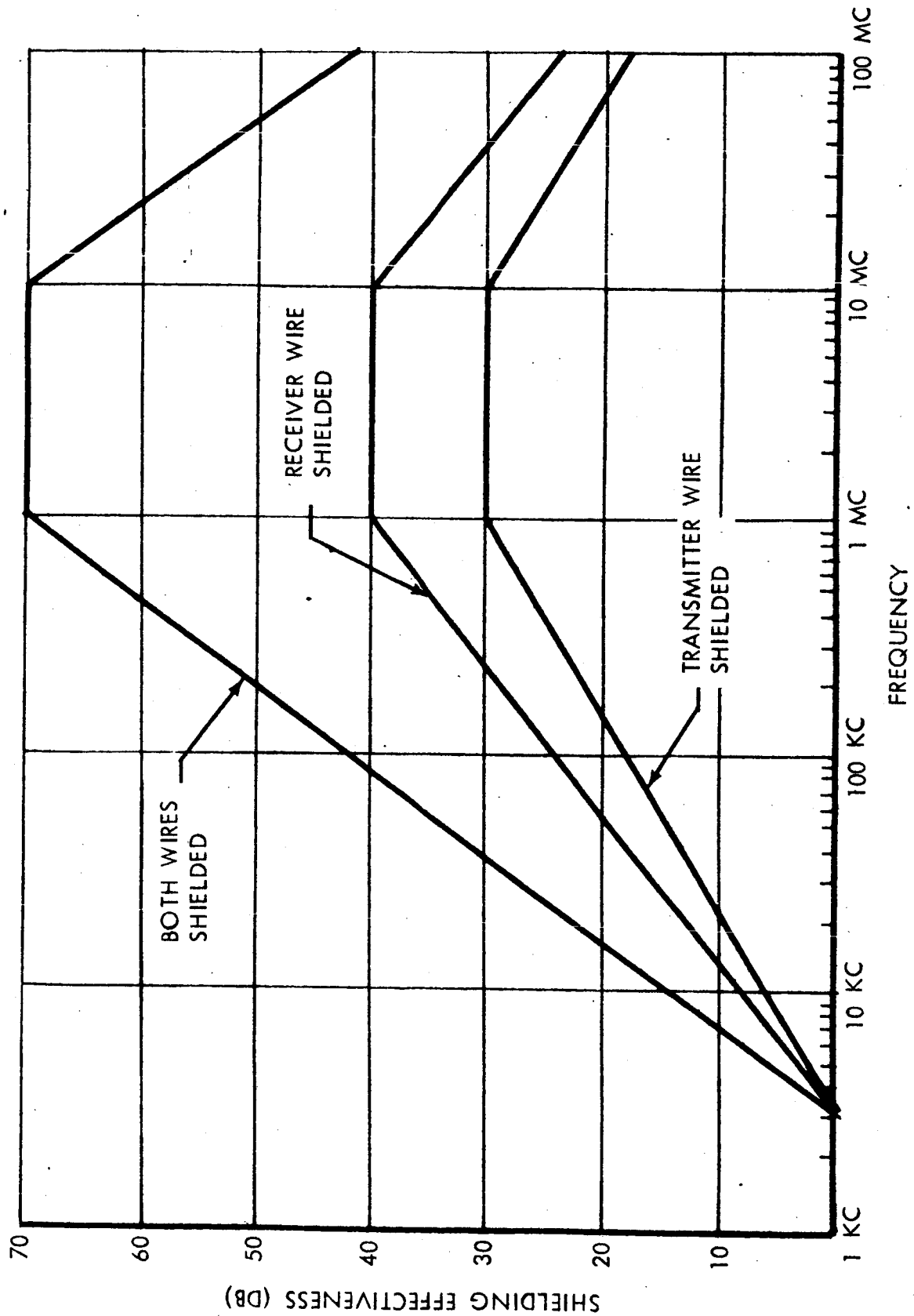
FIGURE 4.13

NEW SHIELDING EFFECTIVENESS ON MAGNETIC COUPLING

## 4.5.4    Twisting Attenuation Factor

Considerable laboratory work has been performed to determine the attenuation effectiveness gained by having a twisted pair rather than two straight wires.

The original computer-prediction program used a value of 14 db if the wires were twisted. The laboratory data indicates that a much more realistic figure could be used.

Testing was performed over the frequency range of 1 Kc to 10 Mc for inductively- and capacitively-coupled circuits. It should be noted that an inductively-coupled circuit has come capacitive coupling and vice versa. This level for capacitive coupling was 40 db below that for inductive coupling. When a wire pair was twisted, the inductive-coupling level dropped 40 db or more. The actual level was below that for the stray-capacitive coupling. Thus, by twisting the wires, inductive coupling is reduced by at least 40 db. Whereas, twisting the wires has negligible effect on capacitive coupling. It should also be noted that twisting both the emitter and receptor pair does not neces-sarily reduce the coupling beyond that obtained by twisting either one or the other.

From this data, it will be observed that the definition of inductive and capacitive circuits needs to be established in such a way that the com-puter can establish an appropriate attenuation level.

## 4.5.5    Test Circuits Used for Checkout

Upon completion of the computer program coding, a number of sample circuits were chosen for checkout of the program. These consisted of samples of each major type of circuit. Typical circuit parameters were chosen, based on information from previous programs. A typi-cal route plan was set up and random wire codes were chosen for each circuit.

There were a total of nine circuits considered and computer calculations were performed for determining interference between each combination. A number of the intermediate steps and calculations were printed out to be compared to hand calculations. During this checkout, several minor programming mistakes were discovered, and several formulas were discovered which had been improperly programmed. These errors were corrected, and it was verified that the computer program was properly calculating the information desired.

## 4.6    COMPUTER ANALYSIS OF INTERFERENCE IN SATURN INSTRUMENT UNIT CIRCUITS

After the computer-prediction program was developed and checked out, its capabilities were applied to an actual system. A portion of the Saturn Instrument Unit in the Saturn launch system was chosen for this purpose. The portion of (Figure 4.14) the Saturn IU examined was the Guidance Signal Processor and its intertie with the FM/FM and PCM Telemetry, Control and Power Distributors and the Command System. Since little information was available on the functioning of the unit, sample circuits were chosen. The primary source of information on circuit parameters was "Technical Manual, Field Maintenance Instructions, Guidance Signal Processor, NASA Model GSP-24 (IBMP/N 6740000)". Interconnecting wiring information was obtained from NASA documents 40M30627 and 10M70390, and NASA drawing 10M20379.

The circuit information in the document was incomplete and scattered throughout it. Thus, a good portion of the required information for interference prediction had to be estimated, based on experience with "similar" types of equipment. This should be kept in mind when evaluating the accuracy of the results.
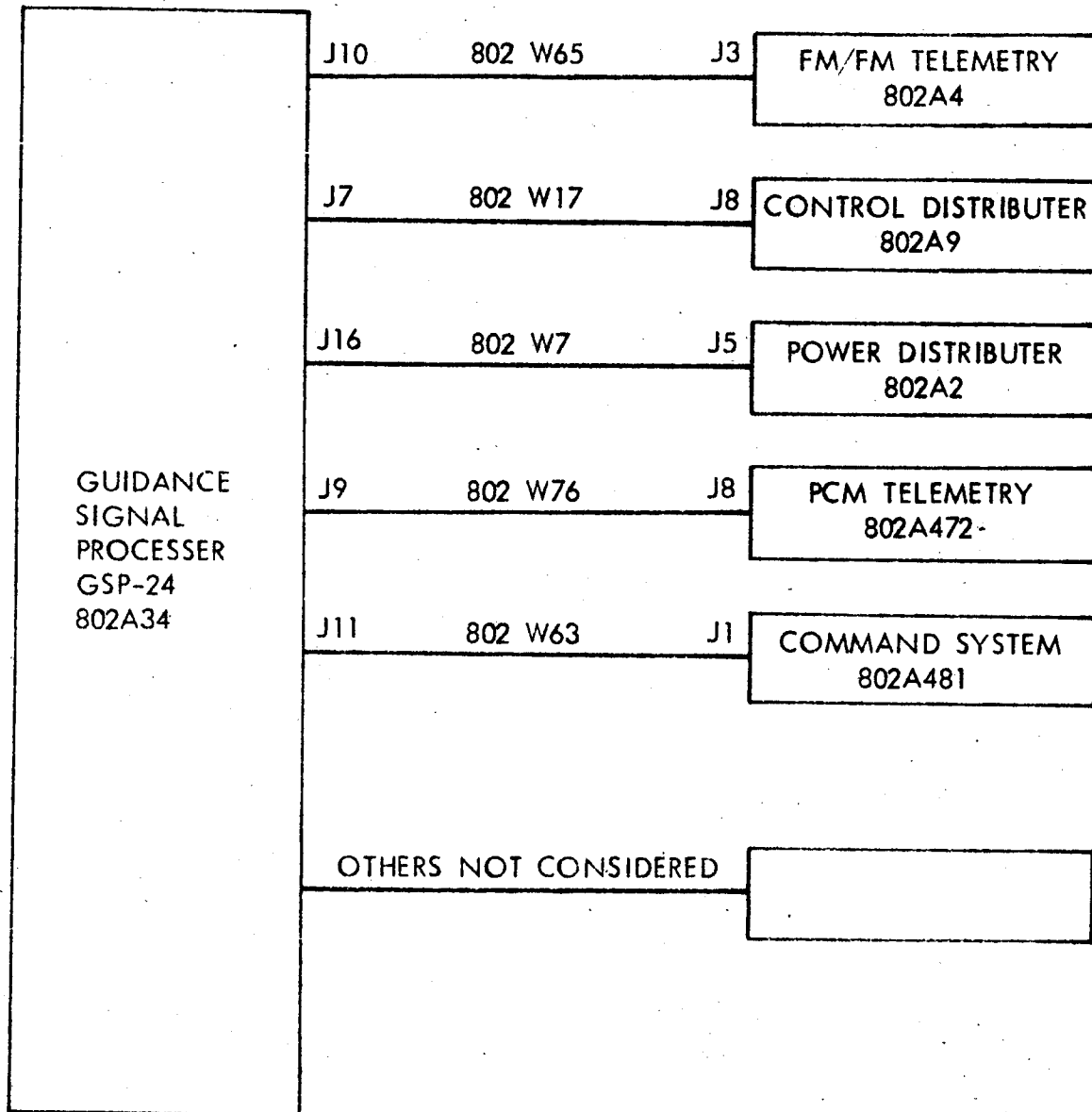
FIGURE 4.14
SATURN INSTRUMENT UNIT CIRCUITS ANALYZED

Actually, this illustrates the usefulness of the program, since results can be obtained even under these conditions. When the computer predicts interference problems between certain circuits, then further analysis can be made in specific circuits rather than all of these circuits. The circuits were chosen that represented a good cross section of circuit functions.

Each wire involved in the cables selected was tabulated and the parameters of the circuits listed as far as were known. Then each circuit was classified into one of the six basic circuit categories.

The parameters were entered on the data sheets, and computer input cards were punched. There were a total of 52 circuits compared for possible interference. Thus, there were 2,704 cases considered. Ordinarily, there is interest in interference signals that reach or exceed a level 6 db below the susceptibility level of the receptor circuit. On this run, there were 196 cases indicated where this was the case. Ninety-four of these indicated levels exceeded the susceptibility level.

An analysis of the results at this point can indicate a great many things about the system. For instance, there are certain receptors that are susceptible to a large number of other circuits, while some emitters are interfering with a large number of circuits. This information narrows the area of investigation to a few specific circuits. These could be poorly designed, but more likely insufficient details were known initially and improper approximations were made. For the sample run on the Instrument Unit, 8 circuits accounted for 146 of the 196 predicted problem areas. The other 50 cases were distributed among 11 other circuits.

## 4.7    FEASIBILITY OF PREDICTION ON LARGER SYSTEMS

In principle, there is no limit to the size of system that can be evaluated for interference prediction by the present computer program. The program could be extended to such larger electronic complexes as the Instrument Unit, booster stages, payload (e.g., LEM, Apollo Command and Service modules), and the ground checkout equipment.

Possible limiting features are the following: computer storage limitations, computer operating time, manpower and time to gather information and fill out data sheets.

As is indicated in Paragraph 4.4.2, the total storage capabilities using drums and tapes is large enough that it is not a consideration. However, the computer operating time becomes the main point of interest. For the 50 circuits that were checked on the Instrument Unit package, the operating time was about 23 minutes. During this time, the emitter and receptor spectra were constructed and 2500 comparisons made for possible interference. About 12.5 seconds were required to construct the spectra and the remainder of the time was spent in checking for possible interference. However, because of time-sharing aspects of the computer, it has not yet been determined what portions of the program required the most time. Thus, the time required for a larger-number circuit has not been fully determined. The indications are that this computer-operating time will be the primary limiting factor. It should be noted that each single comparison requires about one hour to hand calculate.

Checking is underway to define more specifically the aspects of the program that are consuming the majority of the time. The use of core storage for 800 or fewer circuits will decrease the time from that when using tapes or a drum storage. Also, consideration is being given to a modification which will allow identical circuits with different route plans to be treated in a less redundant manner.

The fact of interest for the area of the Instrumentation Unit circuitry that was under consideration is that only 15% of the wires had "different" signals for a given route plan. Whether this is unique or not will remain to be seen. However, the fact remains that of the total number of wires in a system, a large percentage carry the same or similar signals, or are ground-reference lines which are neglected. Raising this to a possible 25%, there would only be 625 circuits to checkout of the approximate 2500 in the Instrumentation Unit.

## 4.8        FUTURE PROGRAM OPTIMIZATION

The greatest possibilities for improvement in the EMI program performance lie in the reduction of program execution time through reducing the time presently used in input-output operations. The present FORTRAN IV program performs much repetitive tape/drum reading of spectra-coupling data and can do no computing while this data is being read into core storage. The incorporation into the program of some means of simultaneous computing and input would thus significantly reduce execution time.

The standard FORTRAN language, however, does not provide for parallel input-output and computing, and thus any parallel processing capability must be implemented especially for each computer system. One means to accomplish such parallel processing is provided by NTRAN, a program system available for use with the FORTRAN IV of the Boeing SRU 1107. The incorporation of the NTRAN capability into the EMI prediction program would thus reduce execution time, but such a version of the program would no longer have the general FORTRAN IV feature of program compatibility with many computer systems. There is, for example, no similar capability currently available with the FORTRAN IV of the Boeing IBM 7094.

Another approach to reducing time spent in reading information from tape or drum is the abvious one of elimination: rather than store all spectra and coupling data on tape or drum as is presently the case, this data could remain in core storage. The desirable feature of general-program compatibility with computer systems having the FORTRAN IV capability would then be retained. A discussion of the limitations placed on the size of a vehicle system to be considered by such a program is given in Paragraph 4.4.2.

## 5.0 CONCLUSIONS & RECOMMENDATIONS

### 5.1 FEASIBILITY OF INTERFERENCE PREDICTION IN CAVITIES

In Section 3.0, some aspects of the electromagnetic theory of cavity resonators have been presented. The purpose of the presentation has been to demonstrate that it is feasible to calculate the interference field everywhere in a vehicle enclosure, and so to obtain the necessary information for interference prediction. When the geometrical structure of the vehicle enclosure forms constant coordinate surfaces of a separable coordinate system, or when it can be reasonably approximated by such a structure, the derivation of the forced field is relatively simple (provided that the equipment boxes do not occupy an appreciable fraction of the total volume). This includes the most important practical types of vehicle enclosures, the rectangular prism, the circular or elliptical cylindrical box, the sphere, the ellipsoid and the circular cylindrical box with an inner conductor.

Present computer techniques are applicable to the calculation of the field quantities from the derived generalized solutions. The computer program would initially consider the Instrument Unit as a regular cavity with the fields expressable as sums of weighted characteristic functions. The hand calculation of the coupled interference, using these complicated expressions, would involve enormous difficulty, but use of a large-scale digital computer will make the prediction calculations relatively easy and inexpensive.

Small irregularities along boundaries may be taken into account in the computer calculation of the characteristic functions through application of perturbation theory. Provision for such a modification of the characteristic functions in the program does not appear to present any major problems. All combinations of emitter-receptor coupling will

be processed. The computer execution will be quite low for each evaluation, but may become substantial after considering all situations. This execution time will not be unacceptably high, however.

Variational methods are available for more complicated structures or for enclosures which contain a large number of equipment boxes.

The theory is valid for arbitrary sources characterized by known electric and magnetic current distributions. Since exact evaluation of the surface currents on an interference radiator appears to be a very difficult task, either by experimental or analytical methods, the basic assumption in this section has been that the radiating device may be represented by equivalent electric and magnetic dipoles. This implies two conditions: first, that the dimensions of the radiator are limited to a fraction of the wavelength of the interfering frequency; and second, that the field in the cavity can be accurately determined only for points some distance away from the source.

The strengths of the equivalent dipoles may be best obtained experimentally by the shielded-room technique. This also implies that the interfering equipment is available for measurements or that specifications on the interference-producing device are established in terms of equivalent electric and magnetic dipoles.

## 5.2     RECOMMENDED FOLLOW-ON RESEARCH EFFORT

The report presents an engineering technique to evaluate the interference caused by radiating equipment in a space vehicle. To extend the range of the applicability of this technique and to test experimentally the analytic assumptions, further research in some areas is required. A program for future work may be best summarized by the following outline.

## I.    Experimental Verification of Interference Prediction

To test the analytical and experimental work of this report, a full-scale simulation of a typical space system enclosure is proposed. Construction and design of such a model would be directed toward obtaining measurements which confirm theoretical assumptions and indicate problem areas which need further investigation.

The simulation would use a shielded room to represent a vehicle enclosure. Initially, electric and magnetic probes will be mounted on the walls and measurements made of the fields coupled between probes will be compared to analytic predictions. Actual equipment-type boxes will also be mounted on the walls and excited to represent electric or magnetic dipoles. Variations will be made in the number of boxes installed as well as the location, size, and shape of these boxes.

## II.    Shielded-Room Technique

Further analytical and experimental work is required to establish a general method of determining the equivalent dipoles of an interference radiator. The shielded-room technique described in this report is applicable to low frequencies and to small radiators. An extension of this method is required to include the effects of the resonance of the room and the size of the radiator. As an overall check on the shielded-room technique, a comparison should be made between the field intensity values determined by this technique as opposed to those determined in free space.

## III.    Equivalent Lumped-Circuit Model

Some progress has been made in this report to determine the interference field at distances close to the radiator, but the techniques are not fully substantiated at this time. The most promising approach to this problem is the lumped-circuit method described in Section 3.3 of this report. However, the experimental difficulties encountered due

to stray pick-up and reflecting properties of the surrounding room
have been such that no definite conclusions could have been reached
from the experimental data. Further experiments are needed to
develop a lumped-circuit model of two or more equipment boxes at
close distances.

## IV.    Numerical Methods

The various methods of calculating the electromagnetic field, as pre-
sented in this report, are satisfactory to obtain engineering results
for most cavities. The application of the variational methods requires
certain amounts of preliminary analytical work which may become
excessive when complicated geometrical structures are considered.
A numerical method appears feasible for computer prediction of
electromagnetic fields in any type of cavity. The numerical method is
based on the principle that boundary-value problems can be solved by
replacing the partial differential equation by the corresponding differ-
ence equation, and then solving the latter by a process of iteration.
Some work to develop the method has been done in the past (References
6 and 7), but further research is required to improve the technique.
Full development of this method would allow rapid calculation of the
electromagnetic field in any cavity by means of a digital computer.

## APPENDIX A

## ELECTROMAGNETIC THEORY OF CAVITY RESONATORS

A.1    ELECTROMAGNETIC FIELDS IN IDEAL CAVITIES

The excitation problem of ideal cavities due to electric and magnetic sources is solved by considering the characteristic modes of the cavity. Each mode must satisfy the field equations

$$\nabla \times \vec{E}_i = -j\omega_i \mu \vec{H}_i, \qquad\qquad \nabla \times \vec{H}_i = j\omega_i \epsilon \vec{E}_i,$$

where i is the mode index, $\epsilon$ and $\mu$ are the constitutive parameters of the dielectric medium enclosed by the cavity, and $\omega_i$ is the angular resonant frequency of the mode. By eliminating $\vec{E}_i$ or $\vec{H}_i$ from the above equations, the homogeneous wave equations are obtained

$$\nabla \times \nabla \times \vec{E}_i - k_i^2 \vec{E}_i = 0$$

$$(A.1)$$

$$\nabla \times \nabla \times \vec{H}_i - k_i^2 \vec{H}_i = 0$$

where,

$$k_i = \omega_i (\mu \epsilon)^{1/2}$$

Each of these wave equations, coupled with the boundary condition

$$\vec{n} \times \vec{E}_i = 0 \quad \text{on S,}$$

where $\vec{n}$ is the unit normal directed outward from the cavity boundary S, is a characteristic value problem.

# REFERENCES

1) Morse, P. M. and H. Feshbach, Methods of Theoretical Physics, McGraw-Hill Book Company, Inc., New York, 1953.

2) Collin, R. E., Field Theory of Guided Waves, McGraw-Hill Book Company, Inc., New York, 1960.

3) Hasserjian, G., Evaluation of Interference by The Use of A Shielded Room, Master's Thesis, Rennsselaer Polytechnic Institute, Troy, New York, 1954.

4) Stoker, W. C., Quine, J. P., and G. Hasserjian, et. al., An Investigation of Electromagnetic Coupling Devices for The Measurement of Noise Fields, Rensselaer Polytechnic Institute, Troy, New York, Signal Corps Contract No. DA 36-039 SC-207, Final Report, 1952.

5) Goubau, G., Electromagnetic Waveguides and Cavities, Pergamon Press, New York, 1961.

6) Motz, H., "Calculation of The Electromagnetic Field, Frequency and Circuit Parameters of High Frequency Resonator Cavities", Journal of the IEE (London), Vol. 93, Part III, pp. 335-338, September 1946.

7) Reynolds, D. K., Private Communication, 1964, U. of Wash.

8) Quine, J. P., Electromagnetic Shielding Principles, Rensselaer Polytechnic Institute, Troy, New York, 1956.

Hence, for real $\epsilon$ and $\mu$, the characteristic values are real, and the mode factors $\overrightarrow{E}_i$, $\overrightarrow{H}_i$ form a complete orthogonal set. By normalizing the mode vectors such that

$$\iiint \epsilon \; \overrightarrow{E}_i \cdot \overrightarrow{E}_j^* \; dV = \begin{cases} 0 & i \neq j \\ 1 & i = j \end{cases} \quad \text{and}$$

$$\iiint \mu \; \overrightarrow{H}_i \cdot \overrightarrow{H}_j^* \; dV \quad \begin{cases} 0 & i \neq j \\ 1 & i = j \end{cases}$$

any field due to sources in the cavity can be expressed as

$$\overrightarrow{E} = \sum_i A_i \overrightarrow{E}_i$$

$$\overrightarrow{H} = \sum_i B_i \overrightarrow{H}_i \, , \qquad \text{(A.2)}$$

where $A_i$ and $B_i$ are constants determined by the sources of excitation in the cavity.

For electric current sources, $\overrightarrow{J}$, in the cavity, the fields satisfy equations

$$\nabla \times \overrightarrow{E} = - j\omega\mu \overrightarrow{H}, \qquad\qquad \nabla \times \overrightarrow{H} = j\omega\epsilon \overrightarrow{E} + \overrightarrow{J},$$

where $\omega$ is the angular frequency of the source. The two field equations reduce to the inhomogeneous wave equation

$$\nabla \times \nabla \times \overrightarrow{E} - k^2 \overrightarrow{E} = - j\omega\mu \overrightarrow{J}, \qquad \text{(A.3)}$$

where,

$$k = \omega \sqrt{\mu \epsilon} .$$

By substituting equation (A.3) into the first of equations (A.2) and using the first of equations (A.1), it can be shown that

$$\sum_i A_i \left( \omega_i^2 - \omega^2 \right) \mu \epsilon \vec{E_i} = - j \omega \mu \vec{J} \qquad (A.4)$$

If each side of equation (A.4) is multiplied by $\vec{E_j}^*$ and integrated over the volume, V, of the cavity, the constant $A_i$ is found to be

$$A_i = - \frac{j\omega}{\omega_i^2 - \omega^2} \iiint \vec{J} \cdot \vec{E_i}^* \, dV$$

Hence, the first of equations (A.2) becomes

$$\vec{E} = \sum_i \frac{j\omega \vec{E_i}}{\omega^2 - \omega_i^2} \iiint \vec{J} \cdot \vec{E_i}^* \, dV, \qquad (A.5)$$

and the corresponding $\vec{H}$, obtained from the field equations, is

$$\vec{H} = \sum_i \frac{j\omega_i \vec{H_i}}{\omega^2 - \omega_i^2} \iiint \vec{J} \cdot \vec{E_i}^* \, dV \qquad (A.6)$$

107

Similarly, for magnetic current sources, $\overrightarrow{M}$, within the cavity, the wave equation in $\overrightarrow{H}$ is

$$\nabla \times \nabla \times \overrightarrow{H} - k^2 \overrightarrow{H} = -j\omega\epsilon \overrightarrow{M}$$

which, together with the second of equations (A.2), gives the constant $B_i$

$$B_i = \frac{-j\omega}{\omega_i^2 - \omega^2} \iiint \overrightarrow{M} \cdot \overrightarrow{H}_i^* \, dV$$

Hence, the fields due to a magnetic current source, $\overrightarrow{M}$, in a cavity are

$$\overrightarrow{H} = \sum_i \frac{j\omega \overrightarrow{H}_i}{\omega^2 - \omega_i^2} \iiint \overrightarrow{M} \cdot \overrightarrow{H}_i^* \, dV \tag{A.7}$$

$$\overrightarrow{E} = \sum_i \frac{j\omega_i \overrightarrow{E}_i}{\omega^2 - \omega_i^2} \iiint \overrightarrow{M} \cdot \overrightarrow{H}_i \, dV \tag{A.8}$$

Adding the equations (A.5) and (A.7), the total electric field due to a general source is

$$\overrightarrow{E} = \sum_i \frac{j \overrightarrow{E}_i}{\omega^2 - \omega_i^2} \iiint \left[ \omega\overrightarrow{J} \cdot \overrightarrow{E}_i^* + \omega_i \overrightarrow{M} \cdot \overrightarrow{H}_i^* \right] dV \tag{A.9}$$

Similarly, adding (A.6) and (A.8),

$$\overrightarrow{H} = \sum_i \frac{j \overrightarrow{H}_i}{\omega^2 - \omega_i^2} \iiint \left[ \omega_i \overrightarrow{J} \cdot \overrightarrow{E}_i^* + \omega\overrightarrow{M} \cdot \overrightarrow{H}_i^* \right] dV \tag{A.10}$$

## A.2    PERTURBATIONAL AND VARIATIONAL METHODS

The theory of the skin effect for metallic boundaries permits one to calculate the effect of lossy walls on the characteristic modes and characteristic values of the resonant frequencies. The relation between the tangential electric and magnetic field components on the wall is

$$\vec{n} \times \vec{E} = \frac{1+j}{\sqrt{2}} \sqrt{\frac{\mu \omega}{\sigma}} \vec{H} = Z_s \vec{H},$$

$$Z_s = R_s + jX_s,$$

(A.11)

where $\vec{n}$ is the unit normal directed into the cavity, $\mu$ and $\sigma$ are the magnetic permeability and the conductivity of the metal, and $Z_s$ is its surface impedance. The perturbational expression for the change in resonant frequency can be obtained by considering the fields in the original loss-free cavity and in the cavity with lossy walls

$$\nabla \times \vec{E_0} = -j\omega_0 \mu \vec{H_0}, \qquad \nabla \times \vec{H_0} = j\omega_0 \epsilon \vec{E_0} \qquad (A.12)$$

$$\nabla \times \vec{E} = -j\omega\mu \vec{H}, \qquad \nabla \times \vec{H} = j\omega \epsilon \vec{E} \qquad (A.13)$$

where $\vec{E_0}$, $\vec{H_0}$, $\omega_0$ represent the field and resonant frequency of the original cavity, and $\vec{E}$, $\vec{H}$, $\omega$ represent the corresponding quantities of the perturbed cavity. By scalarly multiplying the second of equations (A.13) by $\vec{E_0}$ and the first of equations (A.12) by $\vec{H}$, and by adding the two equations, the result is

$$\nabla \cdot (\vec{H} \times \vec{E_0}) = j\omega\vec{E} \cdot \vec{E_0} - j\omega_0 \mu \vec{H_0} \cdot \vec{H} \qquad (A.14)$$

Similarly, from the second of equations (A.12) and the first of equations (A.13), it can be obtained

$$\nabla \cdot (\vec{H}_0 \times \vec{E}) = j\omega u \, \vec{H} \cdot \vec{H}_0 - j\omega_0 \epsilon \, \vec{E}_0 \cdot \vec{E} \qquad (A.15)$$

where the vector identity,

$$\nabla \cdot (\vec{A} \times \vec{B}) = \vec{B} \cdot \nabla \times \vec{A} - \vec{A} \cdot \nabla \times \vec{B},$$

has been used. Finally, by adding equations (A.14) and (A.15) and integrating over the volume of the cavity, the change in resonant frequency is given by

$$\omega - \omega_0 = \frac{-j \oiint Z_s \vec{H} \cdot \vec{H}_0 \, dS}{\iiint (\epsilon \vec{E} \cdot \vec{E}_0 - u \vec{H} \cdot \vec{H}_0) \, dV} \qquad (A.16)$$

This is an exact expression for the new resonant frequency due to lossy walls when the impedance condition in equation (A.11) is valid. The perturbational method consists of replacing the unknown fields by the known $\vec{E}_0$, $\vec{H}_0$ fields. The new resonant frequency, $\omega$, becomes complex (i.e., with real and imaginary parts. The excited field near a complex resonant frequency can be calculated by considering the total field (say $\vec{E}$ field in equation (A.9)) as a function of complex frequency, p,

$$\vec{E}(p) = \sum_i \frac{j \vec{E}_i}{p^2 - \omega_i^2} \iiint \left[ p \vec{J} \cdot \vec{E}_i^* + \omega_i \vec{M} \cdot \vec{H}_i^* \right] dV$$

Assuming that the source is frequency independent, $\overrightarrow{E}(p)$ represents a meromorphic function in the complex p-plane which has simple poles at

$$p = \pm \omega_i$$

In the vicinity of the pole $\omega_i$, $\overrightarrow{E}(p)$ may be represented by a Laurent series

$$\overrightarrow{E}(p) = \frac{1}{p - \omega_i} \sum_{n=0}^{\infty} \alpha_n (p - \omega_i)^n$$

within a distance $|p - \omega_i|$ from $\omega_i$ such that

$$|p - \omega_i| \ll |\omega_i - \omega_{i \pm 1}|$$

The field $\overrightarrow{E}(p)$ may be approximated by its first term in the Laurent expansion

$$\overrightarrow{E}(p) = \frac{\alpha_0}{p - \omega_i}$$

where the residue, $\alpha_0$, is simply

$$\alpha_0 = \frac{j \overrightarrow{E_i}}{2} \iiint \left[ \overrightarrow{J} \cdot \overrightarrow{E_i^*} + \overrightarrow{M} \cdot \overrightarrow{H_i^*} \right] dV$$

and

$$\overrightarrow{E}(\omega \rightarrow \omega_i) = \frac{j \overrightarrow{E_i}}{2(\omega - \omega_i)} \iiint \left[ \overrightarrow{J} \cdot \overrightarrow{E_i^*} + \overrightarrow{M} \cdot \overrightarrow{H_i^*} \right] dV \qquad (A.17)$$

when a number of complex resonant frequencies of the perturbed cavity are near each other, as in cases of degenerate modes, the condition

$$\left| p - \omega_i \right| \leq \left| \omega_i - \omega_{i+1} \right|$$

is not fulfilled. In these cases, the total field is obtained by the same reasoning as above

$$\overrightarrow{E(\omega)} = \sum_{r=1}^{k} \frac{j \overrightarrow{E_{ir}}}{2(\omega - \omega_{ir})} \iiint \left[ \overrightarrow{J} \cdot \overrightarrow{E_{ir}^{*}} + \overrightarrow{M} \cdot \overrightarrow{H_{ir}^{*}} \right] dV \qquad (A.18)$$

$$\omega \to \omega_{ir}, \quad r = 1, 2, \ldots k$$

## A.3 DIPOLE SOURCES IN A RECTANGULAR CAVITY

The simplest example of forced fields is a loss-free rectangular cavity which is excited by a point source. Figure A.1 illustrates a rectangular cavity in Cartesian coordinates x, y, z, and of dimensions a, b, c. A z-directed dipole source is shown at a point x', y', z'.

A dipole source in arbitrary direction can always be reduced in three perpendicular components along coordinate axis. Since the selection of the coordinate axis in a rectangular cavity is arbitrary, it is sufficient to consider z-directed electric and magnetic dipoles only in order to find the fields due to arbitrary oriented sources. The total solution is the sum of individual component solutions with a cyclic exchange of coordinate axis and indices $\ell$, m, n.
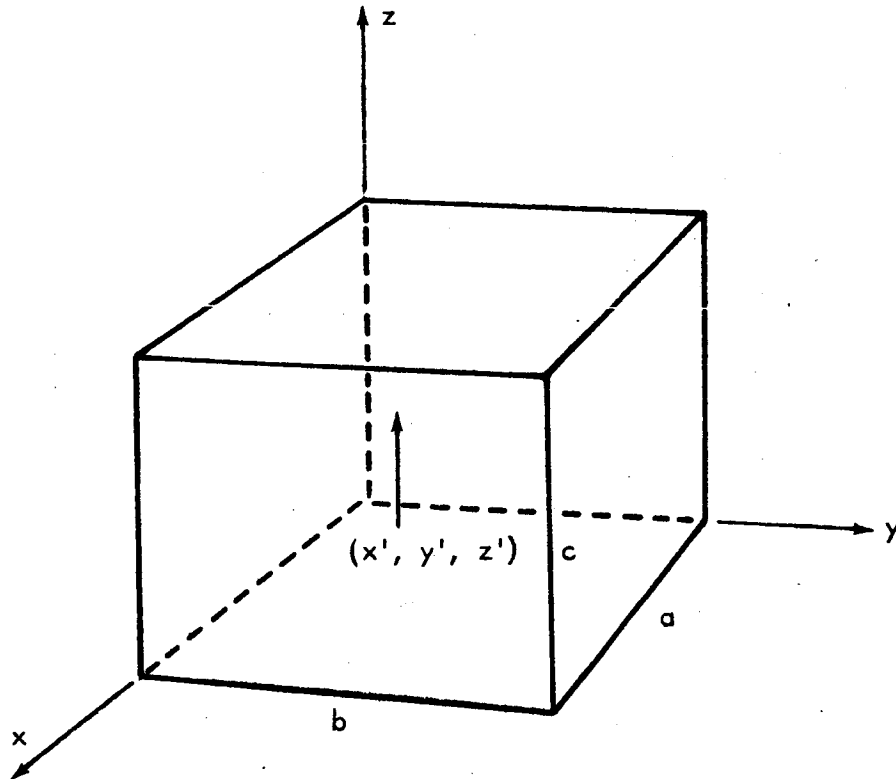
FIGURE A.1 DIPOLE SOURCE IN RECTANGULAR CAVITY

The equation (A.3) with the boundary condition, $\vec{n} \times \vec{E}_i = 0$, yield the following normalized mode vectors for loss-free rectangular cavities:

TM Modes

$$(E_x)_{\ell mn} = A_E \frac{\gamma_n \gamma_\ell}{k_{\ell mn}} \cos(\gamma_\ell x) \, \sin(\gamma_m y) \, \sin(\gamma_n z)$$

$$(E_y)_{\ell mn} = A_E \frac{\gamma_n \gamma_m}{k_{\ell mn}} \sin(\gamma_\ell x) \cos(\gamma_m y) \, \sin(\gamma_n z)$$

$$(E_z)_{\ell mn} = -A_E \frac{\gamma_\ell^2 + \gamma_m^2}{k_{\ell mn}} \sin(\gamma_\ell x) \, \sin(\gamma_m y) \, \sin(\gamma_n z)$$

TM Modes (Cont.)

$$(H_x)_{\ell mn} = -A_H \gamma_m \sin(\gamma_\ell x) \cos(\gamma_m y) \cos(\gamma_n z)$$

$$(H_y)_{\ell mn} = A_H \gamma_\ell \cos(\gamma_\ell x) \sin(\gamma_m y) \cos(\gamma_n z)$$

$$(H_z)_{\ell mn} = 0$$

TE Modes

$$(E_x)_{\ell mn} = -A_E \gamma_m \cos(\gamma_\ell x) \sin(\gamma_m y) \sin(\gamma_n z)$$

$$(E_y)_{\ell mn} = A_E \gamma_\ell \sin(\gamma_\ell x) \cos(\gamma_m y) \sin(\gamma_n z)$$

$$(E_z)_{\ell mn} = 0$$

$$(H_x)_{\ell mn} = -A_H \frac{\gamma_n \gamma_\ell}{k_{\ell mn}} \sin(\gamma_\ell x) \cos(\gamma_m y) \cos(\gamma_n z)$$

$$(H_y)_{\ell mn} = -A_H \frac{\gamma_n \gamma_m}{k_{\ell mn}} \cos(\gamma_\ell x) \sin(\gamma_m y) \cos(\gamma_n z)$$

$$(H_z)_{\ell mn} = A_H \frac{\gamma_\ell^2 + \gamma_m^2}{k_{\ell mn}} \cos(\gamma_\ell x) \cos(\gamma_m y) \sin(\gamma_n z)$$

where $A_E = \frac{1}{\sqrt{\epsilon}} A$, $A_H = \frac{j}{\sqrt{\mu}} A$

$$A = \sqrt{\frac{2^\alpha}{a\,b\,c\,(\gamma_\ell^2 + \gamma_m^2)}} \qquad \alpha = \left. \begin{array}{c} 1 \\ 0 \end{array} \right| \begin{array}{l} \ell,\ m,\ n \neq 0 \\ \ell \text{ or } m \text{ or } n = 0 \end{array}$$

$$k_{\ell mn} = \sqrt{\gamma_\ell^2 + \gamma_m^2 + \gamma_n^2} = \pi \sqrt{\left(\frac{\ell}{a}\right)^2 + \left(\frac{m}{b}\right)^2 + \left(\frac{n}{c}\right)^2}$$

$$\gamma_\ell = \frac{\pi \ell}{a}, \quad \gamma_m = \frac{\pi m}{b} \quad \gamma_n = \frac{\pi n}{c}$$

A point source which represents an electric dipole directed in the z-direction is described by a current distribution of the form

$$J_z = I L \ \delta(x - x') \ \delta(y - y') \ \delta(z - z')$$

where I is the current and L is the length of the dipole, $\delta(x - x')$ is the Dirack delta function

Since only TM modes are excited in the cavity, the volume integral in equations (A.5), (A.6) reduces to

$$\iiint \vec{J} \cdot \vec{E}_i^* \ dv = \iiint J_z (E_z^*)_{\ell mn} \ dx \ dy \ dz = I L \left[ E_z^* (x', y', z') \right]_{\ell mn}$$

The fields are:

$$E_x = -j \frac{4 I L k}{a b c} \sqrt{\frac{\mu}{\epsilon}} \sum_{\ell mn} \frac{2^\alpha}{k^2 - k_{\ell mn}^2} \frac{\gamma_n \gamma_\ell}{k_{\ell mn}^2} \cos(\gamma_\ell x) \sin(\gamma_\ell x') \sin(\gamma_m y)$$

$$x \sin(\gamma_m y') \sin(\gamma_n z) \cos(\gamma_n z')$$

$$E_y = -j \frac{4 I L k}{a b c} \sqrt{\frac{\mu}{\epsilon}} \sum_{\ell mn} \frac{2^\alpha}{k^2 - k_{\ell mn}^2} \frac{\gamma_m \gamma_n}{k_{\ell mn}^2} \sin(\gamma_\ell x) \sin(\gamma_\ell x') \cos(\gamma_m y)$$

$$x \sin(\gamma_m y') \sin(\gamma_n z) \cos(\gamma_n z')$$

$$E_z = j \frac{4 I L k}{a b c} \sqrt{\frac{\mu}{\epsilon}} \sum_{\ell mn} \frac{2^\alpha}{k^2 - k_{\ell mn}^2} \frac{\gamma_\ell^2 + \gamma_m^2}{k_{\ell mn}^2} \sin(\gamma_\ell x) \sin(\gamma_\ell x') \sin(\gamma_m y)$$

$$x \sin(\gamma_m y') \cos(\gamma_n z) \cos(\gamma_n z')$$

$$H_x = -\frac{4\,I\,L}{a\,b\,c} \sum_{\ell mn} \frac{2^\alpha\, \gamma_m}{k^2 - k_{\ell mn}^2} \sin(\gamma_\ell\, x) \sin(\gamma_\ell\, x') \cos(\gamma_m\, y)$$

$$x \sin(\gamma_m\, y') \cos(\gamma_n\, z) \cos(\gamma_n\, z')$$

$$H_y = \frac{4\,I\,L}{a\,b\,c} \sum_{\ell mn} \frac{2^\alpha\, \gamma_\ell}{k^2 - k_{\ell mn}^2} \cos(\gamma_\ell\, x) \sin(\gamma_\ell\, x') \sin(\gamma_m\, y)$$

$$x \sin(\gamma_m\, y') \cos(\gamma_n\, z) \cos(\gamma_n\, z')$$

$$H_z = 0$$

Similarly, a point source which represents a z-directed magnetic dipole is described by a magnetic current distribution of the form

$$M_z = m\,\delta(x - x')\,\delta(y - y')\,\delta(z - z')$$

where m is the dipole moment. For a small loop in xy plane with a current I and area S,

$$m = j\omega\mu\, I\,S$$

The integral in equations (A.7), (A.8) becomes

$$\iiint \overline{M} \cdot \overline{H_i}^* \, dv = \iiint M_z \left(H_z^*\right)_{\ell mn} dx\, dy\, dz = j\omega\mu\, I\,S \left[ H_z^* (x', y', z') \right]_{\ell mn}$$

A z-directed magnetic dipole excite only TE modes, and the fields are given by:

$$E_x = -j \, \frac{4IS\,k}{a\,b\,c} \sqrt{\frac{\mu}{\epsilon}} \sum_{\ell mn} \frac{2^\alpha \, \gamma_m}{k^2 - k\ell_{mn}^2} \cos(\gamma_\ell \, x) \cos(\gamma_\ell \, x') \sin(\gamma_m \, y) \cos(\gamma_m \, y') \sin(\gamma_n \, z) \sin(\gamma_n \, z')$$

$$E_y = j \, \frac{4IS\,k}{a\,b\,c} \sqrt{\frac{\mu}{\epsilon}} \sum_{\ell mn} \frac{2^\alpha \, \gamma_\ell}{k^2 - k\ell_{mn}^2} \sin(\gamma_\ell \, x) \cos(\gamma_\ell \, x') \cos(\gamma_m \, y) \cos(\gamma_m \, y') \sin(\gamma_n \, z) \sin(\gamma_n \, z')$$

$$E_z = 0$$

$$H_x = \frac{4IS\,k^2}{a\,b\,c} \sum_{\ell mn} \frac{2^\alpha}{k^2 - k\ell_{mn}^2} \frac{\gamma_n \, \gamma_\ell}{k\ell_{mn}^2} \sin(\gamma_\ell \, x) \cos(\gamma_\ell \, x') \cos(\gamma_m \, y) \cos(\gamma_m \, y') \cos(\gamma_n \, z) \sin(\gamma_n \, z')$$

$$H_y = \frac{4IS\,k^2}{a\,b\,c} \sum_{\ell mn} \frac{2^\alpha}{k^2 - k\ell_{mn}^2} \frac{\gamma_m \, \gamma_n}{k\ell_{mn}^2} \cos(\gamma_\ell \, x) \cos(\gamma_\ell \, x') \sin(\gamma_m \, y) \cos(\gamma_m \, y') \cos(\gamma_n \, z) \sin(\gamma_n \, z')$$

$$H_z = -\frac{4IS\,k^2}{a\,b\,c} \sum_{\ell mn} \frac{2^\alpha}{k^2 - k\ell_{mn}^2} \frac{\gamma_\ell^2 + \gamma_m^2}{k\ell_{mn}^2} \cos(\gamma_\ell \, x) \cos(\gamma_\ell \, x') \cos(\gamma_m \, y) \cos(\gamma_m \, y') \sin(\gamma_n \, z) \sin(\gamma_n \, z')$$

## A.4    DIPOLE SOURCES IN CYLINDRICAL CAVITY

Another example of forced fields in a loss-free cavity is a dipole source in circular cylindrical cavity.  Figure A.2 shows the cylindrical coordinate system r, $\emptyset$, z and the dimensions of the cavity with radius a and height h.   The coordinates of the source are r', $\emptyset$', z'.
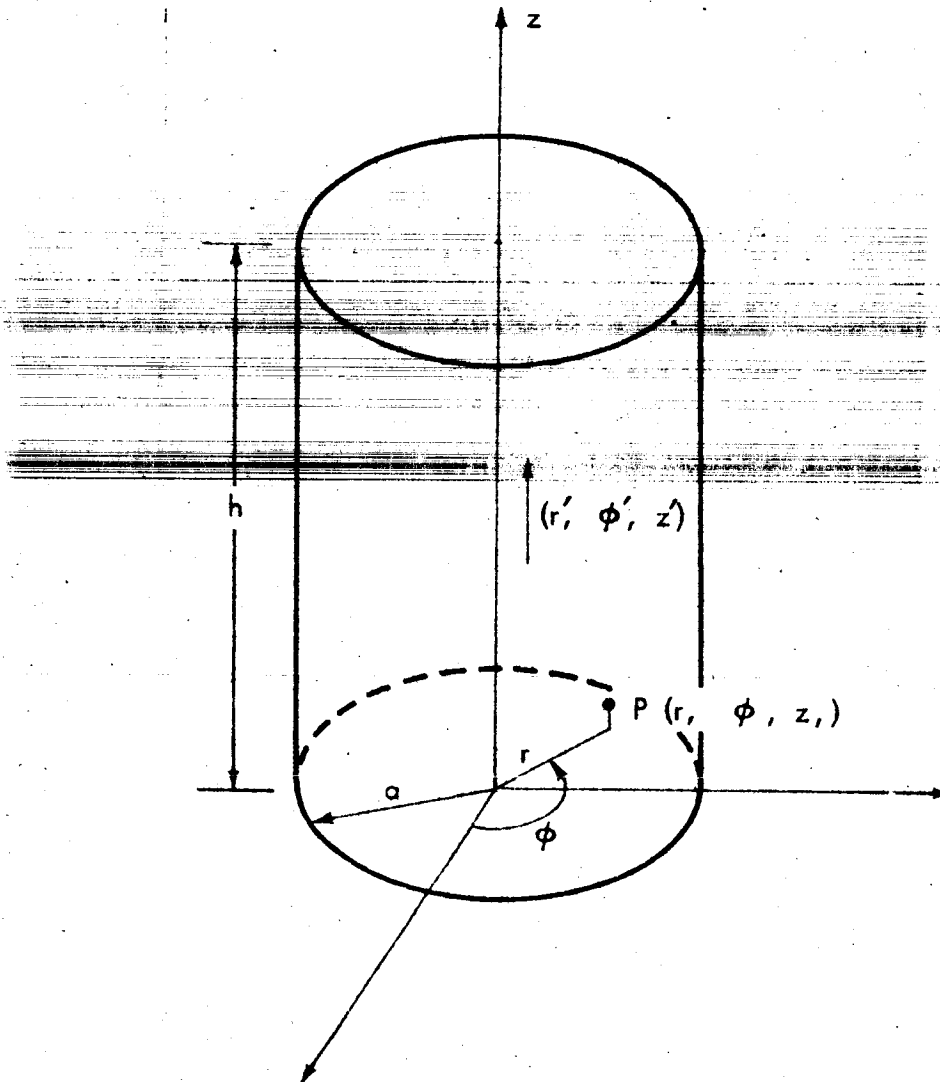
FIGURE A.2

The normalized mode vectors for the TM modes are:

$$(E_r)^E_{\ell mn} = A_E \, \frac{\gamma_n \, \gamma^E_{\ell mn}}{k^E_{\ell mn}} \, J'_\ell \, (\gamma^E_{\ell m} r) \begin{Bmatrix} \cos \ell \varphi \\ \sin \ell \varphi \end{Bmatrix} \sin (\gamma_n z)$$

$$(E_\varphi)^E_{\ell mn} = A_E \, \frac{\gamma_n}{k^E_{\ell mn}} \, J_\ell (\gamma^E_{\ell m} r) \begin{Bmatrix} -\sin \ell \varphi \\ \cos \ell \varphi \end{Bmatrix} \sin (\gamma_n z)$$

$$(E_z)^E_{\ell mn} = -A_E \, \frac{(\gamma^E_{\ell m})^2}{k^E_{\ell mn}} \, J_\ell (\gamma^E_{\ell m} r) \begin{Bmatrix} \cos \ell \varphi \\ \sin \ell \varphi \end{Bmatrix} \cos (\gamma_n z)$$

$$(H_r)^E_{\ell mn} = A_H \, \frac{\ell}{r} \, J_\ell (\gamma^E_{\ell m} r) \begin{Bmatrix} \sin \ell \varphi \\ -\cos \ell \varphi \end{Bmatrix} \cos (\gamma_n z)$$

$$(H_\varphi)^E_{\ell mn} = A_H \, \gamma^E_{\ell m} \, J'_\ell (\gamma^E_{\ell m} r) \begin{Bmatrix} \cos \ell \varphi \\ \sin \ell \varphi \end{Bmatrix} \cos (\gamma_n z)$$

$$(H_z)^E_{\ell mn} = 0$$

where, $k^E_{\ell mn} = \sqrt{(\gamma^E_{\ell m})^2 + \gamma_n^2} = \sqrt{\left(\frac{y_{\ell m}}{a}\right)^2 + \left(\frac{n \pi}{h}\right)^2}$

$$A_E = \sqrt{\frac{1}{\epsilon}} \, A, \quad A_H = \frac{j}{\sqrt{\mu}} \, A, \quad A = \frac{1}{y_{\ell m} \, J'_\ell \, (y_{\ell m})} \sqrt{\frac{2^\alpha}{\pi h}}$$

$J_\ell (\gamma^E_{\ell m} r)$ is the Bessel Function of order $\ell$ and argument $(\gamma^E_{\ell m} r)$, $J_\ell '(\gamma^E_{\ell m} r)$ is its derivative with respect to argument. The quantity, $y_{\ell m}$, is the mth zero of the equation,

$$J_\ell (y_{\ell m}) = 0$$

and

$$\alpha = \begin{cases} 0 \text{ for } \ell = 0, \ n = 0 \\ 1 \quad\quad \ell = 0, \ n \neq 0 \text{ or } \ell \neq 0, \ n = 0 \\ 2 \quad\quad \ell \neq 0, \ n \neq 0 \end{cases}$$

The normalized mode vectors for the TE modes are:

$$(E_r)^H_{\ell mn} = B_E \frac{\ell}{r} J_\ell (\gamma^H_{\ell m} r) \begin{Bmatrix} -\sin \ell \varphi \\ \cos \ell \varphi \end{Bmatrix} \sin (\gamma_n z)$$

$$(E_\varphi)^H_{\ell mn} = B_E \gamma^H_{\ell m} J'_\ell (\gamma^H_{\ell m} r) \begin{Bmatrix} \cos \ell \varphi \\ \sin \ell \varphi \end{Bmatrix} \sin (\gamma_n z)$$

$$(E_z)^H_{\ell mn} = 0$$

$$(H_r)^H_{\ell mn} = B_H \frac{\gamma_n \gamma^H_{\ell m}}{k^H_{\ell mn}} J'_\ell (\gamma^H_{\ell m} r) \begin{Bmatrix} \cos \ell \varphi \\ \sin \ell \varphi \end{Bmatrix} \cos (\gamma_n z)$$

$$(H_\varphi)^H_{\ell mn} = B_H \frac{\gamma_n}{k^H_{\ell mn}} \frac{\ell}{r} J_\ell (\gamma^H_{\ell mn} r) \begin{Bmatrix} -\sin \ell \varphi \\ \cos \ell \varphi \end{Bmatrix} \cos (\gamma_n z)$$

$$(H_z)^H_{\ell mn} = B_H \frac{(\gamma^H_{\ell mn})^2}{k^H_{\ell mn}} J_\ell (\gamma^H_{\ell mn} r) \begin{Bmatrix} \cos \ell \varphi \\ \sin \ell \varphi \end{Bmatrix} \sin (\gamma_n z)$$

where,

$$k^H_{\ell mn} = \sqrt{(\gamma^H_{\ell mn})^2 + \gamma_n^2} = \sqrt{\left(\frac{y'_{\ell m}}{a}\right)^2 + \left(\frac{n\pi}{h}\right)^2}$$

$$B_E = \frac{1}{\sqrt{\epsilon}} B, \quad B_H = \frac{i}{\sqrt{\mu}} B, \quad B = \frac{1}{J_\ell (y'_{\ell m})} \sqrt{\frac{2^\alpha}{\pi h \left| (y'_{\ell m})^2 - \ell^2 \right|}}$$

$$\alpha = \begin{cases} 1 \text{ for } \ell = 0 \\ 2 \quad \ell \neq 0 \end{cases} \quad \text{and} \quad J'_\ell (y'_{\ell m}) = 0$$

As seen from the above for $\ell = 0$, there are two mode vectors for each TM and TE mode, one with $\cos \ell \phi$ and the other with $\sin \ell \phi$ dependency. This degeneracy is removed if the excitation problem is considered or if the cavity has perturbations. Assuming that the radiating equipment is mounted on the curved surface, only r-directed electric dipole and $\phi$- and z-directed magnetic dipoles are important. For the r-directed electric dipole point source, the current distribution is,

$$J_r = I L \frac{\delta (r - r') \delta (\varphi - \varphi') \delta (z - z')}{r}$$

The total field is the sum of TM and TE modes; the volume integral in equations (A.5), (A.6) becomes,

$$\iiint_V \vec{J} \cdot \vec{E_i} \, dv = \iiint J_r \left[ (E_r^E)_{\ell mn} + (E_r^H)_{\ell mn} \right] dv = I L \left\{ E_r^E (r', \varphi', z') + E_r^H (r', \varphi', z') \right\}_{\ell mn}$$

The source coordinate $\emptyset'$ may be assumed zero, $\emptyset' = 0$, without any loss of generality. Since $E_r$ must be a symmetric function of $\emptyset$, the degeneracy is removed since $\cos \ell \emptyset$ must be used for the $E_r$ field component. The total field in the cavity is given by,

$$\vec{E} = I L \sum_{\ell mn} \left\{ \frac{j \omega \vec{E}^E_{\ell mn}}{\omega^2 - (\omega^E_{\ell mn})^2} \left[ E^E_r (r', \varphi', z') \right]_{\ell mn} \right. $$

$$ \left. + \frac{j \omega \vec{E}^H_{\ell mn}}{\omega^2 - (\omega^H_{\ell mn})^2} \left[ E^H_r (r', \varphi', z') \right]_{\ell mn} \right\} $$

$$\vec{H} = I L \sum_{\ell mn} \left\{ \frac{j \omega^E_{\ell mn} \vec{H}^E_{\ell mn}}{\omega^2 - (\omega^E_{\ell mn})^2} \left[ E^E_r (r', \varphi', z') \right]_{\ell mn} \right. $$

$$ \left. + \frac{j \omega^H_{\ell mn} \vec{H}^H_{\ell mn}}{\omega^2 - (\omega^H_{\ell mn})^2} \left[ E^H_r (r', \varphi', z') \right]_{\ell mn} \right\} $$

$$\vdots$$

A z-directed magnetic dipole has TE modes only. Assuming the magnetic current distribution as before,

$$M_z = j \omega \mu 1 S \frac{\delta (r - r') \delta (\varphi - \varphi') \delta (z - z')}{r}$$

the volume integral in equations (A.7), (A.8) is

$$\iiint \vec{M} \cdot \vec{H_i} \, dv = \iiint M_z \, (H_z^H)_{\ell mn} \, dv = j \omega \mu \, I \, S \left[ H_z^H \, (r', \varphi', z') \right]_{\ell mn}$$

The field becomes

$$\vec{E} = j \omega \mu \, I \, S \sum_{\ell mn} \frac{j \omega_{\ell mn}^H \; \vec{E}_{\ell mn}^H}{\omega^2 - (\omega_{\ell mn}^H)^2} \left[ H_z^H \, (r', \varphi', z') \right]_{\ell mn}$$

$$\vec{H} = j \omega \mu \, I \, S \sum_{\ell mn} \frac{j \omega \; \vec{H}_{\ell mn}^H}{\omega^2 - (\omega_{\ell mn}^H)^2} \left[ H_z^H \, (r', \varphi', z') \right]_{\ell mn}$$

Since $H_z$ must be symmetric about the source coordinate $\emptyset'$, only cos $\ell\emptyset$ dependency is used ($\emptyset' = 0$) for $H_z$ with corresponding cos $\ell\emptyset$ or sin $\ell\emptyset$ functions for the other field components.

For the $\emptyset$-directed magnetic dipole, both TM and TE modes are required. Since $H_\emptyset$ is an odd function of $\emptyset$, it has sin $\ell\emptyset$ dependency,

$$(H_\varphi^E)_{\ell mn} = A_H \, \gamma_{\ell m}^E \; J'_\ell \, (\gamma_{\ell m}^E \, r) \; \sin(\ell\varphi) \cos(\gamma_n z)$$

$$(H_\varphi^H)_{\ell mn} = -B_H \, \frac{\gamma_n}{k_{\ell mn}^H} \, \frac{\ell}{r} \, J_\ell \, (\gamma_{\ell m}^E \, r) \; \sin(\ell\varphi) \cos(\gamma_n z)$$

The field for the $\phi$-directed magnetic dipole is given by,

$$\vec{E} = j\omega\mu I S \sum_{\ell mn} \left\{ \frac{j\omega \omega_{\ell mn}^E \; \vec{E}_{\ell mn}^E}{\omega^2 - (\omega_{\ell mn}^E)^2} \left[ H_\varphi^E (r', \varphi', z') \right]_{\ell mn} + \frac{j\omega \omega_{\ell mn}^H \; \vec{E}_{\ell mn}^H}{\omega^2 - (\omega_{\ell mn}^H)^2} \right.$$

$$\left. \left[ H_\varphi^H (r', \varphi', z') \right]_{\ell mn} \right\}$$

$$\vec{H} = j\omega\mu I S \sum_{\ell mn} \left\{ \frac{j\omega \vec{H}_{\ell mn}^E}{\omega^2 - (\omega_{\ell mn}^E)^2} \left[ H_\varphi^E (r', \varphi', z') \right]_{\ell mn} + \frac{j\omega \vec{H}_{\ell mn}^H}{\omega^2 - (\omega_{\ell mn}^H)^2} \right.$$

$$\left. \left[ H_\varphi^H (r', \varphi', z') \right]_{\ell mn} \right\}$$

# APPENDIX B

## DEVELOPMENT OF EMITTER AND
## RECEPTOR SUSCEPTIBILITY SPECTRA

The information in this appendix represents the results of Air Force funded study on the X 20 program (contract AF33(657) 7132).

Classification of all circuits into a few basic types greatly simplifies the procedure of developing emitter and receptor susceptibility spectra for use in a computer-prediction program. Thus, it has been decided to classify all circuits into one of six basic types. These basic circuit types are:

1) Power,
2) Servo,
3) Signal,
4) Switch,
5) Squib,
6) Modulated.

A description of the basic circuit types and the associated spectra is given in the following sections.

## B.1     EMITTER SPECTRA

### B.1.1     Power Circuits

Power circuits are those circuits which are used to transmit the primary power of the vehicle from its source to the using equipment or load.

Power circuit interference is produced by arcing and voltage changes in reactive loads, and by the commutation of diodes or rotating contacts. Due to the high currents switched, the resultant interference voltages will be large in magnitude. The short switching times

involved produce broad frequency spectra. Specifications prescribing
a safe level have been adopted to reduce the probability of power cir-
cuit interference. The limits of MIL-I-26600 have been used as the
assumed generated spectra for power circuits. The broadband con-
ducted measurements of MIL-I-26600 have been extended upward to
100 Mc and downward to zero frequency. The spectra limit is shown
in Figure B.1.
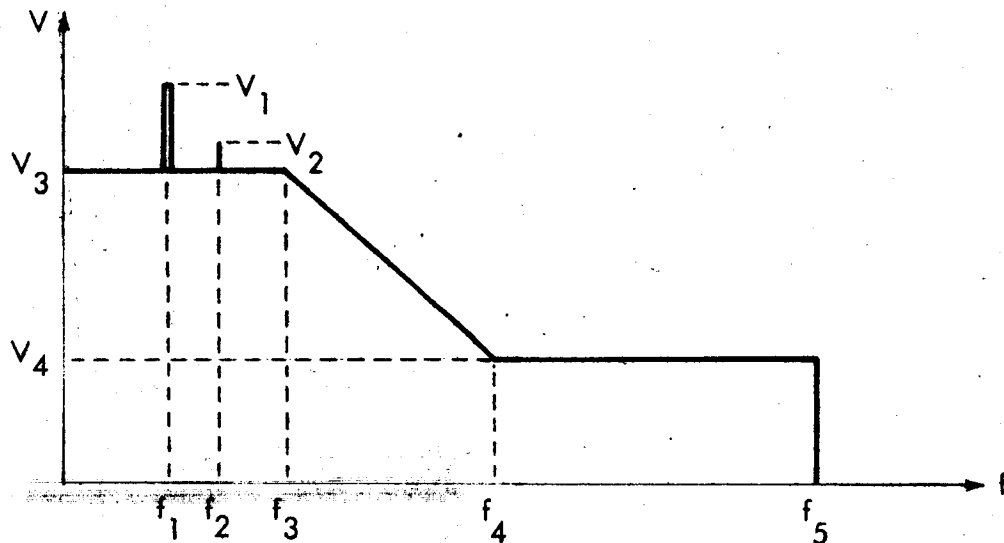


FIGURE B.1    EMITTER SPECTRUM FOR POWER CIRCUITS

AC
Only
$\{$

$V_1$ = voltage amplitude of supply

$f_1$ = frequency of supply (use a band run-
ning from $f_1$ - frequency tolerance
to $f_1$ + frequency tolerance)

DC
Only
$\{$

$V_2$ = maximum allowable ripple voltage
if > 134 db/u v

$f_2$ = frequency of ripple voltage

Also, in Figure B.1,

$$V_3 = 134 \text{ db/}\mu v$$

$$V_4 = 81 \text{ db/}\mu v$$

$$f_3 = 15 \text{ Kc}$$

$$f_4 = 2 \text{ Mc}$$

$$f_5 = 100 \text{ Mc}$$

B.1.2    Switch Circuits

Switch circuits are very much like power circuits in that most power circuits are switched at some time. To avoid conflicting entries, it was necessary to define power circuits as those which would be switched normally only once, and would usually be carrying a steady current. The switch category also includes switches which may be operated only once such as those controlling alarm lights, squibs, ready strings, etc. These circuits are sources of interference, but are virtually unsusceptible to it.

Switch circuit interference is produced because of the reactance of source and load, together with the nonlinear noise generating characteristics of the switching arc. Some switches will not be associated with power circuitry, and test data will be available as a result of qualification testing to either MIL-I-6181D or MIL-I-26600. Where test data is not available, it is reasonable to assume that these switches will produce the same interference spectra as other switches in similar applications.

Therefore, test data from switching operations on previous programs was used as the best available. A review of the data showed that switches could be divided into six general types according to the circuit in which they were used. The TYPE 1 switch circuit consists of a switch (either solid state or toggle) which supplies power to a light.

The TYPE 2 circuit consists of a switch which controls power to acti-vate a relay. The TYPE 3 circuit activates a relay and a light in series. Types 1, 2, and 3 reduced to approximately the same spec-trum and were considered to have the same spectrum in the computer program. The TYPE 4 switch is used with a high-impedance load possessing a large reactive component. The TYPE 5 switch controls a low-impedance load with very little reactance. The TYPE 6 switch controls 400-cycle power to an electronic equipment rack.

The actual measured spectra for switches will exhibit many discon-tinuities, with peaks at some frequencies and nulls at others. Since the peaks and nulls for different circuits do not exactly coincide, the curve shown in Figure B.2 is a summary of the anticipated peak values. Again, either test data or definite design information can be used by the computer to evaluate the need for suppression of switch generated interference.
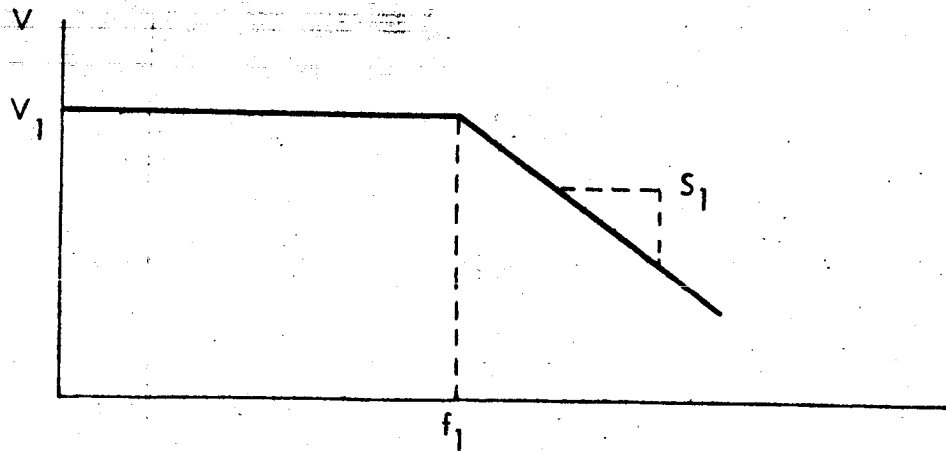


FIGURE B.2    EMITTER SPECTRUM FOR SWITCH CIRCUITS

For switch types 1, 2, and 3:

$$V_1 = 140 \text{ db}/\mu v; \quad f_1 = 7 \text{ Kc}; \quad S_1 = 20 \text{ db/decade}$$

For switch type 4:

$$V_1 = 140 \text{ db}/\mu v; \quad f_1 = 250 \text{ Kc}; \quad S_1 = 20 \text{ db/decade}$$

For switch type 5:

$$V_1 = 150 \text{ db}/\mu v; \quad f_1 = 15 \text{ Kc}; \quad S_1 = 20 \text{ db/decade}$$

For switch type 6:

$$V_1 = 140 \text{ db}/\mu v; \quad f_1 = 200 \text{ Kc}; \quad S_1 = 32 \text{ db/decade}$$

## B.1.3    Signal Circuits

Signal circuits are used to monitor or control the system or carry information. Occasionally, the amplitude of these signals is sufficient to produce interference to other circuitry. Signal circuits have been divided into three sub-types: AC signal, DC signal, and pulse signal. For this study, a DC signal has been defined as one in which the modulation produces no zero crossings, and which is longer than one second in duration. An AC signal has zero crossings, and a pulse signal is less than one second duration.

For pulse signals, the worst case is the square-cornered trapezoidal pulse shown in Figure B.3(a). The voltage spectrum of this pulse, obtained from the Fourier transform of the time function, is given in Figure B.3(b). For the purpose of this study, the negative lobes of the spectrum are considered positive since interference voltage is the primary interest. The "nuisance" value of the circuit is more readily derived through use of the curve of maximum amplitudes shown as $\emptyset(f)$ in Figure B.3(b).

For the AC and DC signals, the worst case would be a continuous spectrum throughout the modulation bandwidth, as shown in Figure B.4. Any actual modulation that would be used would consist of discrete spectral lines of varying amplitudes spaced at intervals within the modulation bandwidth. The assumption of a continuous spectrum at the maximum amplitude will, therefore, indicate a greater probability of interference than could be experienced by the system.

### B.1.4 Modulated Signal Circuits

Modulated signal circuits are those which are used to transmit information within or between communication equipments. These circuits are usually very sensitive and relatively susceptible to interference.

Modulated signal circuits normally transmit more information at higher rates than signal circuits. This is accomplished by utilizing more complex modulation techniques and greater bandwidth. There are three types of modulation considered: (1) frequency modulation (FM), (2) amplitude modulation (AM), and (3) pulse modulation (normally pulse-code modulation - PCM). Each of these modulation techniques is used extensively and combinations of any two, and sometimes all three, may be encountered. This study is concerned with only the video-frequency modulation frequencies. The most complex modulation that can occur in digital circuits on the FM and AM channels is due to white noise. Therefore, if white noise is assumed to occupy the complete bandwidth of the modulating signal, the output of the modulator will produce the most system interference, and hence, the worst-case condition.

In frequency modulation, the frequency of the carrier signal is changed by an amount proportional to the amplitude of the modulating signal. Then, since the amplitude distribution of the white noise modulating signal is Gaussian, the frequency spectrum of the modulated signal would also be Gaussian. The resulting spectrum is shown in Figure B.5.

(a)



(b)
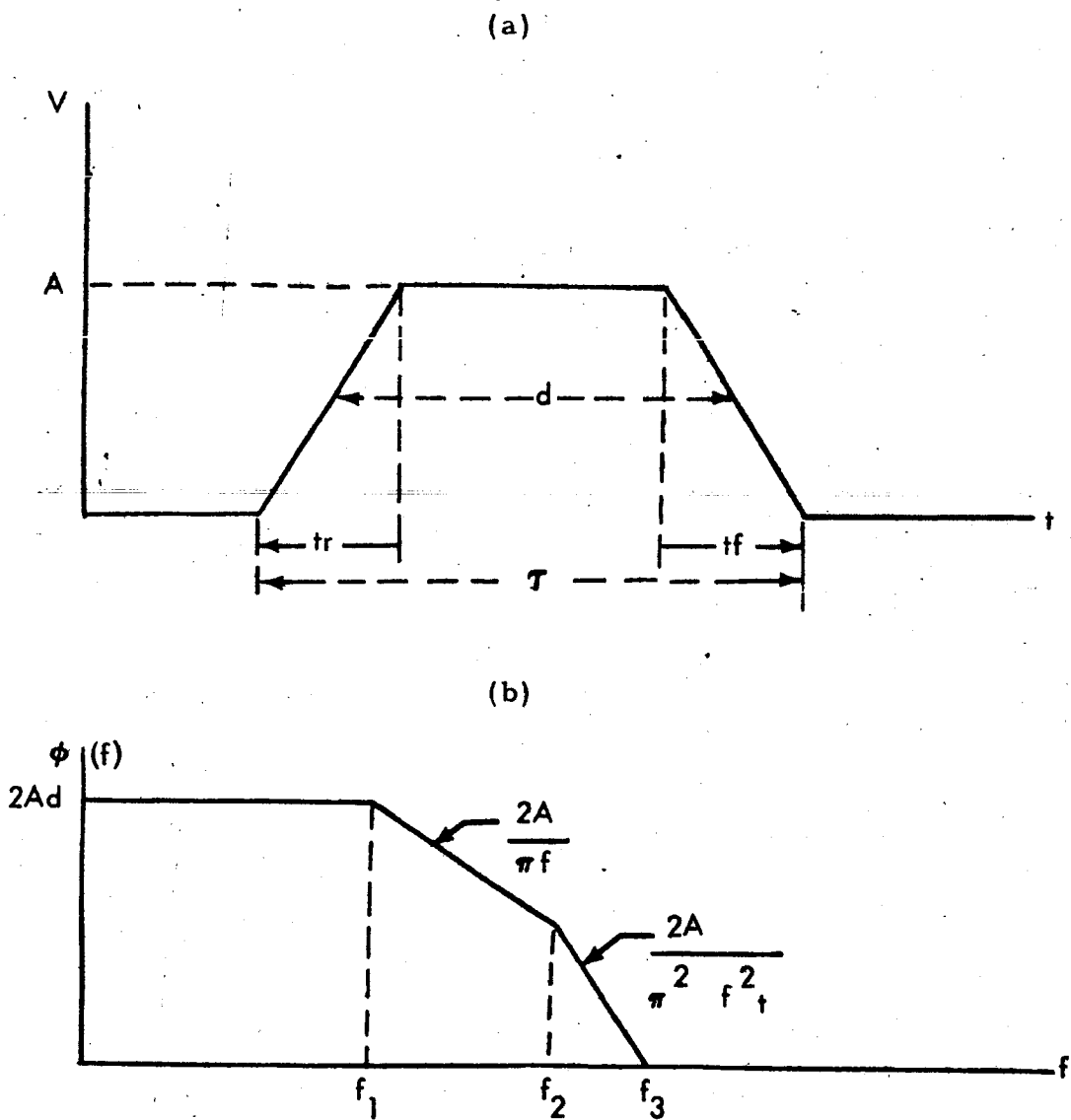


FIGURE B.3    EMITTER SPECTRUM FOR PULSE CIRCUITS

$f_1 = 1/\pi d$

$f_2 = \dfrac{2A}{\pi^2 f^2 t}$

$f_3$ = frequency when curve reaches -20 db

d = duration of pulse at 50% points

t = average of rise and fall time
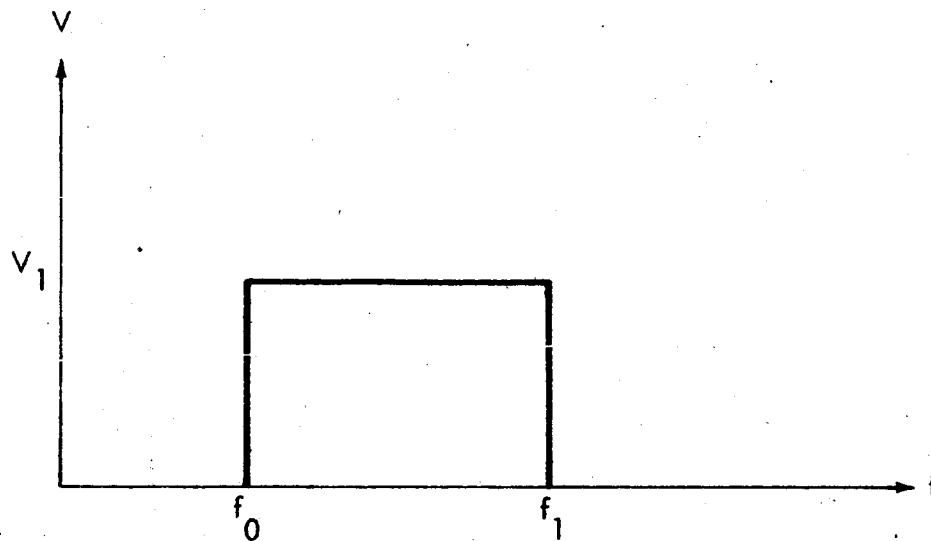
FIGURE B.4    EMITTER SPECTRA FOR DIGITAL CIRCUITS

$V_1$  =  maximum voltage amplitude

$f_0$  =  lower bandpass limit (0 for DC)

$f_1$  =  upper bandpass limit (bandwidth for DC,
             also $f_1$ may be 0 for some DC cases in
             which case there is no coupling possible)

In amplitude modulation, the amplitude of the carrier is proportional
to the amplitude of the input signal.  This process produces two side-
bands centered about the carrier frequency containing the same fre-
quency components as the modulating signal.  White-noise modulation
would have the spectrum shown in Figure B.6.

In pulse-code modulation, the input information is always transformed
into a digital format.  Each parameter is assigned a prescribed num-
ber of discrete values represented by a binary code.  The resultant
PCM signal is a train of pulses with varying widths and repetition
frequencies.

The frequency spectrum of a pulse train consists of a series of dis-
crete spectral lines spaced by the prf with amplitudes following a
curve similar to that of Figure B.3(b). In PCM, however, the prf
is never constant and a continuous shifting of these lines results.
Therefore, a more indicative spectrum and the worst-case condition
would be a continuous spectrum as shown in Figure B.3(b). For the
PCM case, the curve of maximum amplitude must be used since the
pulse width can vary by a factor of n. In computing the worst-case
spectrum for a PCM signal, the widest pulse width should be used to
compute the initial ordinate, and the shortest to compute the curve of
maximum amplitudes. This will produce a spectrum with the maximum
amplitude and the slowest roll-off.
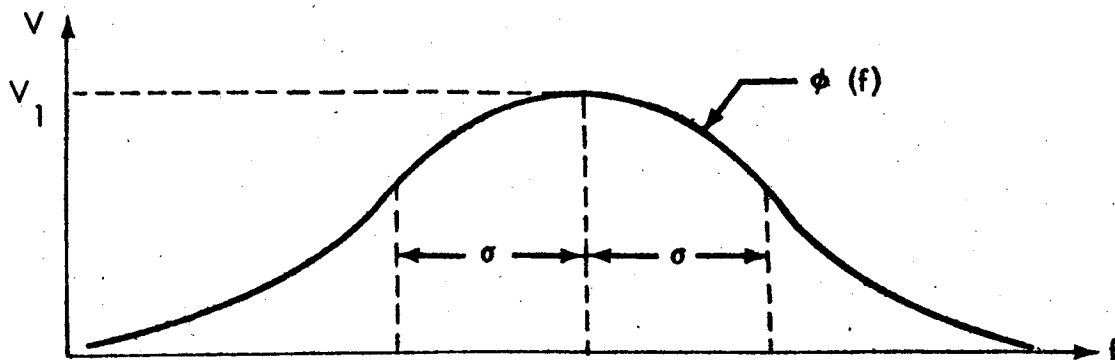


FIGURE B.5    EMITTER SPECTRUM FOR FREQUENCY
MODULATED CIRCUITS

where

$$\varphi(f) = \left[\frac{V^1}{2\pi}\right]\left[e^{-X^2/2}\right]$$

with                                              and

$$X = \frac{f - f_c}{\sigma} \qquad\qquad V^1 = V\left[J_0\left(\frac{\sigma}{\mu}\right)\right]$$

when $\sigma$ = maximum deviation frequency; $\mu$ = highest
modulating frequency; and $V$ = maximum
amplitude of fundamental $f_c$ .
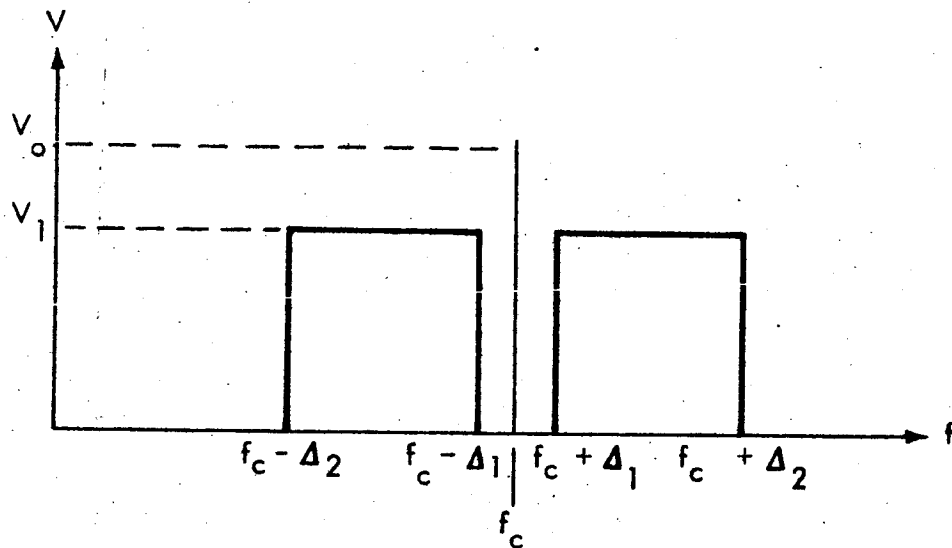
FIGURE B.6   EMITTER SPECTRUM FOR AMPLITUDE
MODULATED CIRCUITS

$V_0$ = maximum amplitude of fundamental $f_c$

$V_1 = \dfrac{m V_0}{2}$ ,  if $m = \%$ modulation/100

$\Delta_1$ = lowest modulating frequency

$\Delta_2$ = highest modulating frequency

## B.1.5   Servo Mechanism Circuits

Servo circuits are those circuits which are used to control the path of
the vehicle. The heart of most servo systems is an amplifier and an
electro-mechanical device. The electro-mechanical devices are
usually not susceptible to interferences, but may be sources. The
amplifier, however, may be susceptible to interference. There are
normally three signals associated with a servo system: the command
input signal, the feedback signal, and the error signal. Interference

generated by servo circuits is similar to that of signal circuitry. The
information rate in servos is low and the modulation bandwidth narrow.
Because the input and the feedback signals of a servo system are nor-
mally very low, they produce little interference and can be neglected.
However, the error signal may be of sufficient amplitude to produce
interference, since it is used to actuate an electro-mechanical device.
As is the case with digital signals, the nature of the interference is
dependent upon the particular signal, and several different signal
spectra may occur. Hence, it is desirable to use worst-case
approximations for the representative spectra.

Although the servo signals will normally produce a very simple spec-
trum, consisting of a few spectral lines of various amplitudes, the
simplified worst case is white noise. The probability of an interfer-
ence indication will be much greater using this assumption than it
would in system operation. The spectrum of a servo circuit signal
may be approximated by the curves in Figure B.7.

B.1.6     Squib Circuits

Squib circuits are those circuits used to fire electro-explosive
devices such as rocket igniter, explosive valves, explosive bolts, etc.
Since squibs are essentially passive devices, they are not sources of
interference; however, they are very susceptible.
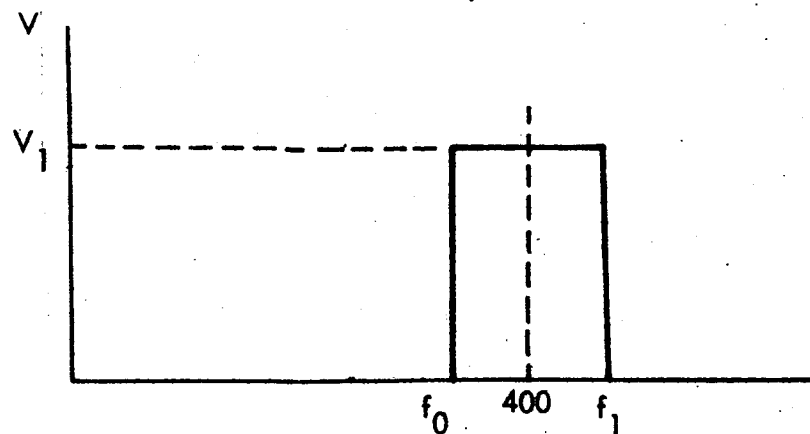


FIGURE B.7     EMITTER SPECTRA FOR SERVO CIRCUITS

In Figure B.7,

$$V_1 = \text{maximum voltage amplitude}$$

$$f_0 = \text{Rx passband lower limit}$$

$$f_1 = \text{Rx passband upper limit}.$$

## B.2 RECEPTOR SUSCEPTIBILITY CRITERIA

### B.2.1 Power Circuits

Power circuits are generally not susceptible to interference, although they can conduct the interference to susceptible circuits. The conducted susceptibility requirements of MIL-I-26600 have been extrapolated into the lower frequencies to produce the curve shown in Figure B.8. When actual test data is available, it can be used to provide a more realistic analysis.

It should be noted that the susceptibility requirements of MIL-I-26600 are not exact for a study of system compatibility. The methods of test described in that specification employ sinusoidal signals, but interference normally encountered on system power lines is a combination of impulsive as well as sinusoidal signals. Since most circuits are responsive to the total energy received, the response to a single sinusoid is only an approximation of the response to normally encountered interference.

This situation has developed largely because a better method is not available; since each source of impulsive interference produces a different spectrum, it is difficult to describe a universal spectrum accurately. Further, if a universal spectrum could be described, the problems of generating it and inserting it into the circuit would seriously hamper its utilization. It may be assumed then that this limitation will always restrict the absolute applicability of this study.
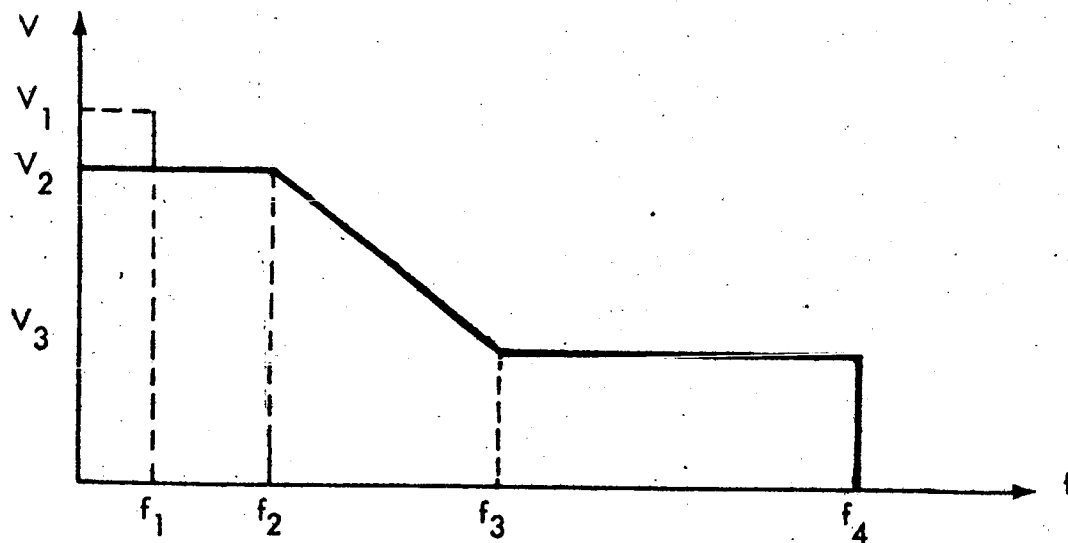
FIGURE B.8     RECEPTOR SUSCEPTIBILITY SPECTRUM
FOR POWER CIRCUITS

$V_1$ = voltage of directly connected supply, if AC

$V_2$ = 130 db/μ v

$V_3$ = 100 db/μ v

$f_1$ = frequency of directly connected supply
(use band as for generated spectrum)

$f_2$ = 15 Kc

$f_3$ = 150 Kc

$f_4$ = 400 Kc

B.2.2     Signal Circuits

Signal circuits are often sensitive due to the normally low-level input signals. Although these circuits may be susceptible to electro-interference, no precise definition of allowable susceptibility criteria exists. Thus, it was necessary to evolve approximations to the

probable susceptibility of signal circuits, based upon the circuit characteristics, as follows: (1) signal circuits will be most sensitive to interference which contains components within the circuit's normal passband; and (2), signal circuits will be less sensitive to higher-frequency interference components. The spectra shown in Figure B.9 is the best available estimate of signal circuit susceptibility, and was developed from experience with similar circuits and generally accepted design practices. The nomenclature used in defining the parameters in the figure refers to data sheet entries. The slope of 10 db per decade for roll-off of sensitivity has been investigated in the laboratory for several typical circuits and is considered conservative.

Some receivers may exhibit a characteristic which does not start at zero frequency; in which case, the spectrum of Figure B.9(b) is used.
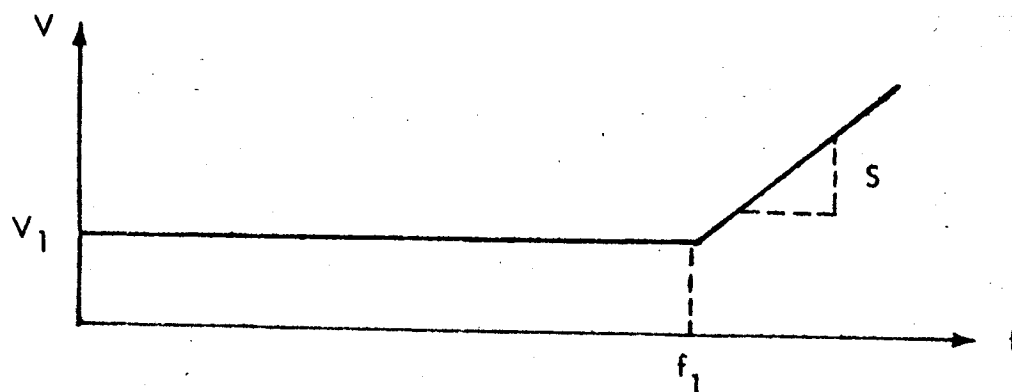


FIGURE B.9(a)   RECEPTOR SUSCEPTIBILITY SPECTRA
FOR SIGNAL CIRCUITS

$V_1$ = 1/2 the tolerance of critical parameter, if in volts, or

$V_1$ = 1/10 maximum voltage amplitude, if above is not in volts, or

$V_1$ = the tolerance of the critical parameter is in volts and the circuit carries an analog label.

Also, in Figure B.9(a), the slope S is assumed to be 10 db/decade.
If Rx bandpass is unknown, let

$f_1$ = 2 BW for DC signal (unless BW = 0)

$f_1$ = 2 upper bandpass limit for AC signals

$f_1$ = 10/pulsewidth for pulse circuits

If Rx bandpass is known, or if BW = 0, let

$f_1$ = Rx bandpass "to".
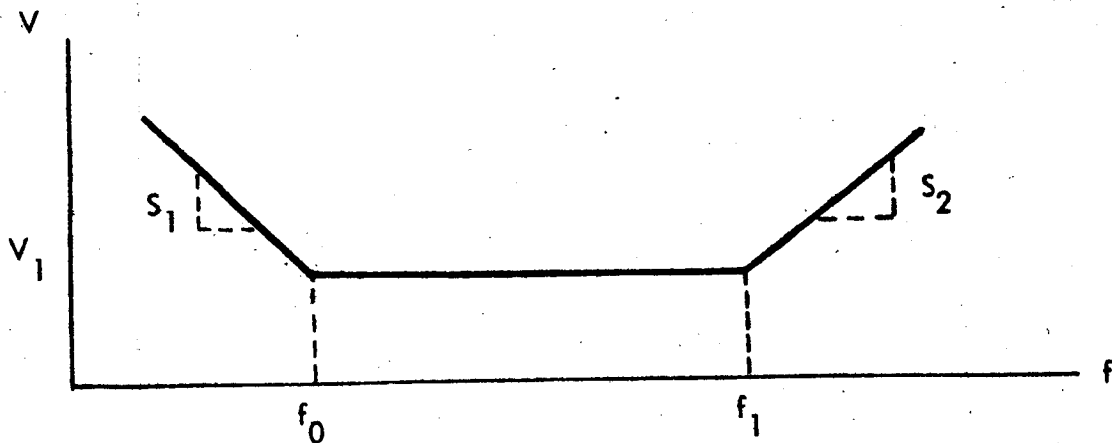


FIGURE B.9(b)    RECEPTOR SUSCEPTIBILITY SPECTRA
FOR SIGNAL CIRCUITS

$f_0$ = Rx bandpass "from", and

$S_1 = S_2$ = 10 db/decade,

with $V_1$ and $f_1$ as previously defined for Figure B.9(a).

## B.2.3 Modulation Signal Circuits

Modulation signal circuits differ from digital circuits in that the circuit bandwidth is usually much narrower and, within this frequency band, modulation circuits can be considered more sensitive. However, the level at which malfunction can occur is dependent on the particular circuit. In general, modulation circuit input signals will be of a relatively constant amplitude with a low dynamic range. An estimated malfunction level would be 40 db below the maximum amplitude at the normally-received signal. The resultant susceptibility spectra is shown in Figure B.10.
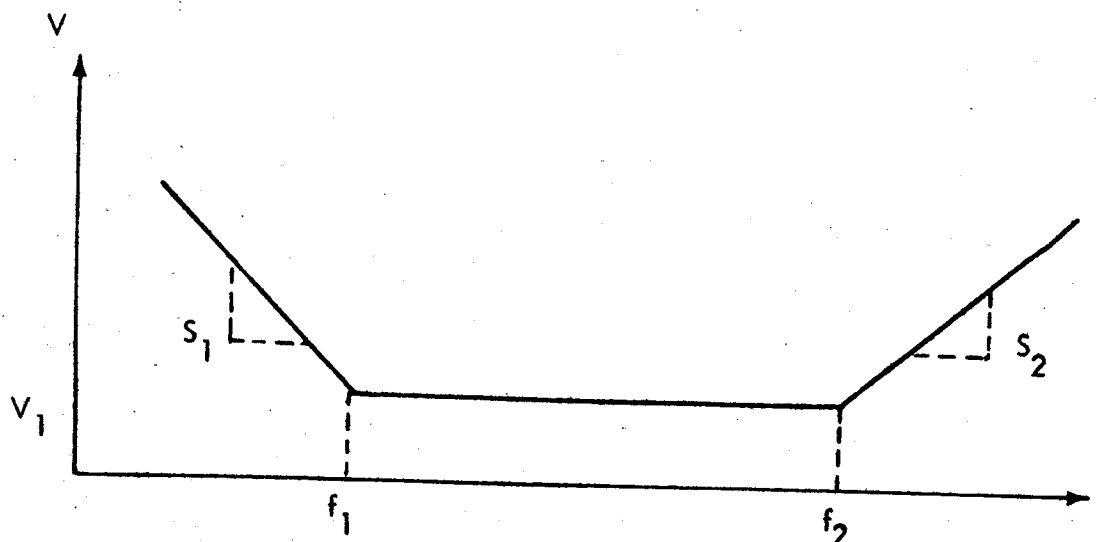


FIGURE B.10    RECEPTOR SUSCEPTIBILITY SPECTRA FOR MODULATED SIGNAL CIRCUITS

$V_1$ = maximum amplitude of fundamental - 40 db

$f_1$ = Rx bandpass "from"

$f_2$ = Rx bandpass "to"

$S_1 = S_2 = 10$ db/decade

The pcm cases will generally have $f_1$ equal to zero but will be identical to the above in all other respects.

### B.2.4    Servo Mechanism Circuits

An interference voltage in a servo system can cause a false error
signal which would result in an incorrect positioning of the electro-
mechanical device. The interference can be introduced into the system
via: (1) the command input circuit, (2) the feedback loop, or (3)
the error circuit. In (1) and (2), the interference may be amplified
and the resultant actuation could be greater than if the interference
were introduced directly in the error circuit. The spectra used in
this analysis have been derived from design information and typical
measured interference data from various programs.

Separate spectra have been devised for the command input and the feed-
back circuits because of differences in the circuit terminations. The
spectrum for the command input circuit is shown in Figure B.11(a),
and the spectrum for the feedback circuit is shown in Figure B.11(b).
The major differences are the extended frequency range of the feed-
back loop and the greater sensitivity of the input circuit. The
command input circuits will be most sensitive to frequencies from DC
to 20 cps, from 380 to 420 cps, 1600 cps and 3.5 Kc. Therefore, the
worst-case spectrum with maximum circuit sensitivity would be flat
and include frequencies from DC to above 3.5 Kc.

From DC to 3.5 Kc, it is possible for the interference signals to modu-
late the error signal and produce undesired positioning. Above 3.5
Kc, the interference signal can saturate the servo amplifiers and pro-
duce a nonlinear response to the desired input signals. The amplitude
required to saturate the servo amplifiers is estimated to be approxi-
mately 35 volts; however, for purposes of treating a worst-case
condition, a lower value is used for this analysis. See Figure B.11(a).

The feedback circuits will be sensitive to frequencies from DC to 20
cps and from 380 cps to 420 cps. Interference at other frequencies
will produce saturation and a nonlinear response to the desired feed-
back signals. It is anticipated that the feedback circuits will saturate
at levels which are lower than 3.5 volts, thus presenting a greater
degree of susceptibility. See Figure B.11(b).
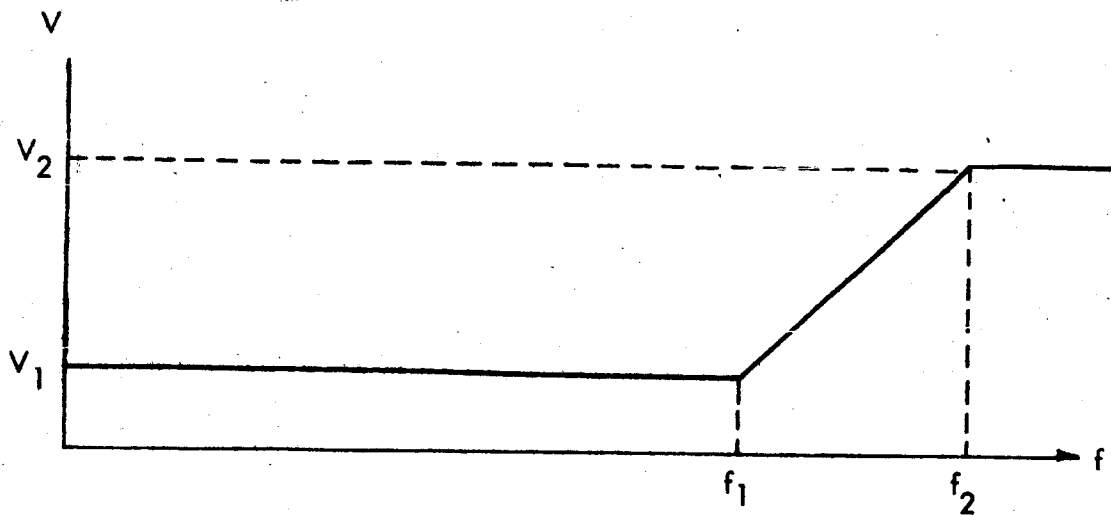
FIGURE B.11(a)    SUSCEPTIBILITY SPECTRA FOR
COMMAND INPUT CIRCUITS

$$f_1 = 3.75 \ \text{Kc}$$

$$f_2 = 37.5 \ \text{Kc}$$

$$V_1 = 20 \quad \text{Mv}$$

$$V_2 = 10 \quad \text{Volts}$$
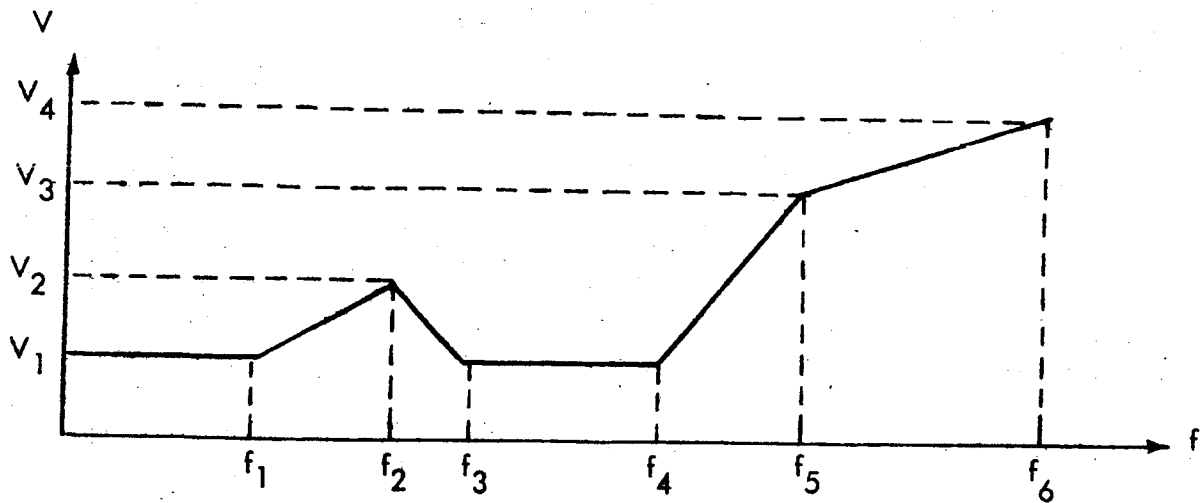


FIGURE B.11(b)    SUSCEPTIBILITY SPECTRA FOR
SERVO FEEDBACK CIRCUITS

For Figure B.11(b),

$$f_1 = 20 \text{ cps}$$

$$f_2 = 180 \text{ cps}$$

$$f_3 = 380 \text{ cps}$$

$$f_4 = 420 \text{ cps}$$

$$f_5 = 4.2 \text{ Kc}$$

$$f_6 = 42 \text{ Kc}$$

$$V_1 = 20 \text{ Mv}$$

$$V_2 = .2 \text{ V}$$

$$V_3 = 2.0 \text{ V}$$

$$V_4 = 4.0 \text{ V}$$

## B.2.5    Electro-Explosive Devices (EED's)

Since EED's can be sensitive to interference and are potentially dangerous if premature detonation occurs, a great deal of investigation has been performed to learn more about their characteristics. The Franklin Institute sponsors the Hazards of Electro-Magnetic Radiation to Ordnance (HERO) Congress annually to discuss the progress of the various investigations. A number of papers in the HERO proceedings for 1961 were used in the development of this analysis.

All EED's are specified in terms of a no-fire current and a sure-fire current. For the purpose of this analysis, a no-fire power of one-half watt will be used as a worst-case condition. The voltage limit will be used rather than the current, because the computer program is set up to compare voltage rather than power or current levels. Since the squib complex impedance is a function of frequency and generally unknown, but the resistance is known and is relatively constant, the no-fire or sure-fire voltage can be calculated and compared with

other voltages in the system. As the frequency of the interference signal is increased into the RF region, the bridge wire becomes a mismatched termination to the circuit and much of the energy is reflected back down the line. Empirical data on many different squib configurations have demonstrated a pronounced roll-off in the EED sensitivity at frequencies above 50 Mc. The estimated squib susceptibility spectrum is shown in Figure B.12. This spectrum applies only to interference introduced into the EED by way of its input leads. A more extensive study would be required to investigate the probability of detonation due to radiation through the EED case.
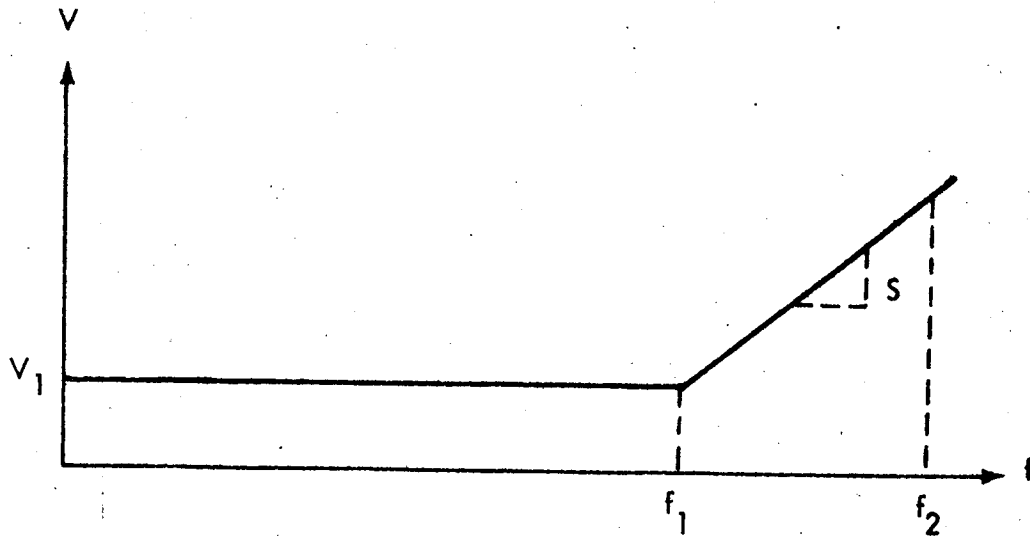


FIGURE B.12   RECEPTOR SUSCEPTIBILITY SPECTRUM
FOR SQUIB CIRCUITS

$$V_1 = 10 \log_{10} \frac{Z_L}{2} + 120 \ \text{db}/\mu\text{v}$$

$$f_1 = 100 \ \text{Mc}$$

$$S = 10 \ \text{db/octave}$$

$$f_2 = 400 \ \text{Mc}$$

$$Z_L = \text{squib input impedance}$$

APPENDIX C

DERIVATION OF OPTIMUM
CABLE-COUPLING EQUATIONS

The information in this appendix represents the results of previous
Boeing-funded basic research.

The purpose of this appendix is to analyze the equivalent circuit of the
cable network between two adjacent circuits and recommend an opti-
mum solution for use in the computer prediction program. Five
methods have been selected to determine the accuracy and complexity
of each method in the solution of the basic coupling network of
Figure C.1.

## C.1    METHOD I.    COMPLETE LOOP EQUATIONS

Method I is the most accurate and also the most complex solution to
the basic cable-coupling network of Figure C.1. It requires the
computer to solve a matrix of four loop equations to obtain the cur-
rents in each loop, and from the currents to arrive at the voltages
across the susceptible loads.
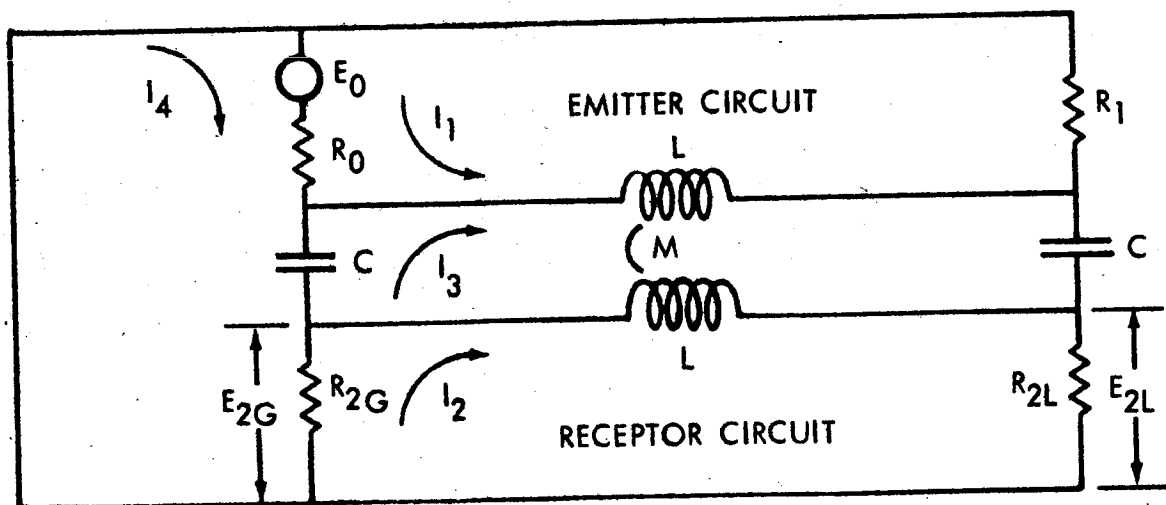


FIGURE C.1    CABLE-COUPLING NETWORK
EQUIVALENT CIRCUIT

The loop equations for the above network are:

$$(R_0 + R_1 + X_L) I_1 + X_M I_2 + (X_L - X_M) I_3 + R_0 I_4 = E_0$$

$$X_M I_1 + (R_{2G} + R_{2L} + X_L) I_2 + (X_M - X_L) I_3 - R_{2G} I_4 = 0$$

$$(X_L - X_M) I_1 + (X_M - X_L) I_2 + 2(X_L - X_M + X_C) I_3 - X_C I_4 = 0$$

$$R_0 I_1 - R_{2G} I_2 - X_C I_3 + (R_0 + R_{2G} + X_C) I_4 = E_0$$

where

$$X_C = -j \frac{1}{\omega C} \qquad X_L = j \omega L \qquad X_M = j \omega M$$

These equations are solved for the appropriate currents and the generator and load end voltage-transfer ratios,

$$\frac{E_{2G}}{E_0} \quad \text{and} \quad \frac{E_{2L}}{E_0} \quad \text{are found.}$$

## C.2    METHOD II.   CAPACITIVE & MAGNETIC COUPLING CALCULATED SEPARATELY & THEN ADDED TOGETHER

Method II is the solution of the modified basic network shown in Figure C.2 and is considerably less complex than Method I, but gives nearly the same results except at the higher frequencies. This method treats the capacitive and magnetic coupling separately and ignores any interaction between them. Capacitive coupling is obtained by solving the circuit with the mutual inductance equal to zero. Then the magnetic coupling is obtained by setting the capacity between wires equal to zero. The total coupling is then the sum of these two. By placing the total

lumped capacity in the center of the circuit, making the pi circuit into a tee circuit, no loop equations are necessary, and the solution becomes much simpler than Method I. Except at frequencies above 20 Mc, the additions of the capacitive and magnetic coupling gives accurate results. As shown by the equations, the capacitive and inductive coupling add in phase at the generator end of the susceptible cable. They are $180^{\circ}$ out of phase at the load end of the susceptible cable, and thus cancel so that the net result is the difference between the two.
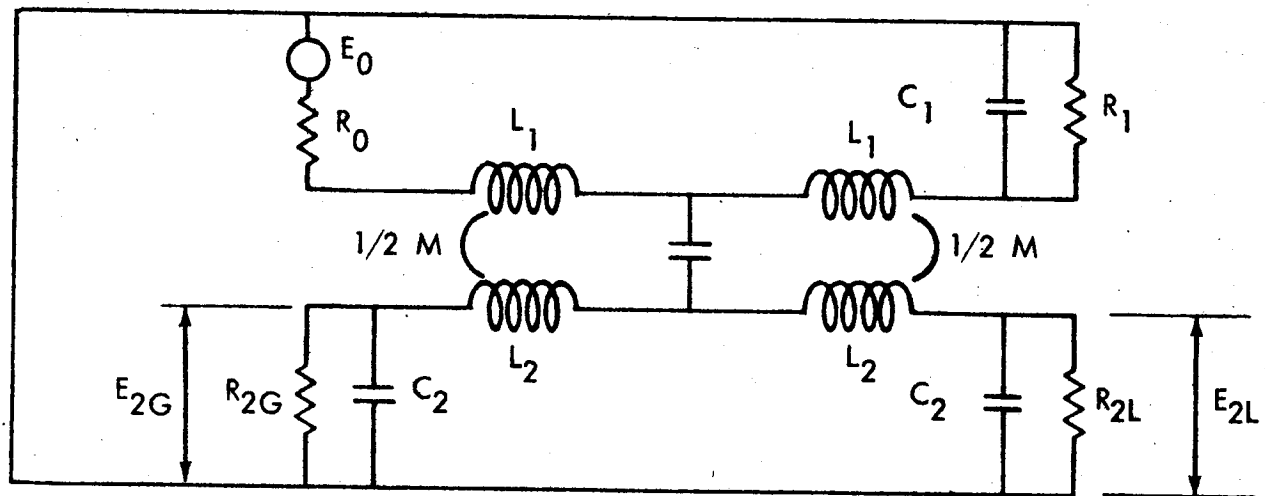


FIGURE C.2.

The voltage transfer ratio found in the solution of the network of Figure C.2 is:

$$\frac{E_{2G}}{E_0} = Z'_{2G} \left[ \frac{1}{Z_{2G}} \frac{Z_1 Z_2}{\left[ (R_0 + X_{L1})(Z_1 + Z_2 + X_C) + Z_1(X_C + Z_2) \right]} + \frac{X_M}{(R_0 + X_{L1} + Z_1)(Z_{2G} + Z_{2L})} \right]$$

147

$$\frac{E_{2L}}{E_0} = Z'_{2L}\left[\frac{1}{Z_{2L}} \frac{Z_1 Z_2}{\left[(R_0 + X_{L1})(Z_1 + Z_2 + X_C) + Z_1(X_C + Z_2)\right]} - \right.$$

$$\left. \frac{X_M}{(R_0 + X_{L1} + Z_1)(Z_{2G} + Z_{2L})}\right]$$

where,

$$X_C = -j\frac{1}{\omega C_3}; \qquad X_{C1} = -j\frac{1}{\omega C_1}; \qquad X_{C2} = -j\frac{1}{\omega C_2}$$

$$X_{L1} = j\omega L_1; \qquad X_{L2} = j\omega L_2; \qquad X_M = j\omega M$$

$$Z_1 = X_{L1} + \frac{R_1 X_{C1}}{R_1 + X_{C1}}; \qquad Z_{2G} = \frac{R_{2G} X_{C2}}{R_{2G} + X_{C2}}; \qquad Z'_{2L} = \frac{R_{2L} X_{C2}}{R_{2L} + X_{C2}}$$

$$Z_{2G} = X_{L2} + Z'_{2G}; \qquad Z_{2L} = X_{L2} + Z_{2L}; \qquad Z_2 = \frac{Z_{2L} Z_{2G}}{Z_{2L} + Z_{2G}}$$

## C.3 METHOD III. NEGLECTING CAPACITANCE TO GROUND & THE RECEPTOR CIRCUIT SELF INDUCTANCE

Method III analyzes the modified basic cable network as shown in Figure C.3. The reason for the modification is that the capacitance to ground and the self-inductance of the cables are negligible at low frequencies and only slightly reduce the coupling at high frequency; these terms can be neglected without impairing accuracy. Neglecting them greatly simplifies the equations.

CAPACITIVE COUPLING        MAGNETIC COUPLING
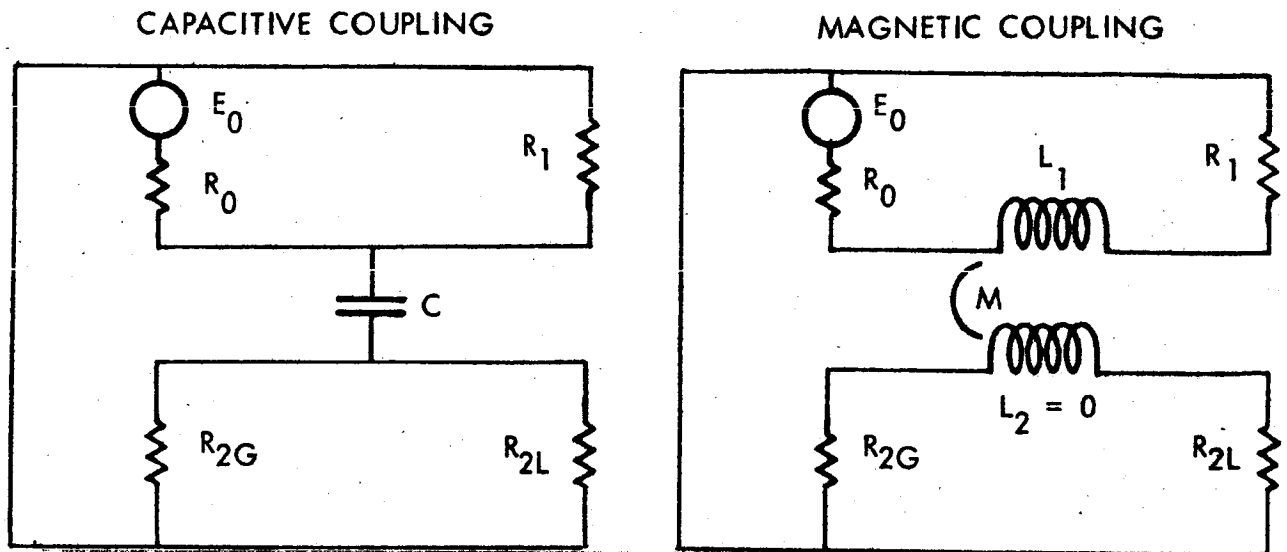


FIGURE C.3.

The solution of the equivalent circuits of Figure C.3 gives the
following voltage-transfer ratios:

$$\frac{E_{2G}}{E_0} = \left[\frac{R_1}{R_1 + R_0} \times \frac{R_2}{\sqrt{R_2^2 + X_C^2}}\right] + \left[\frac{X_M}{(R_1 + R_0)^2 + X_L^2} \times \frac{R_{2G}}{R_{2G} + R_{2L}}\right]$$

$$\frac{E_{2L}}{E_0} = \frac{MAX}{OF} \left[\frac{R_1}{R_1 + R_0} \times \frac{R_2}{\sqrt{R_2^2 + X_C^2}}\right] \text{ or } \left[\frac{X_M}{\sqrt{(R_1 + R_0)^2 + X_L^2}} \times \frac{R_{2L}}{R_{2G} + R_{2L}}\right]$$

where,

$$X_C = -j \frac{1}{\omega C}$$

$$X_L = j \omega L_1$$

$$R_2 = \frac{R_{2G} R_{2L}}{R_{2G} + R_{2L}}$$

$$X_M = j \omega M$$

## C.4 METHOD IV. ALL IMPEDANCES CONSIDERED AS REAL QUANTITIES

Method IV considers the solution of the modified basic cable network of Figure C.4.

This method is the same as Method III except the complex reactances are considered to be real numbers. At low frequencies, this simplification makes no difference because it is the capacitive reactance alone that limits the capacitive coupling and the resistance of the susceptible loads that limits the inductive coupling.

Likewise, at high frequencies, this simplification makes no difference because both couplings approach unity for both Methods III and IV. However, in the middle frequency range of about 3 Mc, Method IV gives coupling 3 db lower than Method III.

Since 3 db is small compared to other errors in input data to the prediction program, and since Method IV actually more nearly agrees with the true curve, this method is favored because of its simplicity.

CAPACITIVE COUPLING | MAGNETIC COUPLING
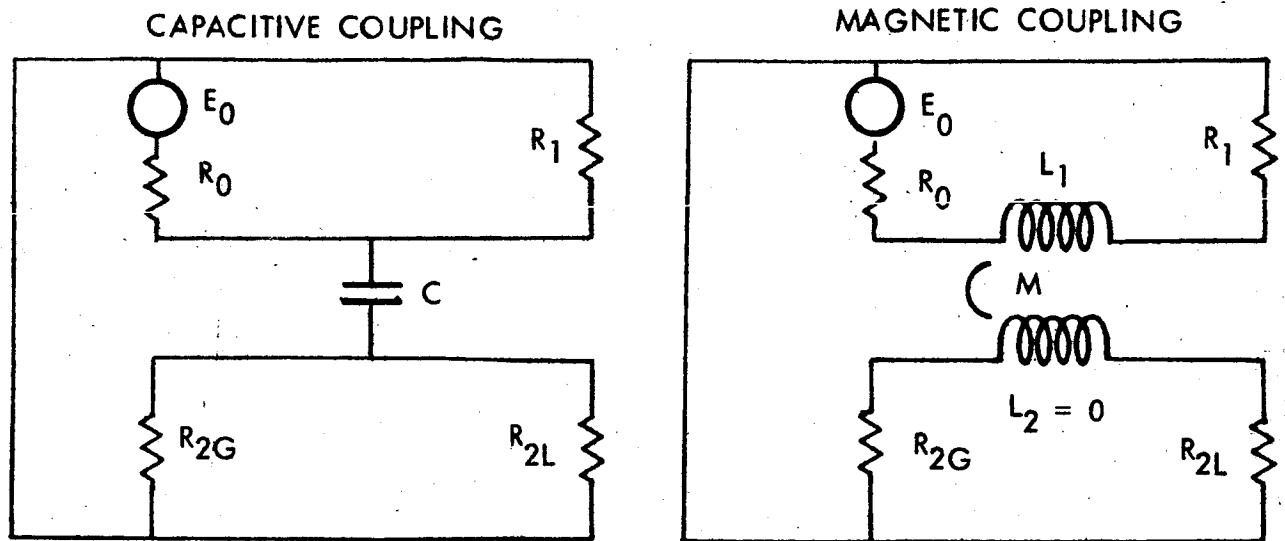


. FIGURE C.4.

The solution of the equivalent circuits of Figure C.4 gives the voltage-transfer ratios as:

$$\frac{E_{2G}}{E_0} = \left[\frac{R_1}{R_1 + R_0} \times \frac{R_2}{R_2 + X_C}\right] + \left[\frac{X_M}{R_1 + R_0 + X_L} \times \frac{R_{2G}}{R_{2G} + R_{2L}}\right]$$

$$\frac{E_{2L}}{E_0} = \frac{MAX}{OF} \left[\frac{R_1}{R_1 + R_0} \times \frac{R_2}{R_2 + X_C}\right] \text{ or } \left[\frac{X_M}{R_1 + R_0 + X_L} \times \frac{R_{2L}}{R_{2G} + R_{2L}}\right]$$

where,

$$X_C = - \frac{1}{\omega C} \qquad\qquad X_L = \omega L_1$$

$$R_2 = \frac{R_{2G} R_{2L}}{R_{2G} + R_{2L}} \qquad\qquad X_M = \omega M$$

## C.5    METHOD V.    STRAIGHT-LINE APPROXIMATION

Method V considers as negligible all self inductance and shunt capacity to ground for both the emitter and receptor circuit. Also, the capacitive and inductive coupling are considered separately. For these assumptions, the modified basic cable network is shown in Figure C.5.



CAPACITIVE COUPLING                     MAGNETIC COUPLING

(a)                                     (b)
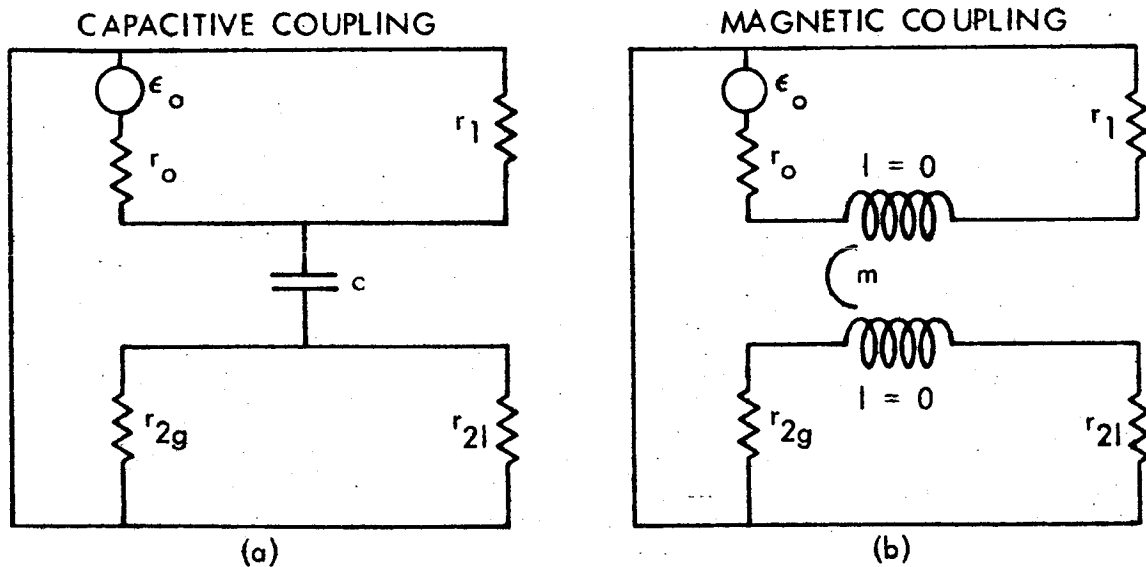
FIGURE C.5.

First, the capacitive coupling is considered and Figure C.5(a) is redrawn as shown in Figure C.6.
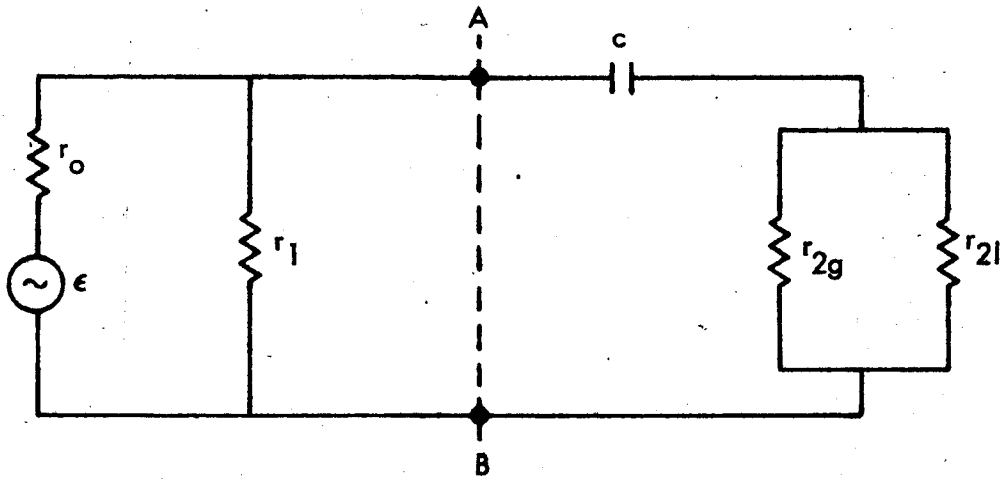


FIGURE C.6.

Applying Thevenin's theorem to the left side of the AB plane, the circuit reduces to that of Figure C.7.
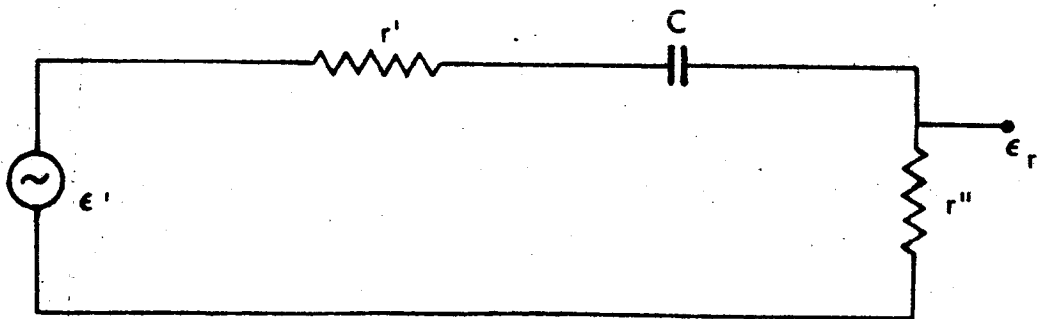


FIGURE C.7.

where,

$$\epsilon' = \frac{r_1}{r_1 + r_0} \; \epsilon_0$$

$$r' = \frac{r_0 \, r_1}{r_1 + r_0}$$

$$r'' = \frac{r_{2g} \, r_{2\ell}}{r_{2g} + r_{2\ell}}$$

The emitter circuit current that is coupled to the receptor circuit through capacitive coupling produces the same voltage, $\epsilon_r$, across the generator and load end of the receptor circuit. This voltage is found by considering the circuit of Figure C.7 as a voltage divider where,

$$\epsilon_r = \frac{r''}{r'' + jX_C + r'} \; \epsilon'$$

after substituting the original circuit parameters, the voltage-transfer function is found to be:

$$\frac{\epsilon_r}{\epsilon_0} = \left( \frac{r_{2g} \, r_{2\ell}}{r_{2g} + r_{2\ell}} \right) \left( \frac{r_1}{r_1 + r_0} \right) \frac{1}{\left[ \dfrac{r_{2g} \, r_{2\ell}}{r_{2g} + r_{2\ell}} + \dfrac{r_0 \, r_1}{r_1 + r_0} + jX_C \right]}$$

This last expression can be simplified by the condition that:

$$X_C \gg \frac{r_{2g} \, r_{2\ell}}{r_{2g} + r_{2\ell}} \; ,$$

$$X_C \gg \frac{r_0 \, r_1}{r_1 + r_0}$$

This condition is satisfied for typical circuits up to 10 Mc. The voltage-transfer function is then given by

$$\frac{\epsilon_r}{\epsilon_0} = \left(\frac{r_1}{r_1 + r_0}\right)\left(\frac{r_{2g}\, r_{2\ell}}{r_{2g} + r_{2\ell}}\right)\left(\frac{1}{X_C}\right) \qquad (C.1)$$

Examining the inductive coupling, the loop equations for Figure C.5(b) are:

$$\ell_0 = i_1\, (r_0 + r_1) - i_2\, X_M$$

$$0 = -i\, X_M + i_2\, (r_{2g} + r_{2\ell})$$

Solving this set of equations for $i_2$, the receptor circuit induces current; the load end voltage-transfer ratio is found to be

$$\frac{\epsilon_\ell}{\epsilon_0} = \frac{r_2\, X_M}{(r_1 + r_0)\, (r_{2g} + r_{2\ell}) - X_M^{\,2}} \qquad (C.2)$$

Since below 10 Mc, $X_m^2 << (r_1 + r_0)(r_{2g} + r_{2\ell})$, this reduces to

$$\frac{\epsilon_\ell}{\epsilon_0} = \frac{r_{2\ell}\, X_M}{(r_1 + r_0)\, (r_{2g} + r_{2\ell})} \qquad (C.3)$$

The voltage induced in the susceptible cable is equal to this constant current times the mutual reactance which increases with frequency by 6 db per octave. Thus, the inductive coupling also increases by 6 db per octave. Therefore, the sum of the two, which are in phase at the generator end of the susceptible cable, also increases by 6 db per octave. This straight line is extended to unity coupling at some high frequency. Above this frequency, the coupling is taken as unity. As shown by the curves, this method gives accurate solutions at all frequencies except at the corner frequency, where it is 6 db too large. However, it gives worst-case coupling, and is quite satisfactory for a prediction program in which the first sorting of data determines only possible interference pairs. The advantages of simplicity in programming the computer far exceeds the disadvantage of including a few additional questionable cases.

Although the capacitive coupling and the inductive coupling are out of phase at the load end of the susceptible cable, it is unwise to depend on them cancelling each other and giving a coupling value less than either. A more reasonable approach is to consider the coupling to be equal to the larger of the two. In the computer program, the process of taking the maximum of two equations is simple. As a general rule, for impedances greater than 300 ohms, this larger coupling is capacitive. For impedances less than 300 ohms, it is inductive.

In Method V, the straight-line approximation method, the curve of coupling versus frequency, need not be calculated at several frequencies. The value of frequency at which the straight line of 6 db per octave slope reaches zero is sufficient data to define the coupling over the whole frequency range.

The corner frequency for the capacitive coupling curve is derived by setting the coupling equal to unity and solving for frequency:

$$f_C = \frac{(R_1 + R_0)\,(R_{2G} + R_{2L})}{2\pi\,C\,R_1\,R_{2G}\,R_{2L}}$$

Similarly, the generator end voltage-transfer ratio is found as,

$$\frac{\epsilon_g}{\epsilon_0} = \frac{r_{2g} X_M}{(r_1 + r_0)(r_{2g} + r_{2l})}$$

Thus, the complete solution of the equivalent circuit of Figure C.5 for the voltage-transfer ratios is found by combining equations (C.1), (C.2), and (C.3):

$$\frac{E_{2G}}{E_0} = \frac{1}{X_C}\left[\frac{R_1}{R_1 + R_0} + \frac{r_{2g}\, r_{2l}}{r_{2g} + r_{2l}}\right] + \left[\frac{X_M}{R_1 + R_0} \times \frac{R_{2G}}{R_{2G} + R_{2L}}\right] \qquad (C.4)$$

$$\frac{E_{2L}}{E_0} = \frac{MAX}{OF}\quad \frac{1}{X_C}\left[\frac{R_1}{R_1 + R_0} + \frac{r_{2g}\, r_{2l}}{r_{2g} + r_{2l}}\right]\ or\ \left[\frac{X_M}{R_1 + R_0} \times \frac{R_{2L}}{R_{2G} + R_{2L}}\right] \qquad (C.5)$$

A closer examination of equations (C.4) and (C.5) for Method V show that both the capacitive coupling and the magnetic coupling increase linearly with frequency until they reach unity coupling.

To consider worst-case coupling at all frequencies, this straight-line approximation for the coupling provides the best method. It is by far the simplest method to calculate as shown in the equations.

Here again, the coupling at the generator end of the susceptible line is equal to the sum of the capacitive and inductive coupling, both of which are straight lines. For the capacitive coupling, the current is limited only by the capacitive reactance which falls off with frequency by 6 db per octave. Thus, the capacitive coupling increases by 6 db per octave. For the magnetic coupling, the current in the source cable is limited by only the load resistance and does not vary with frequency.

Likewise, the corner frequency for the magnetic coupling curve is:

$$f_M = \frac{(R_1 + R_0)(R_{2G} + R_{2L})}{2\pi M R_{2G}} .$$

The corner frequency for the load-end coupling curve is

$$f_L = \text{Minimum of } f_C \text{ or } f_M$$

The corner frequency for the generator-end coupling curve is:

$$f_G = \frac{f_C f_M}{f_C + f_M} = \frac{(R_1 + R_0)(R_{2G} + R_{2L})}{2\pi R_{2G}(M + C R_1 R_{2L})}$$

$f_G$ and $f_L$ are the required parameters to define the coupling.

## C.6  THEORETICAL COMPARISON OF THE FIVE METHODS

Calculations were made using the derived voltage-transfer ratios to determine the accuracy of each method. For this comparison, the loads were chosen as 300 ohms so that the capacitive coupling and magnetic coupling were about equal. The voltage-transfer ratios are plotted against frequency in Figures C.8 to C.11. for both ends of the receptor cable and two different cable configurations. These figures show that Method I agrees most accurately with measured values. However, the simplified methods show good agreement, particularly up to 10 Mc.

## C.7  RECOMMENDED METHOD

Table I, Paragraph 4.2 gives the accuracy of the five methods of calculating cable coupling and the computer time required to make one frequency run for each method. The accuracy is not seriously impaired and the computer time is reduced considerably by the simpler methods.

158

Therefore, based on the foregoing analysis, Method V has been selected and incorporated into the computer interference-prediction program.

## C.8 FORMULAS FOR CAPACITANCE & MUTUAL INDUCTANCE

The formulas used in the computer-prediction program for determination of intercable capacity and mutual inductance are given below.

### Capacitance between Two Wires above A Ground Plane

$$C = \frac{(7.35 \times 10^{-12}) \, (\ell) \left[ \log \frac{S_{12}}{D} \right] \left[ K_{eff} \right]}{\left[ \log \left( \frac{4h}{d} \frac{1}{\sqrt{2 - \sqrt{d/D}}} \right) \right]^2 - \left[ \log \frac{S_{12}}{D} \right]^2} \quad \text{in farads}$$

where,

$$K_{eff} = K_0 + \frac{\left[ \frac{d_1}{d} \right]^2 - 1}{\frac{1}{2} \left[ \frac{d_1}{d} + \frac{D}{d} \right]^2 - 1} (K_1 - K_0)$$

and,

$$S_{12} = \sqrt{D^2 + 4h^2}$$

## Mutual Inductance between Two Wires above A Ground Plane

$$M = (1.405 \times 10^{-7}) \; (\ell) \; \left(\log \frac{S_{12}}{D}\right) \quad \text{in henries}$$

where,

| | | |
|---|---|---|
| $\ell$ | - | Length of wires (in feet) |
| $D$ | - | Separation of wires (in inches) |
| $h$ | - | Height above ground plane (in inches |
| $d$ | - | Diameter of the wire conductor (in inches) |
| $d_1$ | - | Diameter of the wire including the insulation (in inches) |
| $K_0$ | - | Relative dielectric constant of air $(K_0 = 1)$ |
| $K_1$ | - | Relative dielectric constant of the wire insulation |

Notes

1) The factor $\dfrac{1}{\sqrt{2 - \sqrt{d/D}}}$ in the capacitance equation was

determined from measured values of capacitance.

2) $K_{eff}$ was determined from theoretical considerations and accounts for the increase of the effective dielectric constant as the wires are in close proximity, due to the influence of the wire insulation.

3) References for the equations:

M) Diddens, P. A., <u>Design Procedure for The Reduction of Low Frequency Interference in Electrical Wiring Systems</u>, The Martin Company, 1960: p. 20.

C) Loc. Cit.; p. 7.

THE LOAD END OF THE SUSCEPTIBLE CABLE FOR TWO PARLLEL WIRES,
EACH 10 FEET LONG, SPACED AS CLOSE TOGETHER AS THE INSULATION
PERMITTED AND ONE INCH ABOVE A GROUND PLANE

FIGURE C.8

FIGURE C.9

THE GENERATOR END OF THE SUSCEPTIBLE CABLE FOR TWO PARALLEL WIRES, EACH 10 FEET LONG, SPACED AS CLOSE TOGETHER AS THE INSULATION PERMITTED AND ONE INCH ABOVE A GROUND PLANE

⊙ = MEASURED VALUES

METHOD I
METHOD II
METHOD III
METHOD IV
METHOD V

FREQUENCY~MC

VOLTAGE TRANSFER RATIO~DB

FIGURE C.10

THE LOAD END OF THE SUSCEPTIBLE CABLE FOR TWO PARALLEL WIRES, EACH 10 FEET LONG, SPACE ONE INCH APART AND ONE INCH ABOVE A GROUND PLANE

⊙ = MEASURED VALUES

THE GENERATOR END OF THE SUSCEPTIBLE CABLE FOR TWO PARALLEL WIRES, EACH 10 FEET LONG, SPACED ONE INCH APART AND ONE INCH ABOVE A GROUND PLANE

FIGURE C.11

# APPENDIX D

## PROGRAM INPUT PREPARATION
## AND MAJOR SUBROUTINES

### D.1    PROGRAM INPUT PREPARATION

The data card input to the program consists of three sections.

### D.1.1    Wire Route Input

The wire route input section consists of one or more sets of wire routes. Each wire route card set consists of one Type # 1 card and one or more Type # 2 cards:

#### Card Type # 1

| Columns | Format | Contents |
|---------|--------|----------|
| 1 - 3 | A3 | The alphanumeric name or number assigned this wire route |
| 7 - 10 | I3 | The number of station-angle pairs defining this wire route |

#### Card Type # 2

| Columns | Format | Contents |
|---------|--------|----------|
| 1 - 10 | E10.0 | First station in wire route |
| 11 - 20 | E10.0 | First angle in wire route |
| 21 - 30 | E10.0 | Second station in wire route |
| 31 - 40 | E10.0 | Second angle in wire route |
| 41 - 50 | E10.0 | Third station in wire route |
| 51 - 60 | E10.0 | Third angle in wire route |
| 61 - 70 | E10.0 | Fourth station in wire route |
| 71 - 80 | E10.0 | Fourth angle in wire route |

As many cards of Type # 2 are used as necessary to completely list all the station-angle pairs describing the wire route.

The final wire route card set is followed by a card having the word END punched in columns 1 - 3.

### D.1.2    Circuit Description Input

The circuit description input consists of two or more sets of description cards, where there is one such set for each circuit to be considered. The first card of each circuit set contains information which is common to all circuit sets: circuit identification, circuit type number, wire route, and wire code. Each circuit description set is completed by one or more additional cards, the number and formats of the cards depending on the circuit type.

The card formats and the input arguments to be punched on the cards of each of the six types of circuit description sets are indicated in the following six input data format sheets.

The last circuit description data card set is followed by a card with the word END punched in columns 1 - 3.

To complete the data card input to the program, two final cards follow the END card of the circuit description sets. The first such card is of the form:

| Columns | Format | Contents |
|---------|--------|----------|
| 1 - 10 | F10.0 | Interference safety margin - dbs |

The input of an interference safety margin of X db means that if an emitted signal is within X db of interfering with signal receptor in another circuit, the circuits involved constitute an interference pair. The second card has the word INITIALIZE punched in columns 1 - 10.

### D.1.3    Overall Deck Set-Up

A complete data deck has the following overall form.

    1st  wire route card set
    2nd wire route card set

    last wire route card set
    END card
    1st  circuit description card set
    2nd circuit description card set

    last circuit description card set
    END card
    interference safety margin card
    INITIALIZE card


## D.2    DESCRIPTION OF MAJOR SUBROUTINES

The program flow chart of Figure 4.5 shows the manner in which the
computer-prediction program has been developed.  The Spectrum
Generation Program (SGP) serves as the FORTRAN main program
and performs the following major functions:

1)    SGP reads and stores the wire routes to be used;

2)    SGP reads in the circuit name and type for each circuit;

3)    SGP calls the proper subroutine to read the rest of the
      characterizing data for the circuit and construct the
      required spectra;

4)    SGP writes the constructed spectra for each circuit on
      tape or drum for use later in the EMI program for
      comparison of pairs of emitter-receptor spectra.


After each circuit has been processed in Steps 2, 3, and 4, above,
SGP calls subroutine Circuit Interference Prediction (CIP).  It is
evident that SGP itself is primarily a control program, reading
and writing data rather than making computations.  The input data is
read from the normal system input unit.

The output from SGP and its spectra-generating subroutines is stored on tapes/drums currently assigned as follows:

| Physical Unit | Logical Unit | Information Stored |
|---|---|---|
| Tape A | 1 | Input data for circuits |
| Tape B | 2 | Same as above |
| Tape C | 3 | Same as above |
| Drum 1, 3rd area | 8 | Spectra and coupling data for Rx circuits |
| Drum 2, 4th area | 11 | Spectra and coupling data for Tx circuits |
| Drum 2, 3rd area | 12 | Same as above |

## D.2.1    Spectra-Constructing Routines

There are six spectra-generating subroutines, one for each type cir-cuit, called by SGP. Each such routine constructs a Tx and/or Rx spectrum, and writes the input data for the circuit currently being processed on the appropriate tapes.

The transmission of information between SGP and each of the six spectrum-generating subroutines is through COMMON storage. The circuit name, circuit type, wire code, and wire route (i.e., the information read by SGP from the first input card for a given circuit) is stored by SGP in a common block having the label CKTBLK. The coupling data read from the remaining input cards for the circuit by the appropriate spectrum-generating routine and the constructed spectra are passed to SGP by use of a common block labelled SPCTRA.

The list of variables (using the program variable names) in each of these common blocks is as follows:

| Common Block Name | Variable | |
|---|---|---|
| CKTBLK | ORID | Order description for the circuit |
| | CIRCUIT | Name or number assigned this circuit |
| | CONNI | Connector |
| | CTACTI | Contact |
| | COMNZ | Connector |
| | CTACTZ | Contact |
| | ID | Circuit type number |
| | ROUTE | Name or number of wire route of this circuit |
| | IWIRE | Wire code |
| SPECTRA | FTX array | Frequency values in Tx spectrum log frequency |
| | VTX array | Amplitude values in Tx spectrum db/$\mu$v |
| | N | Number of points in Tx spectrum |
| | FRX array | Frequency values in Rx spectrum log frequency |
| | VRX array | Amplitude values in Rx spectrum db/$\mu$v |
| | M | Number of points in Rx spectrum |
| | ZG | Complex generator impedance - ohms |
| | ZL | Complex load impedance ohms |
| | PWCD | Power supply type |
| | FREQ | Ripple frequency - cps |

The proper spectrum-generating subroutine is chosen by SGP according-ing to the circuit type number (variable name ID in the CKTBLK list above):

| Circuit Type Number | Circuit Type |
|---|---|
| 1 | power |
| 2 | servo |
| 3 | signal |
| 4 | switch |
| 5 | squib |
| 6 | modulated signal |

### D.2.1.1 Subroutine PWRSGN (Power Circuits)

PWRSGN is called by SGP to read the input data for power circuits and to construct Tx and Rx spectra as described in Paragraphs B.1.1 and B.2.1.

### D.2.1.2 Subroutine SRVSGN (Servo Circuits)

SRVSGN is called by SGP to read the input data for command input and feedback-type servo circuits and to construct Tx and Rx spectra as described in Paragraphs B.1.5 and B.2.4.

### D.2.1.3 Subroutine DGTSGN (Signal Circuits)

DGTSGN is called by SGP to read the input data for signal circuits and to construct Tx and Rs spectra as described in Paragraphs B.1.3 and B.2.2.

### D.2.1.4 Subroutine SWCSGN (Switch Circuits)

SWCSGN is called by SGP to read the input data for switch circuits and to construct a Tx spectrum as described in Paragraph B.1.2.

### D.2.1.5    Subroutine SQBSGN (Squib Circuits)

SQBSGN is called by SGP to read the input data for squib circuits and to construct an Rx spectrum as described in Paragraph B.2.5.

### D.2.1.6    Subroutine MDCSGN (Modulated Signal Circuits)

MDCSGN is called by SGP to read the input data for modulated signal circuits and to construct Tx and Rx spectra as described in Paragraphs B.1.4 and B.2.3.

### D.2.1.7    Subroutine PULSE

PULSE is called by DGTSGN to compute the envelope of the Fourier spectrum of a trapezoidal pulse.

One type of signal frequently used is a trapezoidal pulse. The power spectrum of such a signal resembles a damped sine wave; it has maximum amplitude at zero frequency and zero amplitude at infinite frequency. The envelope of the spectrum is used as an approximation, since too many points would be required to adequately define the actual spectrum.

For example, consider the square pulse shown below.
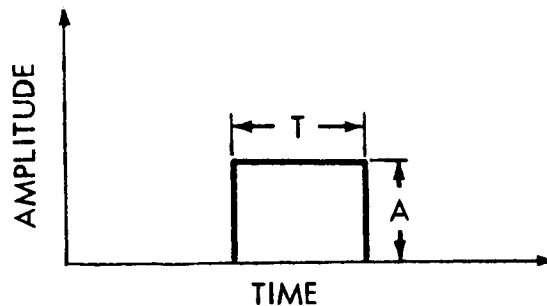
The power spectrum of this pulse and envelope have the form
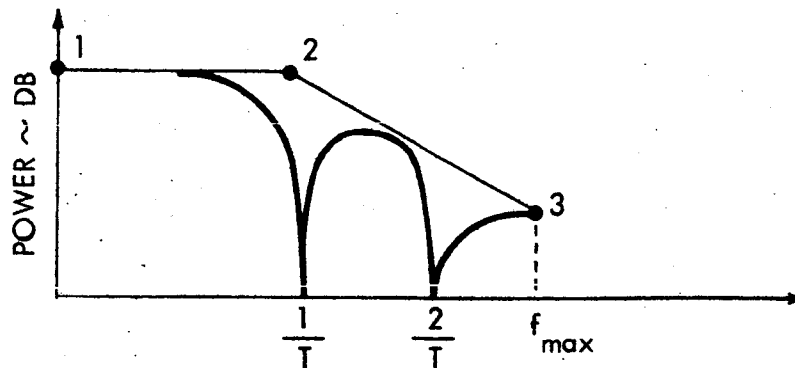


The envelope is described by the points 1, 2, 3, and the line segment joining them.

The list of input and output arguments for PULSE is as follows:

| Variable Name | In | Out | Meaning |
|---|---|---|---|
| A | X | | Pulse height - volts |
| T | X | | Pulse width at bottom - microseconds |
| TR | X | | Rise time - microseconds |
| TF | X | | Fall time - microseconds |
| VTH | X | | Amplitude at which the spectrum ends - db/mv |
| VBR array | | X | Amplitude values in pulse spectrum - db/$\mu$ v |
| FBR array | | X | Frequency values in pulse spectrum - megacycles |
| JJ | X | | JJ = 1, trapezoidal pulse JJ = 4, square pulse |

### D.2.2 CIP (Circuit Interference Program)

CIP and the subroutines called by CIP constitute that portion of the EMI program which compares receptor susceptibility spectra with emitter interference spectra for the purpose of prediction of possible interference. CIP is in subroutine form and is called by SGP.

CIP performs the following major functions for each pair of possible interference circuits:

1) Reads Tx and Rx spectra and coupling data from tape or drum;

2) Determines the amount of coupling between the two circuits;

3) Computes an interference spectrum (an attenuated emitter spectrum) and compares it with the Rx susceptibility spectrum;

4) Prints diagnostic information for each potential interference pair.

The amount of coupling between circuits is dependent upon the amount of mutual wire length for the circuits. The wire route information read from the input cards by SGP is passed to CIP via a COMMON block labelled WROUTE. The arrays in the WROUTE block give the name and the set of station-angle pairs for each wire route.

### D.2.2.1 Subroutine SPCMPR

SPCMPR is called by CIP and subroutine ATTEN to substract one spectrum from another.

The FORTRAN-calling sequence and a description of the input and output arguments for SPCMPR are as follows:

CALL SPCMR (FB, VB, NB, FA, VA, NA, FC, VC, NC).

| Argument | In | Out | Meaning |
|---|---|---|---|
| FB | X | | Frequency array for Curve B |
| VB | X | | Voltage array for Curve B |
| NB | X | | Number of points in Curve B |
| FA | X | | Frequency array for Curve A |
| VA | X | | Voltage array for Curve A |
| NA | X | | Number of points in Curve A |
| FC | | X | Frequency array for Curve C |
| VC | | X | Voltage array for Curve C |
| NC | | X | Number of points in Curve C |

(Here, Curve C = Curve A - Curve B)

D.2.2.2    Subroutine MUTUAL

MUTUAL is called by CIP to compute the mutual wire length for a Tx and Rx circuit pair.

The FORTRAN-calling sequence and a description of the input and output arguments for MUTUAL are as follows:

CALL MUTUAL (Z1, A1, Z2, N1, A2, N2, RADIUS, LENGTH).

| Argument | In | Out | Meaning |
|---|---|---|---|
| Z1 | X | | Station array for first wire route |
| A1 | X | | Angle array for first wire route |
| N1 | X | | Number of station-angle pairs in first wire route |
| Z2 | X | | Station array for second wire route |
| A2 | X | | Angle array for second wire route |
| N2 | X | | Number of station-angle pairs in second wire route |
| RADIUS | X | | Radius of the shell in which the circuits are located |
| XL LENGTH | | X | Mutual wire length |

All angles are in degrees, and the mutual wire length and the station values are in inches.

D.2.2.3     Subroutine ELMNTS

ELMNTS is called by CIP to compute coupling parameters for a Tx - Rx circuit pairs.

The calling sequence and a description of the input and output arguments for ELMNTS are as follows:

CALL ELMNTS (ITWIRE, IRWIRE, H, XLNGTH, XM, XC,
                    ISLD, ADAT)

| Argument | In | Out | Meaning |
|----------|----|----|---------|
| ITWIRE | X | | Tx wire code |
| IRWIRE | X | | Rx wire code |
| H | X | | Circuit height above ground plane - inches |
| XLNGTH | X | | Mutual wire length - inches |
| XM | | X | Mutual inductance - henries |
| XC | | X | Mutual capacitance - farads |
| ISLD | | X | Wire shielding code: |

                                    0 - neither wire shielded
                                    1 - Rx wire shielded
                                   10 - Tx wire shielded
                                   11 - both wires shielded

| ADAT | | X | Attenuation due to twisting: |

                                   14 db   if either wire twisted
                                    0 db   if neither twisted

The wire codes, shielding and twisting data, and wire diameters neces-
sary for the computation of the output argument are collected in tables
within ELMNTS. Mutual capacitance XC and mutual inductance XM
are computed using the formulas in Paragraph C.8.

## D.2.2.4    Subroutine ATTEN

ATTEN is called by CIP to compute: (1) an attenuation spectrum for
a Tx - Rx pair, and (2) the interference spectrum obtained by sub-
tracting this attenuation spectrum from the Tx emitter spectrum.

The basic attenuation spectrum is defined by three points as follows:

| Log Frequency | Voltage Attenuation - db |
|---|---|
| 0 | $20 f_2$ |
| $f_2 = \log(cf)$ | 0 |
| 8 | 0 |

The "corner frequency" cf is computed depending upon the relative ordering of the load ends of the Tx and Rx circuit:

1)     If both loads are on the same ends of the circuits,

$$cf = \text{minimum } (f_c, f_m), \text{ where}$$

$$f_c = \frac{(Z_{\ell 1} + Z_{g1})(Z_{g2} + Z_{\ell 2})}{2\pi \ C \ Z_{\ell 1} Z_{g2} Z_{\ell 2}},$$

$$f_m = \frac{(Z_{\ell 1} + Z_{g1})(Z_{g2} + Z_{\ell 2})}{2\pi \ M \ Z_{g2}} \text{ and}$$

$Z_{\ell 1}$   =   load impedance, Tx circuit - ohms

$Z_{\ell 2}$   =   load impedance, Rx circuit - ohms

$Z_{g1}$   =   generator impedance, Tx circuit - ohms

$Z_{g2}$   =   generator impedance, Rx circuit - ohms

C     =   mutual capacitance - farads

M     =   mutual inductance - henries

2) If the loads are at opposite ends of the circuits,

$$cf = f_g = \frac{(Z_{\ell 1} + Z_{g1})(Z_{g2} + Z_{\ell 2})}{2\pi Z_{g2}(M + C Z_{\ell 1} Z_{\ell 2})} .$$

If either or both wires are shielded, the minimum of the attenuation produced by inductive and capacitive shielding at any frequency is added to the basic attenuation curve. The inductive and capacitive shielding spectra information, as defined in Paragraph 4.5.3, is in table form within ATTEN.

If either wire is twisted, an additional amount of attenuation, given in the calling sequence to ELMNTS, is also added at each point of the basic attenuation spectrum.

The final attenuation spectrum is subtracted from the Tx spectrum to obtain the interference spectrum which is returned to CIP by ATTEN.

A description of the input and output arguments for ATTEN is as follows:

| Argument | In | Out | Meaning |
|---|---|---|---|
| XM | X | | Mutual inductance - henries |
| XC | X | | Mutual capacitance - henries |
| ZG1 | X | | Complex generator impedance Tx circuit - ohms |
| ZG2 | X | | Complex generator impedance Rx circuit - ohms |
| ZL1 | X | | Complex load impedance Tx circuit - ohms |

| Argument | In | Out | Meaning |
|---|---|---|---|
| ZL2 | X | | Complex load impedance Rx circuit - ohms |
| VTX | X | | Amplitude array, Tx spectrum - db/µv |
| FTX | X | | Frequency array, Tx spectrum - log frequency |
| NTX | X | | Number of Tx spectrum points |
| VINT | | X | Amplitude array, interference spectrum - db/µv |
| FINT | | X | Frequency array, interference spectrum - log frequency |
| NINT | | X | Number of interference spectrum points |
| ISLD | X | | Wire shielding code, as in |
| ADAT | X | | Twisting attenuation, as in |
| IORIDI | X | | Order ID, Tx circuit |
| IORID2 | X | | Order ID, Rx circuit |
| CORNER | X | | Corner frequency - cf |